RENEWABLE ENERGY: RESEARCH, DEVELOPMENT AND POLICIES

M. Dhurgadevi, PhD
P. Sakthivel, PhD
K. Gunasekaran, PhD
EDITORS

The Future of WIND ENERGY

NOVA

Renewable Energy: Research, Development and Policies

www.novapublishers.com

Renewable Energy: Research, Development and Policies

Technical Challenges in the Commercialization of Transformers for Solar Photovoltaic Technology Applications
Bonginkosi Allen Thango (Author)
2021. ISBN: 978-1-68507-214-8 (Softcover)
2021. ISBN: 978-1-68507-249-0 (eBook)

Biofuel Production from Microalgae, Macroalgae and Larvae: Processes and Conversion Technologies
Man-Kee Lam, PhD, AMIChemE (Editor)
Jun-Wei Lim, PhD, ChM, MRSC (Editor)
Yoke-Wang Cheng, PhD (Editor)
Inn-Shi Tan, PhD, FHEA, Grad I.E.M (Editor)
2021. ISBN: 978-1-68507-116-5 (Hardcover)
2021. ISBN: 978-1-68507-159-2 (eBook)

Applied Soft Computing Techniques for Renewable Energy
Amit Kumar Thakur (Editor)
Rajesh Singh (Editor)
Ajay Kumar Kaviti (Editor)
Anita Gehlot (Editor)
J.V Muruga Lal Jeyan (Editor)
2020. ISBN: 978-1-53618-180-7 (Hardcover)
2020. ISBN: 978-1-53618-209-5 (eBook)

Waste-to-Energy (WtE)
Eduardo Jacob-Lopes, PhD (Editor), Leila Queiroz Zepka, PhD (Editor) and Maria Isabel Queiroz (Editor)
2019. ISBN: 978-1-53614-431-4 (Hardcover)
2018. ISBN: 978-1-53614-432-1 (eBook)

More information about this series can be found at
https://novapublishers.com/product-category/series/renewable-energy-research-development-and-policies/

M. Dhurgadevi, P. Sakthivel
and K. Gunasekaran
Editors

The Future of Wind Energy

nova
science publishers
www.novapublishers.com

https://doi.org/10.52305/NUYF7030

Library of Congress Cataloging-in-Publication Data

ISBN: 979-8-88697-344-0(eBook)

Published by Nova Science Publishers, Inc. † New York

Contents

Preface

Wind Energy is one of the oldest forms of energy from a natural source. Today, wind energy is one of the most mature renewable energy technologies and forms a critical stabilizing pillar for the entire portfolio of renewable energy sources. Wind energy supports a strong domestic supply chain. Wind has the potential to support over 600,000 jobs in manufacturing, installation, maintenance, and supporting services by 2050. Wind is becoming increasingly important for electricity generation — and turbines are getting bigger, taller and more efficient. About 7% of the world's electricity already comes from wind power.

This book provides fundamental concepts of wind energy systems and discusses the design issues for the future as well the challenges in wind energy research. The future of wind energy relies on Artificial Intelligence, Cloud Computing, IoT, Block chain and Big data analytics for Wind energy generation and monitoring. Energy optimizations are also very much needed. Recently, electricity generation using wind power has received much attention all over the world. Wind energy is a free, renewable resource, so no matter how much it is used today there will still be the same supply in the future.

Chapter 1 discusses with the economic integration of wind energy in the Economic Community of West African States (ECOWAS) between 2010-2020. Chapter 2 provides risk analysis based selection of the best supply chain using the Gray approach for wind energy system. Chapter 3 depicts a review of surface hardness improvement techniques for wind turbine gears.

Chapter 4 provides a comparison of Artificial Neural Network techniques in the prediction of wind speed using combinations of metrological variables.

Chapter 5 presents a machine learning approach for thermodynamic analysis in wind turbines with optimization.

Chapter 6 elicits the design, modelling and analysis of wind turbine gear and modified wind turbine blades.

Finally, this book covers hardware as well software analysis of the generation of wind energy and status of wind energy with modification of wind turbine also.

Chapter 1

The Economic Integration of Wind Energy: An Analysis of the ECOWAS Sub-Region

David Alemzero* **and Sun Huaping**
School of Economics and Finance, Jiangsu University Zhenjiang, Jiangsu, China

Abstract

This study evaluates the economic integration of wind energy in the Economic Community of West African States (ECOWAS) between 2010 and 2020. Due to the theoretical and economic potential of the sub-regions, wind energy is the only energy source that can cost-effectively meet the energy needs of the sub-regions. For this reason, the study uses data from the World Bank Development Indicators using Panel Vector Auto Regression to analyze the determinants underpinning the economic integration of wind energy. The Panel VAR estimate shows a significant direct link between fossil fuel consumption and private sector investment in renewable energy. This implies that the sub-region consumes a significant amount of fossil fuels, hence the need to increase clean energy investments to move the sub-region towards a low-carbon future. Another significant lag variable is the power consumption per capita in the sub-region. Per capita, electricity consumption in the sub-region is woefully insufficient. Therefore, wind energy can ensure access via the development of small community wind farms where the national power grid cannot be extended to. When assessing the economic justification of wind integration, the LCOE for wind power is 2.98 cents per kilowatt for the lowest cost scenario, compared to nuclear power's 2.26 per kilowatt hour. The FEVD shows that 13.4% of renewable energy investments are self-explanatory within the first and last periods. The FEVD for wind energy illustrates the short-term variance of 16.4 percent and increases to

* Corresponding Author's Email: awelingazure@gmail.com.

In: The Future of Wind Energy
Editors: M. Dhurgadevi, P. Sakthivel and K. Gunasekaran
ISBN: 979-8-88697-232-0

51.1 percent in the following years after system shocks. This implies that the expansion of wind capacity in the sub-region is expected to increase in the long term. This serves as a blueprint for integrating wind energy into the sub-region.

Keywords: wind energy, ECOWAS, PVARs LCOE, economic integration, JEL classification: Q4, Q42, Q4

Introduction

Wind energy integration can ensure energy security in the Economic Community of West African States (ECOWAS). The ECOWAS sub-region has made more progress in access to electricity than any sub-region in Africa, but access is still constrained and presents development challenges. The West African Power Pool (WAPP) is the sub-regional body responsible for providing the sub-region's electricity needs; However, it currently only covers about 30% of the electricity needs of the sub-regions (Goldwind, 2013). The subregion includes 15 countries with a population of approximately 375 million people with over 54 percent access to the national electricity grid (ECREEE, 2018.). The total primary energy supply within the sub-region was 8885 per joule in 2018, with biofuels and waste accounting for 70 percent of the supply (IRENA, 2022). Overall, wind energy generated one percent of the 75 terawatts of electricity delivered in 2018 (IRENA, 2022). Oil and natural gas dominate the primary supply sources with twenty percent and eight point eight respectively (IRENA, 2022). In addition, some countries have per capita electricity consumption below 40% and national electricity access below 10%. Access to modern cooking solutions is also below one percent in various economies within the sub-region. The solution lies in the economic integration of wind energy, which can create an energy economy while reducing energy poverty and ensuring energy security (Knobloch et al., 2020; Millstein et al., 2022; Role et al., 2022). Energy presents financial and technical challenges. The pace of energy system transformation is underpinned by many factors such as the cost of research and development and the deployment of renewable energy and decentralized technologies. As integration of new technologies into energy systems increases, there is a need to minimize losses and optimize capital investments due to system constraints.

To back up this claim, the study (ECREEE 2018: De La Pea et al., 2022, 2022; Pan & Dong, 2022) discovered that the ECOWAS sub-region lost 36%

of the electricity generated in 2018, totaling 26,207 GWh. This shows the high transmission and distribution losses from the member countries. According to Ruth and Kroposki (2014), the world needs about $1.5-2 trillion annually to fund transmission and distribution networks, with over two-thirds of that needed for the transmission and distribution systems to transform energy systems by 2030. Therefore, the motivation of this study is to assess the economic integration of wind energy in the ECOWAS sub-region in order to achieve energy security and universalization, thereby achieving SDG seven by 2030. The African Development Bank predicts that Africa will need $130 billion to $170 billion annually to build infrastructure, but there is a funding gap of $68 billion to $108 billion (AfDB, 2020). Additionally, between 2000 and 2009, West Africa received $5 billion in investments in renewable energy. Between 2000 and 2020, Africa attracted $60 billion in global RES investments, with West Africa receiving 7% of that total (IRENA, 2022). The analysis shows that West Africa has received significant investments in clean energy. Nevertheless, these investments have not boosted wind energy inflows in the sub-region. The devastating effects of climate change have made wind energy integration even more urgent and compelling for the ECOWAS sub-region. According to the study (Baarsch et al., 2020), SSA will lose about 15% of its GDP per capita by 2030 due to climate change.

The ECOWAS sub-region has a fairly good wind speed of 6 m/s at an altitude of 100 meters, enabling it to generate utility-scale wind farms and ensure sustainable consumption. Decentralized renewable energy sources provided electricity to approximately 2.5 percent of rural residents (ECREEE 2018). Due to the technical potential of wind energy and falling costs, it is now economical for the ECOWAS sub-region to use wind energy. This point of view is confirmed as nearly thirty nations have achieved grid parity for solar and other renewable electricity due to economies of scale in deployment (D. Alemzero et al., 2021; M. Liu et al., 2022; Moreno-Munoz, 2019). Additionally, electricity tariffs are projected to double by 2035, and this makes an even stronger case for integrating cheaper wind energy into the ECOWAS subregion, which has some of the highest electricity tariffs in the world (D. Alemzero et al., 2021; Moreno-Munoz, 2019.; Sun et al., 2020b). Likewise, subsidies for wind and renewable energy are gaining importance in several markets in the ECOWAS subregion due to falling costs and political incentives (Alemzero et al., 2021). The backbone of integrating wind energy into the national grid is battery storage due to the variable nature of wind energy. Nonetheless, the cost of batteries has dropped by around 40% to 60%, which has led to growth in the energy storage market (Moreno-Munoz, 2017;

Pool, 2022). Similarly, studies predict that the global energy storage market (ESS) for a smart grid will increase to 73% by 2020 and beyond, supporting wind energy deployment in the region. The challenge of grid integration entails a variety of challenges; important among them is grid flexibility, balancing VRE sources such as wind to ensure power system reliability and reduce costs (Martinot 2016).

Table 1, curated from the Goldwind study of the ECOWAS sub-region, shows that two of the 15 nations have fairly good to excellent wind speeds depending on the altitude measured. According to the study in Table 1, the wind resources of Ivory Coast and Guinea-Bissau are too small for investment (Goldwind, 2013). On the other hand, Liberia and Sierra Leone do not have the potential to generate electricity from wind resources. However, this does not mean that these countries cannot use wind energy since the potential of wind resources is not static but dynamic; it changes over time. With advances in technology, increasing the size of turbines with more swept area in certain locations, wind power could generate power for communities. In addition, an area with a wind speed of about 6 m/s or more meets the requirements for utility-scale wind investments, and locations with 5 m/s meet the requirements for small-scale or municipal wind investments (Grashof, 2019; J. Lee & Zhao, 2021; Olatayo et al., 2018; Ramsi et al., 2020; Ivan, 2017; X. Yao et al., 2020). A mini-wind farm project is operating in Kenya, stimulating local economic development, eradicating poverty and boosting employment (Ivan, 2017).

Table 1. Wind potential at best identified sites

Country	Average wind speed (m/s)	Generation (MWh/y/MW)
Benin	6.5	3006
Burkina Faso	6.5	2999
Gambia	6	2588
Guinea	8	4051
Guinea-Bissau	5	1717
Ivory Coast	4.8	1565
Liberia	-	-
Mali	7.2	3531
Niger	8	4051
Nigeria	7.8	3933
Senegal	6	2588
Sierra Leone	-	-
Togo	5.8	2451

Source: Goldwind.

Methods and Data

In this chapter, panel data from 2010-2020 for the ECOWAS subregion is used to empirically assess the economic integration of wind energy in the subregion to ensure energy security and sustainable consumption and boost economic growth. The study units were chosen based on data availability and the fact that they share similar characteristics in their economic development. These are 15 countries that make up the ECOWAS sub-region: Benin, Burkina Faso, Cabo Verde, Ivory Coast, Guinea, Guinea-Bissau, Gambia, Ghana, Senegal, Nigeria, Niger, Mali, Liberia, Sierra Leone, and Togo. In order to derive reliable estimation results, it makes sense to make a cross-sectional dependency of the variables. Some of the variables are not stationary and can lead to biased estimates. Therefore, in addition to the correlation matrix, the panel unit tests cross-sectionally extended Pesaran and Shin are deployed. The first-generation unit root tests do not encapsulate the impact of international shocks hitting countries, or global dependency due to cross-sectional relationships could affect the finite properties of the panel unit root test. The second-generation panel unit root tests were formulated to deal with this situation, to deal with this anomaly. According to (Das 2019), dealing with the cross-sectional dependency in the transient panel is quite challenging. He attributes this to the stochastic nature of the perturbation term, and the usual unit root measure of the t-statistic achieves finite distributions in the analysis. Therefore, different approaches within second-generation unit root analysis have been discussed. One is the set of constraints on the residual covariance matrix (Das, 2019). In this study, the (Pesaran, 2003) (Moon & Perron, 2004) test and the Bai and Ng (2004) (Das, 2019) tests are applied.

Pesaran (2003) Test

It is assumed that Pesaran formulated an easy-to-understand approach for estimating roots of unity in a cross-sectional dependency scenario alongside serially associated error.

$$y_t = u_i + \emptyset_i\, y_{it} + u_{it} \qquad (1)$$

From the equation (1) u_i represents the deterministic term, and the stochastic disturbance is

$$u_{it} = \lambda_i F_t + \varepsilon_{it} \quad (2)$$

The common latent variable is serially unassociated with zero mean and constant variance and is said to be independently distributed among the two and alongside zero mean and variance.

Bearing in mind models (1) and (2), the study derived the following equation (3).

$$\Delta y_{it} = u_i + (\phi_i - 1)\, y_{it} - 1\lambda_i F_t + \varepsilon_{it} \quad (3)$$

Hence the hypothesis to be evaluated is stated below:

$$H_{o=}\phi_i = 1, \forall i$$

With the opposing one below: $H_1 = \begin{cases} \emptyset_i<1, \ i=1,2\ldots.,N_1 \\ \emptyset_{i=}1, i=N_1,2\ldots..N \end{cases}$

Given in the model, the cross-sectional mean of yt and its past values are used as a proxy variable for the usual latent factor Ft. Pesaran's unit root test (Im et al., 2003) is based on the adjacent Dicky-Fuller regression augmented test of the cross-sectional means of past value levels and first differences of each series.

$$y_{it} = a1_i + a2_i\, y_{it-1} + a3_i \bar{y}_{t-1} + \alpha_{4i}\, \overline{y_t} + e_{it} \quad (4)$$

From equation (7.4)

$$\overline{y_t} = \frac{\sum_{I=1}^{N} y_{it}}{N} \text{ and } \Delta\overline{y_t} = \frac{\sum_{I=1}^{N} \Delta y_{it}}{N}$$

Cross-section-specific augmentation The Dicky Fuller (CDAF) statistic is derived from the estimated coefficient of equation (7.4) for the cross-section unit. The asymptotic null distributions of the CADF statistics are alike and independent of the factor loadings.

Variance Decomposition

A variance decomposition is applied to approximate the amount of variance in the forecast error in projecting $X_{j,T+h}$ as result of the structural shock of ε_{it}.

The h-step forecast errors alongside the orthogonal shocks,

$$\delta_h = x_{t+h} - I\Psi_t = \sum_{s=0}^{h-1} \Phi_s \varepsilon_t + h - s \quad (5)$$

Concerning a specific variable x_i the forecast error attains from:

$$\sigma_{ih} = x_{iT+h} I\psi_t = \sum_{s=0}^{h-1} \theta_i Ist + h - 1 + \cdots + \sum_{s=0}^{h-1} \theta_{iks} \varepsilon k, T + h - s \quad (6)$$

Due to the fact that the structure terms are orthogonal, the variance of the stochastic term of the h-step prediction is:

$$V_{(\delta ih)} = \sigma_{\varepsilon i}^2 \sum_{s=0}^{h-1} \theta_{ils}^2 + \cdots . + \sigma_{\varepsilon k}^2 \sum_{s=0}^{h-1} \theta_{iks}^2 \quad (7)$$

As a result, the amount of variance attributable to shock ε_j is

$$VD_{ij(h)} = \frac{\sigma_{\varepsilon i}^2 \sum_{s=0}^{h-1} \theta_{ils}^2}{\sigma_{\varepsilon i}^2 \sum_{s=0}^{h-1} \theta_{ils}^2 + \cdots . + \sigma_{\varepsilon k}^2 \sum_{s=0}^{h-1} \theta_{iks}^2}$$

Hence, in a VAR that has K variables, there will be k^2 $VD_{ij(h)}$ Values.

Next, the Panel Vector auto regression (PVAR) approach suggested (Neves et al., 2019; Lutz Kilian and Helmut Lütkepohl 2017) is ideal since the analysis handles potentially endogenous variables. Panel VARs usually arise in studies entailing different countries, but they can also be used in various sectors, firms, and plants. Thus, the suitability of this approach is because the study analyses the interaction of different variables concerning different countries within the ECOWAS sub-region. These variables are an investment in energy by the private sector; access to clean cooking solutions; percentage of the total population; rural access to electricity; percentage of the total population; Gross Domestic Product per capita; wind energy capacity; RES capacity; research and development (R&D); energy imports; GDP growth; electric power consumption per head; fossil fuel consumption; and transmission and distribution losses (T&D). This scenario makes it feasible to contribute an extra subscript to a variable. Thus, t^{th} observation i^{th} variable of country n by Q_{nt}. Here, $i = 1, \ldots . M$ and N $n = 1, \ldots . , N$. Hence, utilizing the earlier notation, $K = M.N$. Let Q_{nt}=$(Q1_{nt} \ldots \ldots \ldots Q_{Mnt})$ be an M-dimensional vector and represent by Qn_{t-1} and Q_{t-1} vectors of lags Q_{nt} and all variables within the longitude individually. The model is formulated below, with a complete general covariance matrix $\sum u$ for the entire system of all N

countries, $\sum u$ is the covariance matrix of $u_t = (u'_{1t}, \ldots . u'_{Nt})'$. This longitudinal structure has three unique characteristics. To begin with, the lags are all endogenous variables that get into the model through unit i, explaining the dynamic interdependence among the variables. Next, is u_{nt}overall correlated among n . That is, static interdependence. Thirdly, the covariance, the intercept, and the slope of the shocks might be unit-specific. This explains the cross-section heterogeneity among the units. This makes the P-VARs applied in macroeconomic studies different from the ones applied in microeconomic research (Canova & Ciccarelli, 2014; Moreno-Munoz, 2017).

$$Q_{nt} = V_v + S_n Q_{t-1} + u_{nt} \tag{8}$$

Levelized Cost of Energy (LCOE) Comparison of Wind Energy Including Nuclear

Wind energy has experienced more cost reductions over the past five years than any other RE technology (Wiser et al., 2021). Regarding Africa, (Alemzero et al., 2021) calculated that the cost of wind energy fell by 30% from 2010 to 2019. The levelized cost of electricity is the total amount of energy generated in monetary terms over the lifetime of a facility. It measures the total cost of building and operating a facility over a period of time. It creates space for the comparison of different generations of technologies. Generation and production costs could be given below (Bebi et al., 2021; (IRENA), 2017; Sun et al., 2020). Below is a simplified concept of LCOE.The mathematical formulation is given below:

$$\text{LCOE} = \frac{\left[\sum_{n=-1}^{t=-1} \left(\frac{I_t}{(1+1)^{\bar{t}}}\right)\right]_{\text{foundation}} + \left[\sum_{n=0}^{t=n-1} \left(\frac{f_t + O\&M_t - D_{t+T_t}}{(1+1)^{\bar{t}}}\right)\right]_{\text{Production}}}{\left[\sum_{n=-1}^{t=-1} \left(\frac{G_t}{(1+1)^{\bar{t}}}\right)\right]_{\text{Production}}} \tag{9}$$

The discount rate of r is based on the costs available in a given country, considering the balance between equity and debt investments. The weighted average cost or discount is around 12% but varies by generation type. At the same time, several studies use 11% and 7% as the discount factor for the analysis of wind energy projects (Bebi et al., 2021). In the ECOWAS sub-region, macroeconomic instability leads to high inflation, currency risk, and political risk. In addition, operating and maintenance costs are expressed in dollars as a percentage of the total investment. Wind turbines need maintenance to run efficiently, just like any other piece of equipment. This could typically account for a larger amount of the total annual cost, typically

around 20% to 25% of the LCOE cost (IRENA, 2020). The cost of wind energy fuel is zero. Thus, the topic of crude oil price fluctuations has no influence on the operation of wind farms. This highlights the profound differences between wind farms and traditional sources of energy generation (Bebi et al., 2021; Blanco, 2009; Wai-Hoo & Sovacool, 2014). Similarly, the cost of a wind farm requires a high initial investment compared to conventional energy sources such as natural gas power plants, where 40–70% of the costs are fuel and O&M costs.

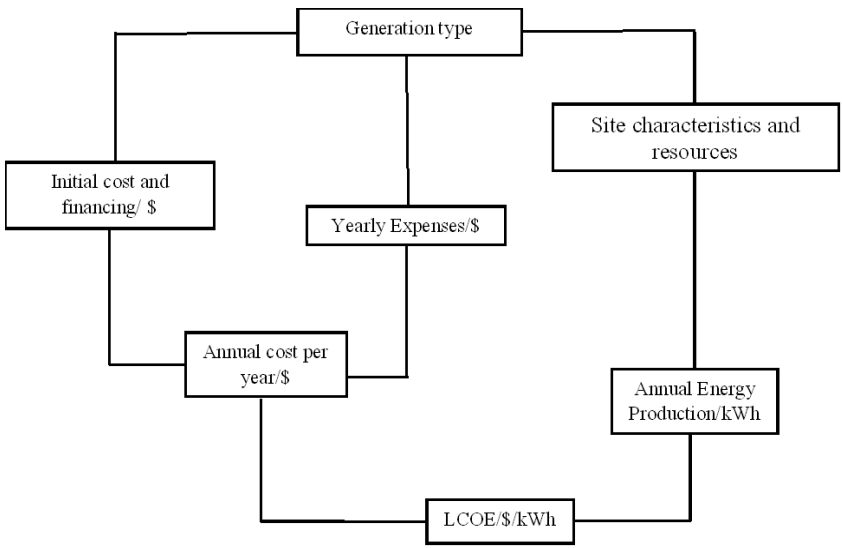

Figure 1. LCOE Concept Source. Author's construct.

Lag Selection Criteria

Panel VAR models are preconditioned, choosing the optimum lags in the two VAR specification moment circumstances. (Abrigo & Love, 2016; Andrews & Lu, 2001) mooted the MMSC premised on GMM equations.

Results and Discussions

Descriptive Statistics

Table 1 contains the descriptive statistics of the analysis. The variable with the highest mean is fossil fuel consumption. This is not a surprise as the ECOWAS sub-region consumes more energy from fossil fuel sources. The next variable

with the highest mean is fuel imports. The variable with the lowest mean is access to clean and modern cooking solutions at 9.425. According to a study (Jewitt et al., 2020; ECREEE, 2018), there have been programmes to improve access to clean cooking solutions through the distribution of LPG, biogas, solar cookers, and ethanol fuel, followed by R&D by millions of people. The data shows that smaller countries like Togo and the French colonies do well in terms of research and development. In fact, investments in renewable energy are beginning to take shape. It has the fourth highest mean. Rural access is also very low in the countries within the sub-region. According to wind energy output, the mean is low. Wind energy is breaking new ground in the sub-region as several countries have already planned or operational wind farm projects. Senegal is a newcomer with its Taiba Ndiaye and Ghana's ongoing Ayitapa wind farm project (Alemzero et al., 2021; Countries et al., 2021; Sun et al., 2020).

Table 2. Descriptive statistics

Variable	Obs	Mean	Std. Dev.	Min	Max
Investrep	165	252.512	548.216	0	2153
Ackg	165	9.425	20.194	0	95.53
Ruralac	165	20.431	21.939	0	95.944
Gdpperca	165	1294.976	847.203	436.627	3482.448
Elcons	165	51.392	80.005	0	375.945
Fuelimprts	163	45373.553	125456.71	-8.192	477684.34
Fosfocon	162	179080.6	192632.03	0	596000
Windcap	164	17.675	164.74	0	2100
Rdm	165	10.809	54.295	0	564.339

Source: Author's calculation.

Table 2 explains the relationship between the variables. The significant variables are the interaction between GDP per capita and access to clean cooking. This explains the importance of integrating wind energy to meet the energy needs of the rural population. Rural people still cook with polluting sources such as biomass, resulting in health risks for the population (Dagnachew et al., 2019; Jewitt et al., 2020). According to the analysis, less than 1% of Liberia and Sierra Leone have access to clean cooking and alternative sources of energy. Meanwhile, Guinea and Guinea Bissau have less than 2% access to clean cooking and alternative solutions. In addition, the correlation between gross domestic product per capita and rural access is the highest. This is very revealing because development is equitable and sustainable when rural residents have equal access to energy. This is even truer

for achieving SDG 7, which calls for universal access to equitable and affordable energy for all by 2030. The higher a nation's GDP per capita, the greater the nation's ability to spend on clean energy sources, especially in the ECOWAS subregion as a developing region (Alemzero, 2022; Bashir et al., 2021; Wai-Hoo & Sovacool, 2014).

Table 3. Correlation Matrix

Variables	**(1)**	**(2)**	**(3)**	**(4)**	**(5)**	**(6)**	**(7)**	**(8)**	**(9)**
(1) Investrep	1.000								
(2) Ackg	-0.036	1.000							
(3) Ruralac	0.283	0.692	1.000						
(4) Gdpperca	0.301	0.596	0.739	1.000					
(5) Elcons	0.269	0.059	0.172	0.146	1.000				
(6) Fuelimprt	-0.114	-0.160	-0.221	-0.221	-0.075	1.000			
(7) Fosfocon	-0.270	-0.168	-0.322	-0.158	-0.221	0.387	1.000		
(8) Windcap	0.052	0.020	0.015	0.053	0.194	-0.023	-0.044	1.000	
(9) Rdm	-0.015	0.093	0.074	-0.015	0.097	-0.027	0.023	-0.021	1.000

Source: Author's calculations.

Table 4 is the cross-sectional dependency test of the second-generation unit root tests from Pesaran. This is done to establish the stationarity of the variable. Since the series are likely to be non-stationary over time between the countries studied, it makes economic sense to determine their stationarity by applying the cross-dependency of the second-generation root of unity tests. Concerns about panel heterogeneity and non-stationarity, as well as cross-sectional dependency caused by macroeconomic variables The differences in the integration of wind within the ECOWAS subregion are related to certain latent variables such as political institutions, human resources, and other factors needed for wind energy integration, as well as the non-stationarity of macroeconomic variables within the analysis, such as gross domestic product, and the interdependence of national economies through cross-sectional dependency. The Pesaran unit test is based on the assumption that the Dickey-Fuller regression is extended alongside the cross-sectional means of past levels and the first differences of each series. Hence, the unit root must overcome these challenges and deliver consistent and unbiased results (Baltagi, 2021; Eberhardt & Teal, 2011). The table above contains the time trends of different delays for the different variables. Therefore, considering the critical values of the t-bar, the null hypothesis is not rejected. Against this background, the CHIPS results analyzed (Pesaran, 2007) proved that the variables are stationary at the first difference, explaining the cross-sectional correlation between these variables. This makes estimating the panel VAR model possible

once all of these variables are stationary. Some researchers believe that PVAR is best suited for a study of this type where the variables are likely to be endogenous (Love & Zicchino, 2006; Neves et al., 2019).

Table 4. Cross-section dependence test and second-generation unit root test (CIPS)

Variable	Prob. Value	Z[t-bar]	Lags
ACKG	1.00***	13.817	3
ELCONS	1.00***	13.817	4
OFOSFOCON	1.00***	12.911	3
FUELIMPRT	1.00***	12.911	3
GDP_PER_CA	0.156**	-1.011	1
INVESTREP	1.00***	13.817	2
R_& D_	1.00***	13.817	2
RURALAC_	0.987***	2.232	1
WINDCAP	1.00***	13.341	3

The second-generation unit root test is performed under the null hypothesis where in the variables are I(1); and ***, **, * and _ denote statistical significance level at 1%, 5% and 10% individually.

From Table 5, the lag order selection criteria that selected the optimal lags for analysis, namely: the Akaike information criteria, the Schwartz information criteria, and the Hannaquin information criteria, sequentially modified LR test statistic, and the final predictor error, are discussed (Andrews & Lu, 2001). These lags have the minimum values and therefore minimize the selection process. These have information criteria for lag orders of less than one. The PVAR model is therefore estimated at first-order lag one.

Table 5. VAR lag order selection Criteria

Lag	LogL	LR	FPE	AIC	SC	HQ
0	-308.096	NA	202603.9	15.05218	15.38316	15.17349
1	-302.826	8.281376	165663.3	14.84884	15.22120	14.98533
2	-302.78	0.070192	173808.5	14.89427	15.30800	15.04592
3	-275.18	40.74189	49131.30	13.62763	14.08274	13.79445
4	271.519	5.229965*	43451.53*	13.50092*	13.99740*	13.68290*
5	-271.405	0.158272	45533.08	13.54308	14.08093	13.74022
6	-269.839	2.087330	44567.34	13.51615	14.09538	13.72846
7	-269.764	0.097390	46873.92	13.56017	14.18076	13.78764
8	-268.144	2.005710	45853.47	13.53064	14.19261	13.77328

LR: sequential modified LR test statistic (each test at 5% level).
FPE: Final prediction error.
AIC: Akaike information criterion.
SC: Schwarz information criterion.
HQ: Hannan-Quinn information criterion.

PVAR

Table 6 measures the homogeneous VAR equations by fitting a multi-panel regression of each explained parameter to lags of itself, past parameters of other exploratory parameters, and lags of exogenous parameters if any. Thus, the results from Table 6 show that the lagged values of fossil fuel consumption and the lagged values of investment in renewable capacity, a proxy variable for wind integration, are significant. The direction is direct. As the ECOWAS sub-region consumes larger amounts of fossil fuels, it is important to scale up investments in wind capacity and shift their consumption pattern in a sustainable way. So, the importance of the interaction of these variables Also, power consumption per capita is significant. Per capita, electricity consumption in the ECOWAS sub-region is not encouraging, as low as 19 kWh for Guinea-Bissau. Wind integration can improve access to the growing per capita consumption in these countries. The analysis showed, for example, that Guinea-Bissau can generate around 1717 MWh of electricity from wind each year.

Table 7 is performed to find the stability condition of the PVAR model by approximating the modulus of each eigenvalue of the measured equation as in (Canova and Ciccarelli, 2014; Neves et al., 2019; Lutz Kilian and Helmut Ltkepohl, 2017). Table 7 shows that the stability condition of the model is satisfied since all roots are less than uniform and are inside the circle. The stability means that the panel VAR model is invertible and achieves an infinite order of the invertible representation of the vector moving average, which is the basis for approximating the IRF. In Figure 1, a stability condition plot is constructed to represent all the results of the companion matrix lying within the circle, making the model stable.

The IRF plots imply that the variables have a general impact on wind energy integration in the ECOWAS subregion after a shock hits the system. They start from zero and take a straight-line trajectory. That is, they all return to an equilibrium path. This shows the stationary of the variables and gives an accurate picture of the future integration of wind energy, as some of the variables show a direct path in the analysis when a positive outlook is assumed. The response of fuel imports and GDP per capita is direct and outpaces most variables. On the contrary, the response to access to clean cooking and alternative cooking solutions and investment in renewable energy started straight away and tumbled down a negative path. This is revealing as some countries in the sub-region are stagnating in access to modern cooking solutions due to a lack of investment. Suppose the ECOWAS sub-region is set

Table 6. PVAR Results

	investrep																
Investrep		Ackg		ruralac		Gdpperca		elcons		fuelimprt		fosfocon		windcap		Rdm	
L.investrep	0.0524	L.investrep	-0.0075	L.investrep	0.0816	L.investrep	0.33	L.investrep	-0.005	L.investrep	-56.87	L.investrep	-27.88	L.investrep	-0.104	L.investrep	-0.0119
	-0.09		(-1.12)		-1.33		-1.64		(-0.10)		(-0.58)		(-0.37)		(-0.64)		(-0.13)
L.ackg	-14.55	L.ackg	0.739	L.ackg	2.373	L.ackg	-7.233	L.ackg	-3.685	L.ackg	-7257.6	L.ackg	-2999.1	L.ackg	-12.52	L.ackg	-8.64
	(-0.39)		-1.68		-0.47		(-0.41)		(-0.71)		(-0.96)		(-1.06)		(-0.68)		(-0.99)
L.ruralac	-7.912	L.ruralac	-0.239	L.ruralac	2.593	L.ruralac	7.303	L.ruralac	-1.227	L.ruralac	6512.5	L.ruralac	-1660.2	L.ruralac	0.646	L.ruralac	4.713
	(-0.35)		(-0.87)		-0.87		-0.65		(-0.84)		-1.35		(-0.83)		-0.09		-0.82
L.gdpperca	1.422	L.gdpperca	0.0297	L.gdpperca	-0.391	L.gdpperca	-0.361	L.gdpperca	0.062	L.gdpperca	-61.45	L.gdpperca	166.4	L.gdpperca	0.333	L.gdpperca	-0.175
	-0.59		-1.04		(-1.52)		(-0.40)		-0.43		(-0.17)		-0.49		-0.56		(-0.52)
L.elcons	3.259	L.elcons	0.0647	L.elcons	-0.626	L.elcons	-1.562	L.elcons	1.031**	L.elcons	933	L.elcons	296.9	L.elcons	1.842	L.elcons	0.651
	-0.88		-1.29		(-1.21)		(-0.90)		-2.73		-1.19		-0.53		-0.99		-0.74
L.fuelimprt	-21.95	L.fuelimprt	-0.46	L.fuelimprt	6.214	L.fuelimprt	21.94	L.fuelimprt	-1.437	L.fuelimprt	-9226.3	L.fuelimprt	-2627.6	L.fuelimprt	-13.19	L.fuelimprt	-1.805
	(-0.65)		(-0.94)		-1.31		-1.39		(-0.44)		(-1.16)		(-0.42)		(-1.02)		(-0.28)
L.fosfocon	0.0005	L.fosfocon	######	L.fosfocon	-5E-05	L.fosfocon	-3E-04	L.fosfocon	-2E-04	L.fosfocon	0.146	L.fosfocon	1.045***	L.fosfocon	6E-05	L.fosfocon	-3.7E-05
	-0.22		(-0.17)		(-0.23)		(-0.36)		(-1.25)		-0.42		-7.8		-0.11		(-0.20)
L.windcap	0.258	L.windcap	0.0044	L.windcap	-0.058	L.windcap	-0.203	L.windcap	0.038	L.windcap	34.58	L.windcap	17.73	L.windcap	0.0457	L.windcap	-0.012
	-0.74		-0.99		(-1.39)		(-1.47)		-1.15		-0.56		-0.33		-0.45		(-0.24)
L.rdm	-0.259	L.rdm	0.0042	L.rdm	0.0187	L.rdm	0.16	L.rdm	0.176	L.rdm	124.3	L.rdm	53.2	L.rdm	-0.02	L.rdm	0.0978
	(-0.45)		-0.55		-0.2		-0.49		-1.72		-0.84		-1.1		(-0.09)		-0.91
																N	127

to significantly expand this sector's access to alternative cooking solutions. In this case, a business-as-usual approach has to be avoided and a new paradigm for formulating framework conditions to maximize investments has to be developed. Overall, the interaction between investment in RE and variable shocks is less strong as the next few periods take on negative values. Clean energy investments within the ECOWAS sub-region are rightfully very low (Monyei et al., 2022; Onuoha et al., 2022). Ultimately, the responses to wind energy and R&D are direct and encouraging. Increasing innovation is spurring the deployment of wind energy and the supply chain, which is increasing the integration of wind energy in the sub-region.

Table 7. VAR Stability Condition check

Root	**Modulus**
-0.343565 - 0.722790i	0.800288
-0.343565 + 0.7227	0.800288
-0.288015 - 0.376421i	0.473968
-0.288015 + 0.376421i	0.473968
No root lies outside the unit circle.	
VAR satisfies the stability condition.	

Source: Author's Calculation.

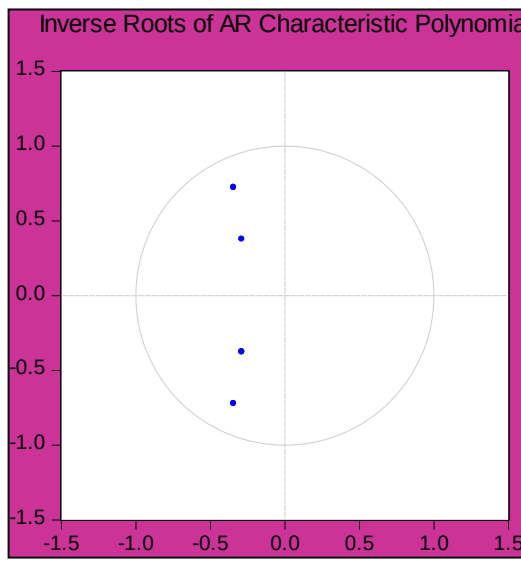

Source: Author's Calculations.

Figure 2. Graph of eigenvalue stability condition.

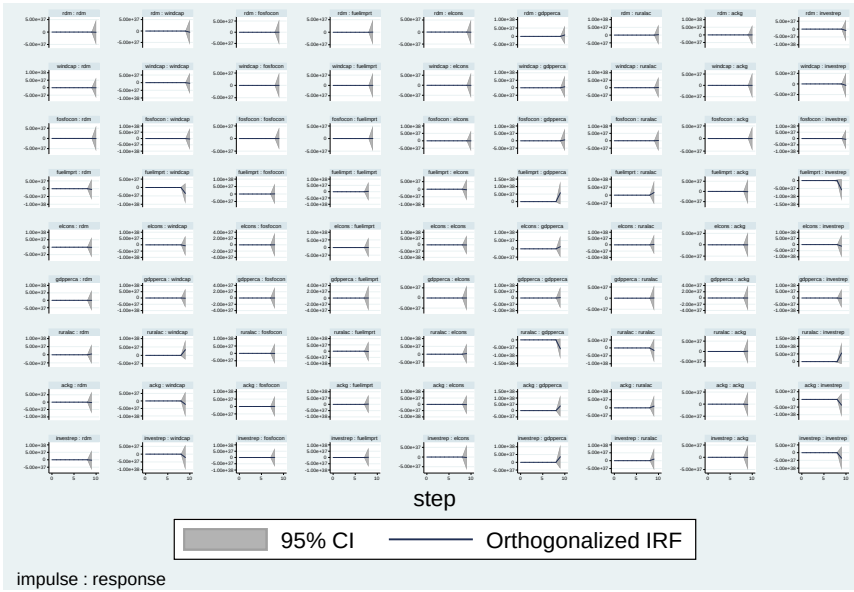

Figure 3. Graphs of orthogonalized IRFs.

Forecast Error Variance Decomposition Analysis

According to the Cholesky decomposition of the residual covariance matrix, the forecast error variance decomposition was analyzed using 1000 Monte Carlo simulations for ten periods. The FEVD represents the percentage of each exploratory variable and highlights the forecast error variance of the different variables. Within the two situations of IRF and FEVD approximation of the VAR, the Cholesky order of the variables was used by replacing the variables in decreasing order of homogeneity, as shown in (Abrigo & Love, 2016; Andrews & Lu, 2001; Love & Zicchino, 2006). Table 6 the short-term variance decomposition of an exogenous shock on the investment in renewable energy accounts for about 13.4% of the InvestRep itself. On the other hand, responding to a shock in access to clean cooking and alternative energy sources produces about 14.8% of the variance in renewable energy investments. Similarly, rural access accounts for 33.2 percent of the short-term investment variance in the second period. In comparison, fuel imports explain 36.7 percent of the variance in investment over the same period, the largest short-term variance. However, the wind cap, electricity consumption per capita, fossil fuel consumption, and research and development have little to no variance impact on InvestREP. In the long run, that is, in year 5, the impact of

the shocks on the system remains the same throughout the period, producing similar impacts on investment and response variables.

Access to clean cooking and alternative cooking solutions has the next highest variance explanation within the model at 83.3 percent in the first period when there is a shock. At the same time, 16.7 percent is self-explanatory due to the size of the investment. The rest of the variables had no decomposition variances on the InvestRep. That concerns the short term. On the other hand, within the long-term horizon, the variables maintain a steady reaction trajectory to shocks that hit the system (Role et al., 2022). Elcons also have a self-explanatory variance of 72.2 percent in the first period. Conversely, the variance within this period is highest at 96% for InvestmentRep, which represents the highest variance. This is because energy consumption is growing due to rapid industrialization and population growth in the ECOWAS sub-region (Goldwind Group, 2013; IRENA, 2021).

A shock accounts for approximately 20.2 percent of the variance in GDP forecast error per capita. Rural access shock causes 26.67 percent of the forecast error variance, while access to clean cooking causes 36.7 percent of the forecast error variance. InvestmentinRep accounts for 17% of the period's short-term forecast error. Over the long term, which includes periods four and five, access to clean cooking solutions explains 14.8 percent of the forecast error variance, while rural areas explain 14.8 percent of the forecast error variance. Because of fuel imports, the forecast variance is 36.7 percent. In both long-term periods, ReinvestRep declares 13.4 percent. Even in the short term, FOSS accounts for 45 percent of forecast deviation in the first period following a shock. Furthermore, rural access accounts for 37.2 percent of short-term access during this time period. More importantly, wind capacity is responsible for 51.5 percent of the variance in forecast errors in the first period following a shock. According to Cross Border Information (CBI), wind energy is the fastest growing renewable energy source in Africa, with a growth rate of 2.5 percent in the first quarter of 2020. As a result, ReinvestRep accounts for 16.4% of the variance. This scenario confirms that the investment is crucial for the integration of wind energy in the ECOWAS sub-region. In contrast, R&D explains approximately 46.1 percent of the variance in forecast error shocks that pass through the system. It is the period over which the variance in forecast error was largely explained by the study variable; the rest had no R&D to explain discrepancies in decomposition analysis. This is expected as R&D investment in the ECOWAS region is almost non-existent in most countries (African Energy Commission, 2018). This is a short term within the first period. 57 percent in the first period and Investrep shows a negligible

variance in this period, the smallest variance in the entire analysis. This analysis is correct because investments in wind energy per se are very low within the ECOWAS sub-region despite the economic and technical potential of wind energy to sustainably meet the region's energy needs (Assoumou & McIsaac, 2022; Bysa, 2020; Mbaziira et al., 2022).

Moreso, A critical look at the results of the FEVD shows that InvestRep explains the forecast error variance across all ten periods but maintains a steady course. This paints a picture of the slow but steady way in which the ECOWAS sub-region is investing in renewable energy and wind. On the other hand, even if the variance is not significantly high, GDP per capita, access to clean cooking, and alternative cooking solutions show a steady trajectory, with the variance of the forecast error still coinciding with rural electricity access. This is synchronous as access to rural areas is very low and wind energy integration is needed to close the access gap. The fuel imports, in particular, explain a strong variance in the forecast error decomposition within the entire analysis. Here's the fact: the ECOWAS sub-region is in an energy deficit and hence these nations depend on imports to meet their domestic electricity needs. Hence the strong and steady variation of these variables. The West African Power Pool (WAPP), which aims to meet the demand to harmonize the idiosyncratic markets into a single market to meet countries' energy needs, is a classic example of the constant variance of this variable. A surprising discrepancy comes from FOSS, fossil fuel consumption, which does not explain any discrepancy at all. This is an outlier as the ECOWAS sub-region consumes most of it from fossil fuel sources. According to the African Energy Commission (2020), fossil fuels accounted for approximately 40.8 percent of Africa's energy consumption in the first quarter of 2020. Another variable that explains the need to integrate wind energy is electricity consumption per capita. Its variance is minimally explained in the analysis. This is due to the low energy consumption within the ECOWAS sub-region. The per capita consumption of Guinea and Guinea-Bissau is about 42 kWh and 19 kWh, respectively. This cannot boost economic growth and development in these countries. Therefore, the need to integrate wind energy to meet energy demand via community wind projects is due to the fact that the entire sub-region has the potential for community wind farm projects. Thus, a wind speed of 5 m/s is required for the integration of small wind farms.

Since the ECOWAS sub-region has a growing population, this demonstrates that the demand for energy consumption per capita will increase in the coming years and justifies the integration of wind energy to meet this growing demand. The sub-region has one of the lowest energy consumption

per capita in SSA, like Sierra Leone, Liberia, and Guinea-Bissau. This fact has also been confirmed (Blimpo et al., 2020).

Levelized Cost of Energy (LCOE) Comparison of Wind Energy Including Nuclear

The diagram below shows electricity generation from wind energy and other generation sources. The levelized cost of bituminous coal was approximately 8.20 cents per kilowatt hour, representing an installation cost of $12,500 in a lower estimate scenario and $1,500 in a higher estimate scenario. On the other hand, the initial levelized cost of wind energy is 2.98 cents per kilowatt at the lowest estimate and about 6 cents at the higher estimate. The service lifespan of a wind energy farm is 20 years. In terms of large-scale solar power, it is 8 cents per kilowatt for the high estimates and 0.805 per kilowatt-cent for the low scenario, as shown in Figure 4 below.

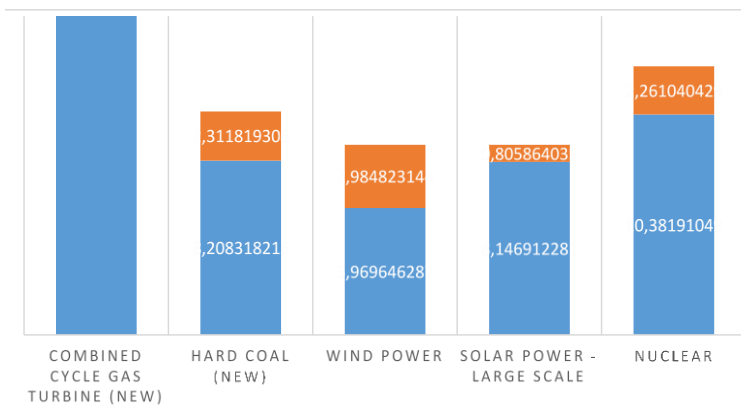

Figure 4. LCOE Comparison of generation sources.

Sensitivity Analysis of Wind Energy and Different Generation Sources

The sensitivity analysis is performed to help investors make an informed decision on the financial indicators and technical factors related to the economic integration of wind energy within the ECOWAS sub-region. Figure 5 shows full load as the highest parameter required for an economic investment in an agricultural project within the ECOWAS sub-region. The full load hours explain the full utilization of a plant. The number of hours a facility can operate to produce electricity. Therefore, it is very important to consider

the full load hour of the location or generation source when constructing a wind farm. It is the most important parameter within the sensitivity analysis. The full load hours make it possible to compare locations, years, and plants in order to normalize the area's energy yield. The full load hour is not static but dynamic over time. The next important variable within the sensitivity analysis is the investment costs. It is particularly high for wind energy within the ECOWAS sub-region, as illustrated by the height of the bar chart. A closer look reveals that wind energy has the highest investment costs for building wind farms in the sub-region. However, the expected investment costs for wind energy will continue to fall from now until 2030, regardless of these currently high costs. The cost of wind turbines overshadows the capital cost of wind energy. Other costs in the form of a control system and land make up a negligible proportion of this aspect. Notably, wind has no variable or marginal costs, fuel costs, or carbon dioxide pollution, as shown in the figure below. These parameters are shown in the figure for traditional energy sources. The hard coal power plant, obviously. Only the conventional source has. This makes integration into the ECOWAS sub-region necessary. The only technical cost of integration is the cost of the network connection, as shown in the figure. This does not prevent the ECOWAS sub-region from using wind energy, since wind energy can be connected to the grid without significant disruptions to the primary reserves of over 10%.

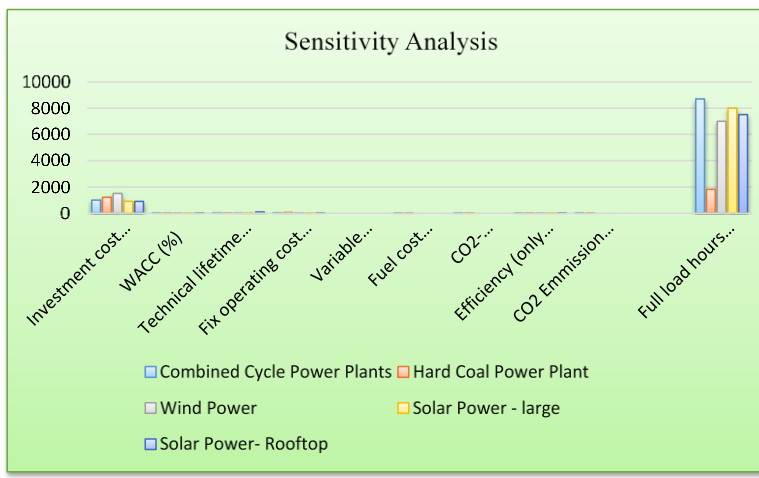

Source: Author's construct.

Figure 5. Sensitivity Analysis.

Conclusion: Summary of Findings

This study analyses the economic rationale for integrating wind energy into the ECOWAS sub-region. The ECOWAS sub-region is one of the largest energy deficit regions in SSA. This was done by applying a panel vector autoregression (PVAR) approach and levelized analysis to determine the drivers and economics of wind energy deployment. The study period extends from 2010 to 2020. The period chosen takes into account that the beginning of the 21st century saw the introduction of renewable energies such as wind energy in the region. The results were varied and interesting and justified the need to integrate wind into the sub-region. First of all, access to clean cooking in the sub-region is negligible. A majority of the population is still dependent on polluting cooking sources that have health and economic impacts. For example, access to modern cooking solutions is around 6% in Benin and 8.9% in Burkina Faso. Mali has declined from 1.02 percent in 2010 to about 0.96 percent in 2016. This corroborates the importance of the per capita electricity consumption variable in the analysis of the panel variables. This implies that the population in the subregion has the lowest overall energy consumption. Another significant variable is the amount of fossil fuel consumption. Fossil fuel consumption is very high in the ECOWAS sub-region. This parameter is significant and reached the highest mean of the analysis. Because of this, there is a need to switch to competitive and environmentally friendly wind energy.

Furthermore, the conclusion equally implies that research and development have at least one non-slight variance declared as FEVD to other variables, with another intrinsic variance of about 46%. This results in the lowest investment in research and development (R&D) among member countries. This explains why R&D investments are scarce in many of the countries studied. Consequently, the economic analysis shows that onshore wind energy integration has the next cheapest generation costs of nearly 3 cents per kilowatt and nearly 7 cents per kilowatt after large-scale solar power within the ECOWAS sub-region of the study. The analysis found that given the affordability of wind integration costs, as the cost of wind deployment continues to decrease through massive economies of scale in terms of cost per kilowatt, the analysis found the sub-regions should implement measures to scale up wind power. Finally, the sub-region has the technical potential (with significant wind speeds) for the development of utility-scale wind farms. Furthermore, the sensitivity analysis shows that of all the parameters that determine the integration of wind farms, the full-hour load is the most

important for determining where to set up a farm and the yield per year. The next important parameter is the investment cost. Besides, the capital cost of wind energy is high, with turbine costs accounting for a larger portion of the cost. The other costs are control systems and land. Furthermore, the conclusion implies that research and development are at least as important as the FEVD explains no less than 46% of variance to other variables other than self-variation. This translates to the least investment in research and development (R&D) among member countries. This explains why R&D investments rarely exist in many of the study countries.

Eventually, the analysis implies that investing in network infrastructure to modernize it is crucial in the long to medium term. This creates additional capacity to transport the increased generation, disruptions, and uncertainties of large amounts of wind energy connected to the national grid. This does not mean that developing countries cannot start integrating wind now because they lack grid capacity; they can do this because they are within the tipping point. Given the above factors, linking access to clean cooking and energy programmes needs to be integrated into national anti-poverty and development policies. Also, a significant increase in funding, both crowd funded and non-crowd funded, is very important in wind energy integration. In terms of innovation, there is little research and development (R&D) investment in the study countries. The ECOWAS sub-region needs to invest in research and development to find innovative ways to achieve the rapid deployment of wind energy. In order to achieve effective and meaningful development and economic growth, there should be adequate and inexpensive energy sources such as wind energy. Finally, diversity refers to the formulation of policies such as rural electrification programs to promote access and create an energy economy in disadvantaged communities.

References

Abbas, Q., Khan, A. R., Bashir, A., Alemzero, D. A., Sun, H., & Iram, R. (2020). *Scaling up renewable energy in Africa: measuring wind energy through econometric approach.*

Abrigo, M. R. M., & Love, I. (2016). Estimation of panel vector autoregression in Stata. *Stata Journal*, 16(3), 778–804. https://doi.org/10.1177/1536867x1601600314

African Energy Comission. (2018). *African Energy database.* 82. https://afrec.au.int/en/documents/20180801/africa-energy-database.

Agency, I. R. E. (2020). Renewable Power Generation Costs in 2019. In *International Renewable Energy Agency.* https://www.irena.org/-/media/Files/IRENA/Agency/Publication/2018/Jan/IRENA_2017_Power_Costs_2018.pdf

Alemzero, D., Acheampong, T., & Huaping, S. (2021). Prospects of wind energy deployment in Africa: Technical and economic analysis. *Renewable Energy*, 179, 652–666. https://doi.org/10.1016/j.renene.2021.07.021.

Andrews, D. W. K., & Lu, B. (2001). Consistent model and moment selection procedures for GMM estimation with application to dynamic panel data models. *Journal of Econometrics*, 101(1), 123–164. https://doi.org/10.1016/S0304-4076(00)00077-4

Assoumou, E., & McIsaac, F. (2022). Côte d'Ivoire's electricity challenge in 2050: Reconciling economic development and climate commitments. *Energy Policy*, 160, 112681.

Baarsch, F., Granadillos, J. R., Hare, W., Knaus, M., Krapp, M., Schaeffer, M., & Lotze-Campen, H. (2020). The impact of climate change on incomes and convergence in Africa. *World Development*, 126, 104699. https://doi.org/10.1016/j.worlddev.2019.104699.

Bai, J., & Ng, S. (2004). A panic attack on unit roots and cointegration. *Econometrica*, 72(4), 1127–1177. https://doi.org/10.1111/j.1468-0262.2004.00528.x

Baltagi, B. H. (2021). *Econometric Analysis of Panel Data* (Springer Texts in Business and Economics) - Sixth Edition. In Springer.

Bebi, E., Malka, L., Konomi, I., & Alcani, M. (2021). An analysis towards a sustainable energy system in albania highly supported by large scale integration of wind resources: A case study of mamaj wind farm. *International Journal of Energy Economics and Policy*, 11(1), 355–372. https://doi.org/10.32479/ijeep.10622

Blanco, I. (2009). *The economics of wind energy*. 13, 1372–1382. https://doi.org/10.1016/j.rser.2008.09.004

Blimpo, M. P., Postepska, A., & Xu, Y. (2020). Why is household electricity uptake low in Sub-Saharan Africa? *World Development*, 133, 105002. https://doi.org/10.1016/j.worlddev.2020.105002

By-sa, C. C. (2020). *Sub-Saharan Africa Market Outlook 2020.*

Canova, F., & Ciccarelli, M. (2014). *VAR Models in Macroeconomics - New Developments and Applications: Essays in Honor of Christopher A. Sims.* https://doi.org/10.1108/s0731-905320130000031014

Fendoğlu, E., & Polat, M. A. (2021). *The Relationship Between R & D Expenditures and Economic Growth: Panel Data Analysis in Selected New Industrializing Countries/ Ar- Ge Harcamaları ile Ekonomik Büyüme Arasındaki İlişki: Seçilmiş Yeni Sanayileşen Ülkelerde Panel Veri Analizi*. 3, 728–747.

Cross Border Infromation (CBi). (2020). *African Energy Atlas 2020-2021*.

Dagnachew, A. G., Hof, A. F., Lucas, P. L., & Vuuren, D. P. Van. (2019). Scenario analysis for promoting clean cooking in Sub-Saharan Africa: costs and benefits. *Energy*, 116641. https://doi.org/10.1016/j.energy.2019.116641

Das, P. (2019). Econometrics in theory and practice: Analysis of cross section, time series and panel data with stata 15.1. In *Econometrics in Theory and Practice: Analysis of Cross Section, Time Series and Panel Data with Stata* 15.1. https://doi.org/10.1007/978-981-32-9019-8

De La Peña, L., Guo, R., Cao, X., Ni, X., & Zhang, W. (2022). Accelerating the energy transition to achieve carbon neutrality. *Resources, Conservation and Recycling*, 177, 105957.

Eberhardt, M., & Teal, F. (2011). Econometrics for grumblers: A new look at the literature on cross-country growth empirics. *Journal of Economic Surveys*, 25(1), 109–155. https://doi.org/10.1111/j.1467-6419.2010.00624.x

Goldwind Group. (2013). *Goldwind Group: Corporate Introduction*. October.

Grashof, K. (2019). Are auctions likely to deter community wind projects? And would this be problematic? *Energy Policy*, 125(August 2017), 20–32. https://doi.org/10.1016/j.enpol.2018.10.010

Hurlin, C., & Mignon, V. (2007). *Second Generation Panel Unit Root Tests To cite this version: HAL Id: halshs-00159842 Second Generation Panel Unit Root Tests*. 1–25. https://halshs.archives-ouvertes.fr/halshs-00159842

Im, K. S., Pesaran, M. H., & Shin, Y. (2003). Testing for unit roots in heterogeneous panels. *Journal of Econometrics*, 115(1), 53–74. https://doi.org/10.1016/S0304-4076(03)00092-7

International Renewable Energy Agency (IRENA). (2017). Renewable energy auctions. In *Renewable Energy Auctions: Analysing 2*016 (Vol. 1, Issue 14).

IRENA. (2019). Renewable Energy Market Analysis: GCC 2019. In *IRENA*. https://www.irena.org/publications/2019/Jan/Renewable-Energy-Market-Analysis-GCC-2019

IRENA. (2021). *The Renewable Energy Transition in Africa*/Publications/2021/March/The-Renewable-Energy-Transition-in-Africa./publications/2021/March/The-Renewable-Energy-Transition-in-Africa

Jewitt, S., Atagher, P., & Clifford, M. (2020). Energy Research & Social Science "We cannot stop cooking": Stove stacking, seasonality and the risky practices of household cookstove transitions in Nigeria. *Energy Research & Social Science*, 61(May 2019), 101340. https://doi.org/10.1016/j.erss.2019.101340

Knobloch, F., Hanssen, S. V., Lam, A., Pollitt, H., Salas, P., Chewpreecha, U., Huijbregts, M. A. J., & Mercure, J. F. (2020). Net emission reductions from electric cars and heat pumps in 59 world regions over time. *Nature Sustainability*, 3(6), 437–447. https://doi.org/10.1038/s41893-020-0488-7

Lee, J., & Zhao, F. (2021). Gobal Wind Report 2021. *Global Wind Energy Council*, 75. http://www.gwec.net/global-figures/wind-energy-global-status/

Liu, M., Ju, C., & Huang, R. (2022). Assessing the Effects of Market Power on Electricity Reliability in China: Toward a Green and Reliable Market. *Frontiers in Energy Research*, 9(January), 1–9. https://doi.org/10.3389/fenrg.2021.811565

Love, I., & Zicchino, L. (2006). Financial development and dynamic investment behavior: Evidence from panel VAR. *Quarterly Review of Economics and Finance*, 46(2), 190–210. https://doi.org/10.1016/j.qref.2005.11.007

Martinot, E. (2016). *Grid Integration of Renewable Energy: Flexibility, Innovation, and Experience*. 223–254. https://doi.org/10.1146/annurev-environ-110615-085725

Mbaziira, R., Carmona Moreno, C., Crestaz, E., Farinosi, F., & Biedler, M. (2022). *Establishing common water sector priorities in Africa*.

Millstein, D., Bolinger, M., & Wiser, R. (2022). What can surface wind observations tell us about interannual variation in wind energy output? *Wind Energy*, April 2021, 1–9. https://doi.org/10.1002/we.2717

Monyei, C. G., Akpeji, K. O., Oladeji, O., Babatunde, O. M., Aholu, O. C., Adegoke, D., & Imafidon, J. O. (2022). Regional cooperation for mitigating energy poverty in Sub-Saharan Africa: A context-based approach through the tripartite lenses of access, sufficiency, and mobility. *Renewable and Sustainable Energy Reviews*, 159, 112209. https://doi.org/https://doi.org/10.1016/j.rser.2022.112209

Moon, H. R., & Perron, B. (2004). Testing for a unit root in panels with dynamic factors. *Journal of Econometrics*, 122(1), 81–126. https://doi.org/10.1016/J.JECONOM.2003.10.020

Moreno-Munoz, A. (n.d.). *IET Energy Engineering Series* 98 Large Scale Grid Integration of Renewable Energy Sources.

Neves, S. A., Marques, A. C., & Fuinhas, J. A. (2019). The interactions between conventional and alternative energy sources in the transport sector: A panel of OECD countries. In *The Extended Energy-Growth Nexus: Theory and Empirical Applications*. Elsevier Inc. https://doi.org/10.1016/B978-0-12-815719-0.00008-5

Lutz Kilian and HelmutLütkepohl (2017) *Structural Vector Autoregressive Analysis.* Availablewww.http:cambridge.org/9781107196575

Regional Progress Report on Energy, *Energy Efficiency and Energy Access in the ECOWAS Subregion* (2020). http://www.ecreee.org/document/regional-progress-report-renewable-energy-energy-efficiency-and-energy-access-ecowas-region

Olatayo, K. I., Wichers, J. H., & Stoker, P. W. (2018). Energy and economic performance of small wind energy systems under different climatic conditions of South Africa. *Renewable and Sustainable Energy Reviews*, 98(September), 376–392. https://doi.org/10.1016/j.rser.2018.09.037

Onuoha, F. C., Uzoechina, B. I., Ochuba, O. I., & Inyang, N. F. (2022). Economic expansion, energy sources and environmental quality in ECOWAS sub-region: evidence from a heterogeneous panel non-linear Autoregressive Distributed Lag (PNARDL). *Environmental Science and Pollution Research*, 29(6), 8892–8908. https://doi.org/10.1007/s11356-021-16173-7

Pan, Y., & Dong, F. (2022). Design of energy use rights trading policy from the perspective of energy vulnerability. *Energy Policy*, 160, 112668.

Pesaran, M. H. (2007). A simple panel unit root test in the presence of cross-section dependence. *Journal of Applied Econometrics*, 22(2), 265–312. https://doi.org/10.1002/JAE.951

Pool, P. (2022). BESS Primary Frequency Control Strategies for the West Africa. 1–25.

Ramsi, J., Diógenes, F., Valentim, M., Claro, J., & Rodrigues, J. C. (2020). Energy Research & Social Science Barriers to onshore wind energy implementation: A systematic review. *Energy Research & Social Science*, 60(October 2018), 101337. https://doi.org/10.1016/j.erss.2019.101337

Role, T., Bonds, G., Role, T., & Bonds, G. (2022). *Financing the Energy Transition: The Role, Opportunities and Challenges of Green Bonds Financing the Energy Transition* (Issue December 2021).

Ruth, M. F., & Kroposki, B. (2014). *Energy Systems Integration: An Evolving Energy Paradigm.*

Sun, H., Khan, A. R., Bashir, A., Alemzero, D. A., Abbas, Q., & Abudu, H. (2020a). Energy insecurity, pollution mitigation, and renewable energy integration: prospective of wind energy in Ghana. *Environmental Science and Pollution Research*, 27(30), 38259–38275.

Sun, H., Khan, A. R., Bashir, A., Alemzero, D. A., Abbas, Q., & Abudu, H. (2020b). *Energy insecurity, pollution mitigation, and renewable energy integration: prospective of wind energy in Ghana.*

Version, D. (2017). *How can we stimulate and exploit a market in Africa for small wind turbines.*

Wai-Hoo, A. Y., & Sovacool, B. K. (2014). The economics of wind energy. *Sustainability Matters: Asia's Energy Concerns, Green Policies and Environmental Advocacy*, 2, 317–340. https://doi.org/10.1142/9789814546829_0026

Wiser, R., Rand, J. T., Seel, J., Beiter, P., Baker, E., Lantz, E., & Gilman, P. (2021). *Expert elicitation survey predicts 37% to 49% declines in wind energy costs by 2050.* April.

Yao, X., Yi, B., Yu, Y., Fan, Y., & Zhu, L. (2020). Economic analysis of grid integration of variable solar and wind power with conventional power system. *Applied Energy*, 264(December 2009), 114706. https://doi.org/10.1016/j.apenergy.2020.114706

Chapter 2

A Risk Analysis-Based Selection of the Best Supply Chain using the Gray Approach for Wind Energy Systems

S. Santhosh[1,*], M. Vesvanth[2] and K. V. Siva Suriya[2]

[1]Department of Mechanical Engineering, Sri Krishna College of Technology, Coimbatore, Tamilnadu, India

[2]PG Scholars, College - Audencia Business School, Nates, France

Abstract

Interest in supply chain management has been growing since the late 80s as it is the critical stage of the production system. It mainly focuses on raw materials, work in progress inventory, finished goods inventory, information, and cash flows in the system. It is vital to learn about and investigate the risks connected to the supply chain. Profitability, future development, market share, client satisfaction, competitive edge, and corporate social responsibility are all linked to risk. Risk management processes are key apprehensions for people, companies, and organizations as there is escalating volatility and increasing uncertainty in the supply chain network. Customer demand and customer deliveries contribute mainly to the uncertainties in the supply chain. The next prime uncertainty is the potential requirements. As a result, risk management is the most important aspect of the supply chain, and it is critical to recognize and categorize various types of risks associated with the supply chain in order to select the best supply chain. This paper examines the dissimilar types of risks and uncertainties connected with supply chains.

* Corresponding Author's Email: drssmech@gmail.com

In: The Future of Wind Energy
Editors: M. Dhurgadevi, P. Sakthivel and K. Gunasekaran
ISBN: 979-8-88697-232-0

An effort has been made by the Gray approach to select the finest supply chain for Indian industries.

Keywords: supply chain, Gray approach, risk management

Introduction

Global markets are crossing the boundaries and managing the demands and supply all over the globe. This market is benefiting global companies around the world. To keep down the cost of manufacturing, they are continuously looking into setting up production centers where the product and labour are chipped. Companies procure materials globally from various vendors to their production units located in different parts of the world, and finished goods from these factories are passed to different parts of the world through various distribution chains. This is the supply chain or network that processes raw materials and makes available goods to their consumers. It is not an individual's potential that makes a supply chain efficient, but a group that helps build this chain's proper functioning. It is the supply chain that confirms the success of any firm, and yet it is simultaneously affected by some risk.

Therefore, risk management is a key thing to analyze. Due to its global nature, the supply chain faces more risk than any other area of the company, and it directly impacts the financial performance of the company. Often, a number of forces that drive the supply chain risk include supply shortages, quality and safety challenges, security, terrorism, weather and natural disasters, longer lead times needed for the global environment, etc. Risk planning often falls to the bottom without being met with a crisis. So much motivation is needed that existing planning will be effective. Risk can be managed to get rid of it, but it cannot be eradicated.

Literature Review

Every business is associated with some kind of risk, so risk management is not new in the field of supply chains. Recognizing and mitigating those risks is a primary task for any firm. A number of papers are available on this. The following studies on supply chain risk are: Risks are categorized under two headings, i.e., operation risk and disruption risk. Any risks that are related to customer demand, supply, and cost and include uncertainty come under

operational risk, whereas risks related to the destruction of property, which can be caused by floods, earthquakes, terrorist attacks, or economic crises, come under disruption risk. The strength of disruption risk has more business impact than operation (C. S. Tang, 2006).

A framework has been proposed that presents a planned way to identify and assess risk and its influence on the network level of the supply chain (S. C. Cheng and B. Hon Kam, 2008). They identified and categorized risk into two clusters, i.e., those happening from simplifying the compound system of supply and demand and, secondly, those happening from perturbation from normal activity. The major focus of the research was on the perturbation side (P. R. Kleindorfer and G.H. Saad, 2005). An approach was developed to identify and manage risk in the supply chain. This structured and ready-to-use approach can be divided into phases where tasks are related to risk for identification, measurement, assessment, evaluation, mitigation, contingency planning, control, and monitoring via a data management system (R. Tummala, T. Schoenherr, 2011). A model was created to analyze the risk associated with the food supply chain with interpretive structure modelling (ISM). Risks were identified and their types were clustered into five categories (Samvedi, V. Jain, and F.T.S. Chan, 2013). They studied and came to a point where risk can be quantified in a supply chain and then combined the value into a comprehensive risk index. Risks are here classified as an environmental risk, process risk, demand risk, and supply risk (A. Diabat, K. Govindan, and V.V. Panicker, 2012).

They discussed some of the operational risks of the supply chain, such as utility failure, poor quality, HR problems, IT system failure, theft of information, personnel, and suppliers (A. Samvedi, V. Jain, and F.T.S. Chan, 2013). They prepared a model for congruence to analyse factors influencing risk conditions that would be easy to apply but also accurate, and they also provided empirical evidence about misfit relationships that focused on three categories of risk: supply market complexity, purchase criticality, and technological uncertainty (M. Dadeviren, Y. Hasan, 2008). They reviewed ninety-two research papers and, accordingly, categorized them into risk, supply chain risk, and supply chain risk management. The structure of classification of the risk includes two levels and three categories, such as internal, external, and environmental in the first layer, and the second level consists of several subcategories (J. Gualandris, M. Kalchschmidt, 2015). They formulated a model to analyze the internal and external risks and their alternatives that affect the supply chain and accordingly set the priorities for

them to verify the best supply chain under these deliberations (S. M. Wagner, C. Bode, 2006).

This research includes some of the risks that supply chains usually come across. Economic risk, environmental and societal risk, performance measurement risk, and procurement risk are all prioritized. Economic risk is regarded as one of the most significant risks because it directly affects the firm's financial status and profitability (M. Chand, T. Raj, R. Shankar, and A. Agarwal, 2017). Environmental and societal risk mainly includes disasters and political or economic activaities such as earthquakes, hurricanes, floods, money devaluation, and political, regulatory, and market forces (S. K. Kumar et al., 2010). Procurement risks come into the picture when orders are not completed on time due to deviations in supply time, quality, and quantity (M. Dagdeviren, S. Yavuz, and N. Klnc, 2007). All these risks can affect the supply chain in terms of cost, quantity, quality, and lead time. For managing this risk, some approaches and models have already been utilized: Fuzzy AHP by Degdeviren et al., (2013) and fuzzy AHP by Wang et al., (2013); Fuzzy AHP and fuzzy TOPSIS by Samvedi et al., (2013); the Quality Function Development (QFD) approach by Faisal M.N. (2007); and the Analytical Network Process (ANP) and Multi-Objective Optimization by Rational Analysis (MOORA) by Chand et al., (2006).

Research Design

ABC Limited, headquartered in Coimbatore (India), provides wind energy systems to their customers. It started as a service and supply of wind energy systems to its customers. The demand for wind energy systems has increased in various areas, like the residential and commercial industries. A company likes to expand its manufacturing facilities as demand increases. The company wants to select the best supply chain for supplying its products to its customers. The company has proposed four supply chains, from which the company has to select one based on risk management. The four proposed networks are given in Figure 1. A description of the network is given below.

The first network consists of suppliers; manufacturing units; distribution hubs; retailers; sorting and dismantling units; reprocessing units; and disposal units. The supplier supplies the raw material, which will be converted into a product in the manufacturing unit, and it will be distributed to the retailers by

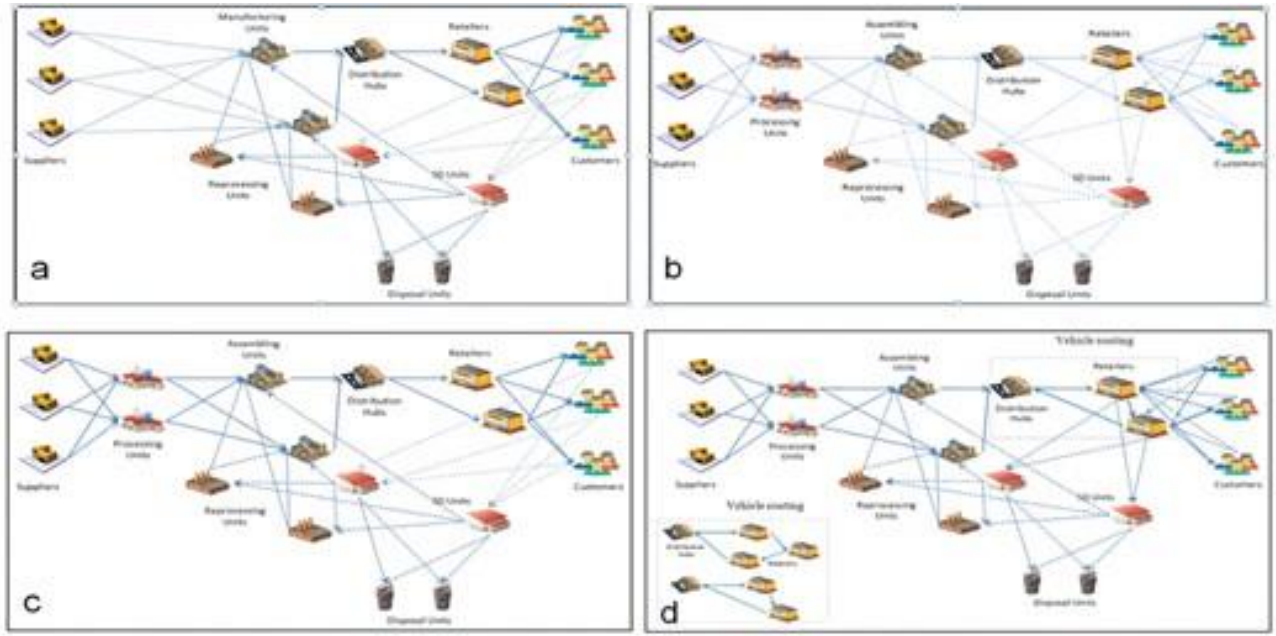

Figure 1. Four proposed supply chains for analysis.

the assembling unit. The end-of-life or end-of-use products are given back to the retailers. Retailers hand over the used products to the sorting and dismantling unit, where the products are disassembled, tested, and sent to the reprocessing unit and disosal unit, respectively.

Table 1. Identified criteria

Id	Criteria	Id	Criteria
C_1	Economic Recession	C_7	Product Performance
C_2	Financial market Instability	C_8	Process performance
C_3	Fuel Price	C_9	Requirement Uncertainty
C_4	Natural Disasters	C_{10}	Supply Disruptions
C_5	Machine Explosive	C_{11}	Unreliable Supplier
C_6	Social and Cultural Grievance	C_{12}	Damage to Cargo

Table 2. Linguistic terms for supply chain ratings

Linguistic Term		Membership Function
Extremely dissatisfied	ED	(0,1)
Dissatisfied	D	(1,3)
Somewhat dissatisfied	SD	(3,4)
Undecided	U	(4,5)
Somewhat satisfied	SS	(5,6)
Satisfied	S	(6,9)
Extremely satisfied	ES	(9,10)

Table 3. Linguistic terms for criteria weights

Linguistic Term		Membership Function
Absolutely Low	AL	(0,0.1)
Very Low	VL	(0.1,0.3)
Low	L	(0.3,0.4)
Medium	M	(0.4,0.5)
High	H	(0.5,0.6)
Very High	VH	(0.6,0.9)
Absolutely High	AH	(0.9,1.0)

In the second network, the manufacturing unit is divided into processing units and assembling units. In the processing unit, the raw materials will be converted into parts, and they will be assembled in the assembling unit. In the third network, the customers give back the used products to the sorting and dismantling unit. In the fourth network, vehicle routing was implemented

between the distribution hub and retailers. In supply chain selection criteria, along with financial risk criteria, some important natural and social risk, performance measure risk, and procurement risk criteria are added and evaluated. These criteria are listed in Table 1. In this work, we use a Gray approach for choosing and evaluating a suitable supply chain. Linguistic terms for alternative ratings and linguistic terms for criteria weightings, respectively, are given in Table 2 and Table 3. The methodology for assessment is explained in the next section of the chapter.

Gray Approach Methodology

In this section, the most suitable supply chain among the projected supply chains is identified by a multi-criteria decision-making approach. After many pilots were run, the Gray approach was found to be suitable for selecting the best supply chain. The Gray approach for evaluating supply chains consists of eight stages, and these approaches are described in fact as follows.

Selection of Evaluation Criteria

In this approach, identifying the criteria and measuring the indicators is the most important step. With the help of a strategic goal, the experts will be brainstorming and will be identifying the criteria.

Assignment of Weight to Criteria and Rating for the Supply Chain

S = (S1, S2, S3… Sn) is the n number of the supply chains, and C = (C1, C2… Cm) is the m number of criteria. Wm (m=1, 2….. i) are the criteria weights. The performance ratings of each decision maker Dk (k=1, 2… K) for each supply chain are denoted by dn (n=1, 2… j).

The evaluation of the criteria and supply chain will be carried out by the decision maker in this step, and they will also determine the linguistic terms for supply chain and criteria.

With reference to the linguistic terms from Tables 2 and 3, the Gray rating for the supply chain and the Gray weight of the criteria are assigned. Calculate the aggregate Gray weight for criteria and rating for the supply chain. Determine the decision matrix.

Rk = (xk, yk), k= 1, 2… K is all the decision-makers Gray weights for criteria and Gray rating for the supply chain. Then R = (x, y) is the aggregated gray weight for criteria, and ratings for supply chains are given by where

$$x = \frac{1}{K}\sum_{k=1}^{K} x_k \qquad y = \frac{1}{K}\sum_{k=1}^{K} y_k \tag{1}$$

The aggregate Gray weight of the criteria and aggregate Gray rating for the supply chain is determined using equation (1). The Gray decision matrix (DM) is determined for the criteria (C) and the supply chain (S) is constructed as follows.

$$R = [r_{mn}]_{i \times j} \; m=1, 2,\ldots, i \; n=1,2,, j \tag{2}$$

Calculated the Weighted Normalized Matrix

Various criteria are scaled to a comparable scale using a linear scale transformation.

The normalized Gray decision matrix R* is given by

$$R^* = [r^*_{mn}]_{i \times j} \; m=1,2,\ldots, i \; n=1,2\ldots..., j \tag{3}$$

where

$$r^*_{mn} = \left(\frac{x_{mn}}{y^*} , \frac{y_{mn}}{y^*} \right)$$

and

$$y^* = \max_{1<n<j} y_{mn}$$

The weights (wl) of the evaluation criteria are multiplied with the normalized Gray decision matrix r*mn to calculate the weighted normalized matrix V for criteria

$$V = [v_{mn}]_{i \times j} \; m=1,2,\ldots, i \; n=1,2,\ldots.., j \tag{4}$$

where vmn = (Wm) (r*mn)

Set the ideal supply chain alternative as a referential supply chain.

The ideal referential supply chain and ideal negative referential supply chain Smax = (V1max, V2max... Vjmax) are obtained from m possible supply chain sets S using

$$S^{max} = \{[\max_{1<n<j}(\bar{v}_{1n}, \underline{v}_{1n})] \ldots [\max_{1<n<j}(\bar{v}_{3n}, \underline{v}_{3n})]\} \quad (5)$$

where n=1, 2… j

Calculate the Gray Possibilities

Contrast Supply Chain Set S with the ideal referential Supply Chain Set Smax.

$$P1 = P(Sn \leq Smax) = 1/i \sum_{m=1}^{i} P(v_{mn} \leq V_n^{max}) \quad (6)$$

Ranking the Supply Chain

In this step, the supply chain with a minimum Pi is better. According to the above procedure, the ranking order of the entire supply chain is determined, and we can select the best from among the set of supply chains.

Computation Experiment

Four supply chains are identified for the company, and the best chain is selected using the Gray approach. Four expert consultants as decision makers have been used in this approach. These decision-makers have examined all the criteria and supply chain, and respective weights and ratings in linguistic terms have been given.

Their Gray membership function has been obtained from Tables 2 and 3 using the linguistic reviews provided to the decision-makers. For these Gray weights, an aggregate Gray weight is computed using equation (1) for the criteria and rating for the supply chain and is shown in Table 4 and Table 5 respectively. From the aggregate Gray decision matrix for supply chain, the weighted normalized supply chain matrix is determined using equation (3) and equation (4) as shown in Table 6.

Table 4. Aggregate Gray criteria weight

Criteria	**Aggregate Gray Weight**	
C_1	0.375	0.475
C_2	0.525	0.725
C_3	0.725	0.875
C_4	0.200	0.350
C_5	0.475	0.575
C_6	0.475	0.575
C_7	0.650	0.850
C_8	0.725	0.875
C_9	0.625	0.775
C10	0.725	0.875
C11	0.825	0.975
C12	0.675	0.925

Using equation (5) for m possible supply chain set S, the ideal referential supply chain Smax is listed below.

Smax = (0.296, 0.475), (0.366, 0.725), (0.564, 0.875), (0.125, 0.350), (0.343, 0.575), (0.327, 0.575), (0.474, 0.850), (0.505, 0.875), (0.478, 0.775), (0.554, 0.875), (0.631, 0.975), (0.559, 0.925)

Table 5. Aggregate Gray Decision Matrix for supply chain

Criteria	**Supply Chain**							
	S_1		S_2		S_3		S_4	
C_1	7.50	9.50	6.50	8.50	5.50	7.50	6.00	9.00
C_2	5.25	6.75	5.75	8.25	5.75	8.25	5.25	6.75
C_3	3.50	4.50	2.25	3.75	2.50	4.00	2.75	4.00
C_4	1.75	3.50	2.25	3.75	1.50	3.25	2.50	4.00
C_5	3.25	4.25	2.75	4.00	3.25	4.50	3.25	4.25
C_6	4.75	6.25	4.75	6.25	5.25	7.25	5.50	8.00
C_7	5.50	7.50	6.75	9.25	5.50	7.50	5.75	8.25
C_8	5.00	6.00	5.75	8.25	5.50	7.50	5.50	7.50
C_9	5.50	7.50	6.50	8.50	5.75	8.25	5.50	7.50
C_{10}	5.50	7.50	6.50	8.50	5.25	6.75	5.50	7.50
C_{11}	5.25	6.75	6.50	8.50	5.75	8.25	5.50	7.50
C_{12}	5.25	6.75	7.25	8.75	5.50	7.50	5.25	6.75

Table 6. Normalized aggregate Gray Decision Matrix for supply chain

Criteria	Supply Chain							
	S_1		S_2		S_3		S_4	
C_1	0.30	0.48	0.26	0.43	0.22	0.38	0.24	0.45
C_2	0.33	0.59	0.37	0.73	0.37	0.73	0.33	0.59
C_3	0.56	0.88	0.36	0.73	0.40	0.78	0.44	0.78
C_4	0.09	0.31	0.11	0.33	0.08	0.28	0.13	0.35
C_5	0.34	0.54	0.29	0.51	0.34	0.58	0.34	0.54
C_6	0.28	0.45	0.28	0.45	0.31	0.52	0.33	0.58
C_7	0.39	0.69	0.47	0.85	0.39	0.69	0.40	0.76
C_8	0.44	0.64	0.51	0.88	0.48	0.80	0.48	0.80
C_9	0.40	0.68	0.48	0.78	0.42	0.75	0.40	0.68
C_{10}	0.47	0.77	0.55	0.88	0.45	0.70	0.47	0.77
C_{11}	0.51	0.77	0.63	0.98	0.56	0.95	0.53	0.86
C_{12}	0.41	0.71	0.56	0.93	0.42	0.80	0.41	0.71

Using equation (6), Gray has the possibility of comparing the supply chain set S with the ideal referential supply chain Smax.

P1 (S1 Smax) = 0.646; P1 (S2 Smax) = 0.563; P1 (S3 Smax) = 0.624; P1 (S4 Smax) = 0.613; P1 (S4 Smax) = 0.613

Using the Gray possibility value, the supply chain is ranked. The Gray possibility betters the supply chain.

S2 > S4 > S3 > S1

From the illustration, it is clear that S2 is the best supply chain shown in Figure 2. The next important supply chain is S4, and S1 is the worst supply chain in this set.

Conclusion

In this chapter, the Gray approach is used to evaluate the financial risk of the supply chain along with the natural and social risks, procurement risks, and supply risks for a manufacturing company. In the proposed method, a brainstorming session was carried out, and 12 criteria were chosen for the assessment of the supply chain. For the chosen criteria and supply chain, an

expert consultant examines and allocates the weights and ratings accordingly. These weights are processed in the Gray approach and a ranking is given to the supply chain. Using the ranking, the best supply chain is selected and used as the supply chain for the company.

Disclaimer

None

References

Cheng S. C, and Hon Kam.B, A conceptual framework for analysing risk in supply networks, *Journal of Enterprise Information Management*, 21(2008) 345-360.

Chand M, Raj T, Shankar R, Analysing the operational risks in supply chain by using weighted interpretive structural modelling (W-ISM) technique, *International Journal of Services and Operations Management*, 18 (2014) 378-403.

Chand M, Raj.T, Shankar R, Agarwal A, Select the best supply chain by risk analysis for Indian industries environment using MCDM approaches, Benchmarking : *An International Journal*, 24 (2017) doi: 10.1108/BIJ-09-2015-0090.

Chand M, Raj T, Shankar R, A comparative study of multi criteria decision making approaches for risks assessment in supply chain, *International Journal of Business Information System*, 18 (2015) 67-84.

Dagdeviren M, Yavuz S, Klnc N, Weapon selection using the AHP and TOPSIS methods under fuzzy environment, *Expert Systems with Applications*, 33 (2007) 870880.

Dadeviren M, Hsan Y. Developing a fuzzy analytic hierarchy process (AHP) model for behavior- based safety management. *Information Sciences* 178(6) (2008): 1717-1733.

Diabat A, Govindan K, Panicker V. V, Supply chain risk management and its mitigation in a food industry, *International Journal of Production Research*, 50 (2012) 30393050.

Faisal M. N, Managing Risk in Small and Medium Enterprises (SMEs) Supply Chains Using Quality Function Deployment (QFD) Approach. *International Journal of Operations Research and Information Systems* (IJORIS) 4(1) (2013) 64-83.

Gualandris J, Kalchschmidt M, Supply risk management and competitive advantage: a misfit model, *The International Journal of Logistics Management*, 26 (2015) 459-478.

Kleindorfer P R, Saad.G H, Managing disruption risks in supply chains, *Production and Operations Management*, 14 (2005) 5368.

Kumar S. K, Tiwari.M. K, Babiceanu.R.F, Minimisation of supply chain cost with embedded risk using computational intelligence approaches, *International Journal of Production Research*, 48 (2010) 37173739.

Li G. D, D. Yamaguchi, M. Nagai, A Gray based decision making approach to the supplier selection problem, *Mathematical and Computer Modeling*, 46, (2007) 573-581

Liu Z, Cruz J M, Supply chain networks with corporate financial risks and trade credits under economic uncertainty. *International Journal of Production Economics*, 137 (2012) 55-67.

Liu T, Matsukawa H, *A review and classification on the supply chain risk management*, Information (Japan), 18 (2015) 2259-2274.

Samvedi A, Jain V, Chan F. T. S, Quantifying risks in a supply chain through integration of fuzzy AHP and fuzzy TOPSIS, *International Journal of Production Research*, Vol. 51(2013) 24332442.

Samvedi A, Vipul J, Felix T. C, Quantifying risks in a supply chain through integration of fuzzy AHP and fuzzy TOPSIS. *International Journal of Production Research* 51(8) (2013) 2433-2442.

Tang C. S, Perspectives in supply chain risk management, *International Journal of Production Economics*, 132 (2006) 451488.

Tummala R, Schoenherr T, Assessing and managing risks using the Supply Chain Risk Management Process (SCRMP), *Supply Chain Management : An International Journal*, 16 (2011), 474-483.

Wagner S. M, Bode C, An empirical investigation into supply chain vulnerability, *Journal of purchasing and supply management*, 12 (2006) 301-312.

Wang X, Chan H K, Yee R W, Diaz-Rainey I, A two-stage fuzzy-AHP model for risk assessment of implementing green initiatives in the fashion supply chain, *International Journal of Production Economics*, 135(2012) 595-606.

Chapter 3

Surface Hardness Improvement Techniques for Wind Turbine Gears

P. Sakthivel[1,*], PhD and R. Mani[2], PhD

[1]Department of Mechanical Engineering, Sri Krishna College of Technology, Coimbatore, Tamilnadu, India

[2]Department of Mechanical Engineering, KSR Institute of Engineering and Technology, Tiruchengode, Tamilnadu, India

Abstract

Wind energy is an eco-friendly and favoured energy source for power generation among various sources of energy. Today, wind energy is the fastest growing sector of renewable energy sources because the wind power plants work efficiently and economically when depended on for continuous and reliable operation. Today, the wind turbine plants are not working up to their complete lifetimes; they fail to achieve the desired life. The wind turbine parts, such as gears, bearings, mechanical brakes, and blades, are failing due to repetitive loads and sudden changes in climatic conditions. The gears, which are the main parts of the wind turbine that failed due to the pitting failure, may have occurred in the region of the gear tooth surface. To avoid this failure and ensure the reliable operation of the wind turbines, companies are offering surface solutions optimised for wind turbine components. Improved surfaces can be achieved by depositing thin coatings or by heat treating the steel components. To achieve accurate process control, the nitriding process parameters need to be modelled and controlled to meet the specifications.

Keywords: wind turbine, gear, pitting, surface coating

* Corresponding Author's Email: skt4design@gmail.com

In: The Future of Wind Energy
Editors: M. Dhurgadevi, P. Sakthivel and K. Gunasekaran
ISBN: 979-8-88697-232-0

Introduction

Wind turbine plants can be found in enormous landscapes or coastal areas. Most industrialised nations use this environmentally friendly technology for electrical energy generation to meet their energy needs. When compared to nuclear-generated energy, wind energy generation is more cost-effective where disposal, final storage, and risk factors are taken into consideration. During the 1980s, the first wind power plant farms were installed. Since then, the generation of wind energy has spread quickly in Germany and other countries. One million tonnes of steel are used every year for the production of wind turbines in Germany. This is three times more than in the ship building industry. As the world slowly turns away from nuclear power, wind energy becomes more important. Later in 2010, the power generated was 238,000 MW; in 2012, the world-wide installed power was 282,587 MW. By 2015, it had increased to 460,000 MW. Hence, power generation increases by 15% every year. China is the biggest producer of wind energy, which, jointly with the USA and Germany, produces about 60% of the worldwide installed capacity. With approximately 15%, Denmark is at the next highest level, with 28% of energy production, followed by Spain and Portugal.

The wind power plant requirements are very diverse and are affected by differences in local and meteorological conditions. In the case of offshore plants, corrosion due to salt and dampness will result in the failure of the power plant. Re-powering will play a major role due to the increase in size and performance of wind turbine plants. Repowering replaces older plants with newer, higher performance power plants. In addition to minimising down-times, performance and efficiency are to be taken by the wind power plants. They have to withstand enormous and often changing forces from external influences. The drive train of a wind power plant is subjected to high loads and stresses. Simultaneously, this makes them susceptible to higher maintenance and repairs. In particular, downtime caused by drive train and gearbox damage is high. To maximise plant profitability, downtime and maintenance work have to be minimized. The general causes of wind power plant failures are wear and component fatigue, such as on gearwheels, which lead to long downtimes.

The materials used in gear box construction have to withstand enormous stresses, diverse forces, high impact momentum and torsion. The main purpose of the gearboxes is to change the speed of rotation and torque. To achieve high efficiency, slow rotor rotational speeds in the range of 6–20 rpm can be transformed into high speeds in the range of 900–2000 rpm. The

approximate transmission capacity of modern wind energy power plants is 144 million rotations of the rotor shaft or 15 billion rotations of the generator shaft. For guaranteeing a high and reliable performance level, steel is used, which has enormous wear and fatigue strength. The material must have high toughness and vibration strength to resist the strong stresses. The gear flanks are very much protected against wear and pitting, and so the flanks are designed in such a way to withstand wear and fatigue from high frictional forces. High surface pressure is exerted on the gear tooth when engaged, and plastic deformation has to be prevented on the ductile outer zone.

Literature Survey

A literature survey has been done on various methods of surface coating techniques and is presented in this section.

Gas nitriding is one of the techniques that are thermo-chemical surface treatments in which nitrogen is transferred from an ammonia atmosphere into the surface of steel at temperatures within the ferrite and carbide phase region. (Pye D., 2003; Somers & Marcel A. J., 2000). After nitriding, a compound layer and an underlying diffusion zone are formed near the surface of the steel.

Next is plasma nitriding, which uses plasma-discharge technology at a lower temperature to introduce nascent nitrogen onto the steel surface. It is another well-established surface hardening process in steel (Baldwin et al., 1998), and is also known as ion nitriding. In this method, plasma is formed by high-voltage electrical energy in a vacuum. Nitrogen ions are accelerated to impinge on the work piece, which is connected as a cathode. The ion bombardment heats the work piece, cleans the surface and provides the nascent nitrogen for diffusion into the steel material (J. R. Davis, 2002).

Wind turbine gearboxes are designed to survive in extreme environmental conditions, most notably high wind forces, desert heat, and arctic cold. Regardless of how strong the design and materials are, the typical gearbox fails to meet its design life (Wallace (Jack) Titus and AFC-Holcroft, 2010). Statistical studies by the National Renewable Energy Laboratory have shown that, on average, a gearbox's time to repair can be as short as five years, give or take, when the economic payback model requires 20 years. Other preliminary studies indicate that the gearbox and/or planetary carrier systems are subjected to higher-than-anticipated stresses and that the materials used may not have the strength to resist the stresses encountered. Historically, pit furnaces and the pit quench have been employed to case harden these and other

large gears because, for treat, there just has been no other choice. In addition, pit furnaces can be energy hogs, especially when carburizing cycles of 35 hours or longer are common.

In the next paper, a study of pulsed nitriding in AISI H13 tool steel is carried out at a low temperature (400°C) for several durations. Despite the low temperature, the author proposed that x-ray diffraction reveals a nitrogen-enriched compound (Fe2-3N, iron nitride) that forms on the surface within the first hour of the process (L. F. Zagonela et al., 2012). The result shows that the material hardness increases linearly with the concentration of nitrogen, reaching up to 14.5 GPa at the surface while the Young Modulus remains unaffected. Nitrogen profiles show a case depth of about 43 μm after nine hours of the nitriding process. From these results, it is clear that pulsed plasma nitriding is highly efficient even at low temperatures.

In the next survey, a low-alloy steel AISI 4340 (Sule Yildiz Sirin et al., 2008) was investigated by the author under different process parameters, including time and temperature. The result shows that the ion nitriding process improves the fatigue strength and fatigue limit. Up to a 91% improvement in fatigue strength has been attained with this surface treatment. The author found that the subsurface 'fish eye' type formation is the most suitable fatigue crack initiation mechanism.

Actually, the life time of wind turbines is designed for around 20 years, but existing gearboxes experience failure only after 5 years of operation (Adam M. Ragheb and Magdi Ragheb, 2010). Wind turbine profits are influenced by factors such as the cost of replacing the gearbox and the length of downtime. For example, replacing a simple gearbox on a 1.5 MW wind turbine may cost the operator well over $250,000. A gearbox replacement costs about 10% of the wind turbine's construction and installation cost, which affects the estimated income from a wind turbine.

Gear Material Selection and Gear Failures

Power transmission gears are manufactured from a wide variety of steels and cast iron. In all categories of gears, materials can be chosen only after careful consideration of the performance demanded by the application end-use and total manufactured cost. Key design considerations require an analysis of the type of applied load, whether gradual or instantaneous, and also the mechanical properties like bending fatigue strength or wear resistance, which will define core strength and heat-treating requirements. The process of gear

manufacturing involves the collection of raw materials and the manufacturing of gears. The reasons for hard machining are from different sources shown in Figure 1. Each area in the gear tooth profile sees different service demands. Major issues like tooth bending and contact stress, resistance to scoring and wear, and fatigue are given more consideration during forces that will act on the gear teeth.

Good surface hardness and high residual compressive stress are desired to improve endurance or bending fatigue life. A combination of high hardness and adequate subsurface strength is necessary to prevent the spalling effect and handle contract stress and wear.

Material selection properties include tensile, yield, and impact strength, as well as elongation properties. Repairing or replacing a failed wind turbine gearbox is an extremely expensive undertaking. Gearbox failures can be caused by fundamental design issues, manufacturing defects, lubricant system failures, high loading or many other reasons. A correct failure mode diagnosis is the first step in identifying the actions that can be taken to avoid additional failures. Five of the most common gear and bearing failure modes, along with tips on identification and potential means of prevention, are provided below.

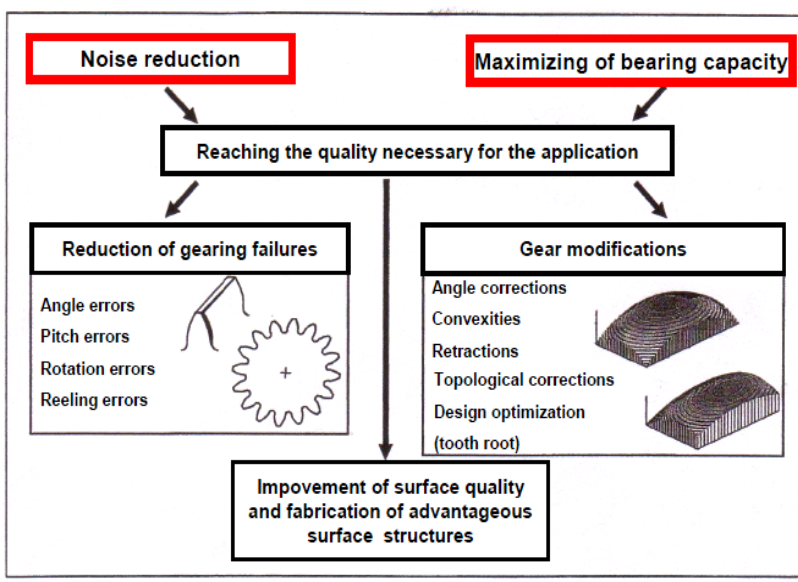

Figure 1. Reasons for hard machining.

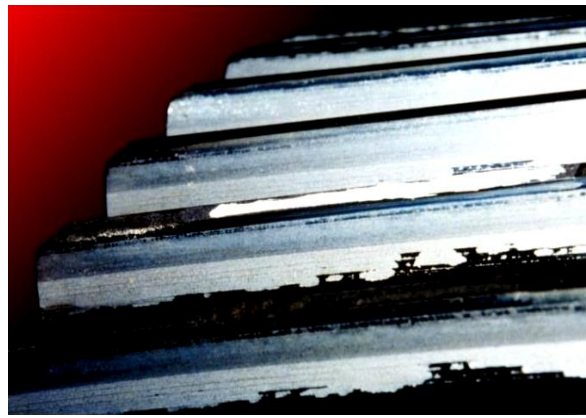

Figure 2. Micro pitting.

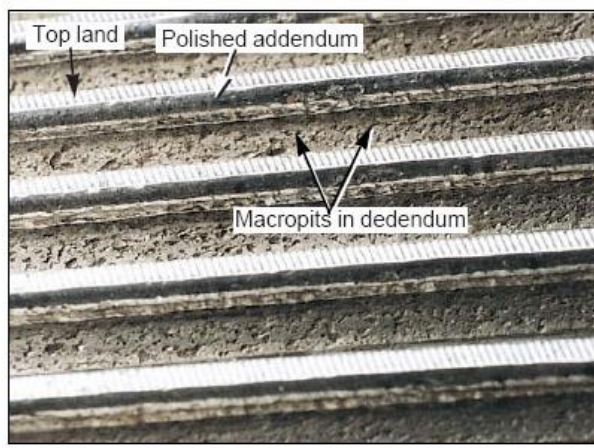

Figure 3. Macro pitting.

Micro Pitting

Micro pitting is a form of localised material surface damage that occurs under rolling and sliding contact operating in the boundary lubrication region. Micro pitting can affect both gears and bearings. Failures due to micro pitting are very common in wind turbine gearboxes. Micro pitting results in a matte finish surface in affected areas, as seen in Figure 2. Changing the type of lubricant and reducing component surface roughness are two methods for preventing micro pitting failures.

Macro Pitting

Macro pitting occurs when the contact stress in the gear or bearing exceeds the fatigue strength of the material, which is shown in Figure 3. It can affect both gears and bearings. Wind turbine gears and bearings are typically designed for a 20-year service life, and macro pitting that occurs before the end of the design life is an indication that one or more design assumptions, such as contact stress, material properties, lubricant condition, or applied load, were not met. Beach marks due to the presence of corrosion and lubricant in the crack are sometimes present and indicate a fatigue progression process. Macro pitting failures can be prevented by reducing loads, improving gear/bearing profiles to reduce stress, increasing material strength through alloy selection or a heat treatment process.

Bending Fatigue

Bending fatigue occurs when the stress exceeds the capability of the gear material at the root of the gear tooth. This is due to excessive loads, incorrect heat treatment, inclusions in the steel or a cut in the root of the tooth. Fracture surface appearance will vary depending on whether the failure was high or low cycle fatigue. Features such as ratchet marks are occasionally present and indicate multiple crack origins. This failure can be prevented by increasing gear material strength, decreasing load, and optimising the gear root fillet geometry.

Fretting Corrosion

Fretting corrosion can affect gears and bearings. It occurs when two contacting surfaces have small oscillating relative motions with no lubricant film between the surfaces. It occurs in wind turbine gearboxes due to transportation or spending time with no rotation. This type of corrosion can be identified by the presence of ruts along the lines of contact, along with the presence of reddish brown or black wear debris. This can be prevented by minimising the amount of time that a gearbox spends without rotating or by improving transportation conditions, depending on the cause of the fretting corrosion.

Axial Cracking

Axial cracking occurs in bearings always on the bearing inner ring. The cracks developed in the axial direction, perpendicular to the direction of rolling. Axial crack failures are most likely to occur in through-hardened bearings. This type of failure can be prevented by using case-carburized bearings, applying a black oxide coating, ensuring that the appropriate amount of retained austenite is present, and ensuring the correct level of interference fit exists between the bearing inner ring and the shaft on which it is mounted. Case-core separation, plastic deformation, scuffing, polishing, adhesion, abrasion, sub-case fatigue, erosion, electric discharge, cavitation, corrosion, are some additional forms of cracking. Whatever may be the type of failure mode, proper and prompt identification is needed to prevent a reoccurrence of any gearbox failure.

Methodology

Sulzer Metco Company has already established surface coating techniques for braking devices, valve parts, hydraulic components, and gears. The coating technique depends on the service demands. Thin film coatings are deposited by Physical Vapor Deposition or Plasma-Assisted Chemical Vapor Deposition. For heat treatment processes like case hardening and carburizing, nitriding is used. The following methods are generally used for surface coating techniques:

Case Hardening

The method of case hardening is used to generate high hardness in the outer zone and toughness, as well as an elastic core at the same time. Drive shafts require a ductile outer zone and a tougher core due to high torsion and impact loads. Case hardened gears and drive shafts are to fulfil the required surface hardness, hardness of the outer zone and ductility with a tough core. The shaft and gear withstand wear and the specific high pressures required for wind turbine applications. Case hardening takes place at a high temperature of 950°C to 1050°C, such that the carburizing and tempering processes can cause deformation. Regular carburizing depth ranges are between 0.1 and 4.0 mm. Based on the high case hardness, the post-deformation of teeth is not a

problem, although the post-treatment may lead to reduced case hardness. Shafts and large gears have to be aligned after the case hardening process. The range of hardness values for case hardened steels after hardening is 45-64 HRC.

Nitriding

The nitriding process (shown in Figure 4) is a heat treatment that diffuses nitrogen atoms into the surface of a metal to create a case-hardened surface. It is largely used on steel, but it is also on titanium, aluminum, and molybdenum. Usual applications include gears, die-casting tools, crankshafts, camshafts, forging dies, cam followers, valve parts, extruder screws, extrusion dies, injectors, and plastic-mold tools. The processes are named after the medium used to donate. The three main methods used are: gas nitriding, salt bath nitriding, and plasma nitriding.

Figure 4. Nitriding Process.

Gas Nitriding

The gas nitriding process is shown in Figure 5. The main donor is a nitrogen-rich gas, generally ammonia (NH3). It is sometimes known as ammonia nitriding. When ammonia comes into contact with the heated work piece, it disassociates into nitrogen and hydrogen. The nitrogen atom then diffuses onto the surface of the substance, creating a nitride layer. This process has been around for a while, but only recently have efforts been made to investigate its

thermodynamics and kinetics. Researchers are doing this to accurately control the process. The thickness and phase constitution can be selected for the nitriding layers (shown in Figure 6) and the process optimised for the particular properties. The temperature range for the gas nitriding process is 480°C–650°C.

Figure 5. Gas Nitriding.

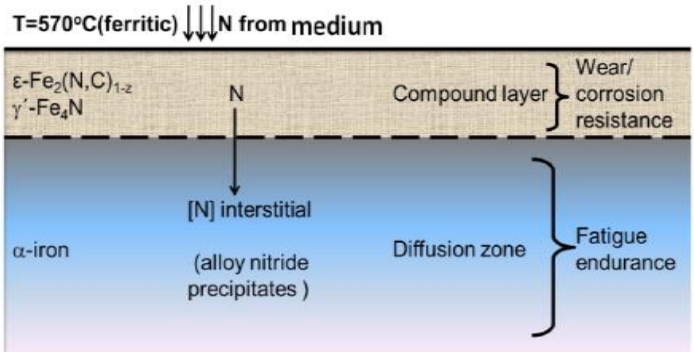

Figure 6. Diffusion zone of Nitrided iron.

Salt Bath Nitriding

In this process, the nitrogen-donating medium is a nitrogen-containing salt such as cyanide salt. Salts are also used to donate carbon to the work piece surface during the salt bath process. Nitrocarburizing temperatures range between 550 and 590 degrees Celsius.

Plasma Nitriding

Plasma nitriding is preferable for an industrial surface hardening process for metallic materials. In this technique, strong electric fields are used to produce ionised molecules of the gas around the surface to be nitrided. Such a highly active gas with ionised molecules is called plasma. Usually, pure nitrogen gas is used for the plasma nitriding process.

Generally, steels are surface treated with plasma nitriding. The advantage of plasma nitriding is related to the close control of the nitrided microstructure, which allows nitriding with compound layer formation. During the process, the performance of metal parts is improved, and the working lifespan is also boosted. For instance, mechanical properties of austenitic stainless steel like wear can be significantly reduced and the hardness of tool steels can be doubled on the surface. A plasma nitrided part is usually ready for use, and it does not require machining, polishing, or any other post-nitriding processes. So the process is user-friendly, saves energy and causes little or no distortion.

Plasma nitriding can be done at temperatures ranging from 260°C to over 600°C. Stainless steel can be nitrided to maintain the corrosion resistance properties at moderate temperatures without the formation of chromium nitride precipitates.

Carburizing

Carburizing (shown in Figure 7.) is a type of heat treatment process to produce a surface which is wear resistant while preserving the value of toughness and strength of the core. Carburizing increases the strength and wear resistance by diffusing carbon into the surface of the steel. This treatment is suitable for after machining with low carbon steel parts, as well as high alloy steel bearings, gears, and other components. Usually, the temperature at which the carburising and carbonitriding processes take place is 815°–1010°C. Most of the carburizing process is done by a fit furnace or sealed atmosphere furnace for heating the components. Gas carburizing allows for accurate control of both the process temperature and the carburizing atmosphere. The carbon potential of the gas can be lowered to allow diffusion, avoiding surplus carbon in the surface layer.

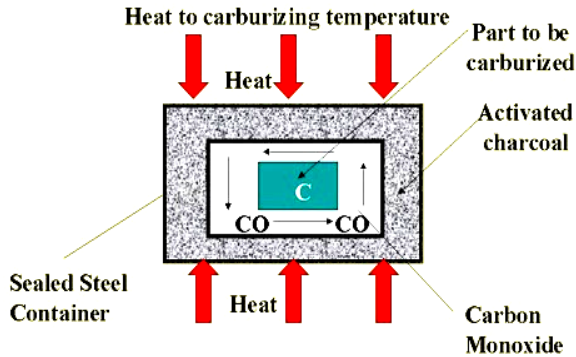

Figure 7. Carburising Process.

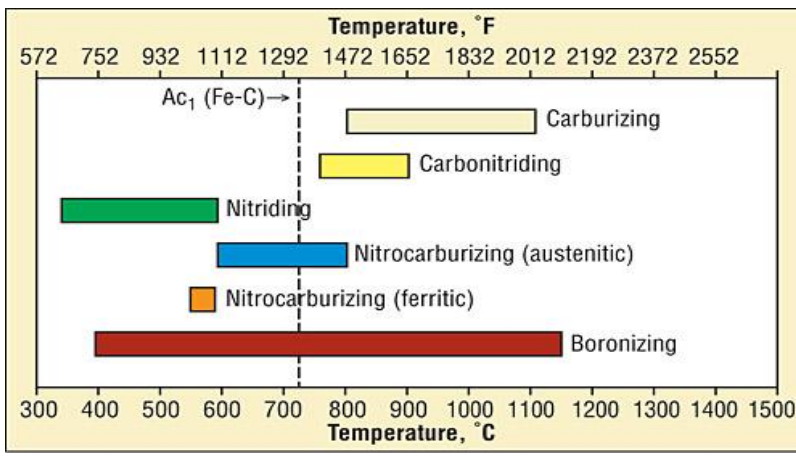

Figure 8. Oxide layer and diffusion zone.

After carburizing, the work is slowly cooled for later quench hardening or quenched directly into oil. A quench selection is made to attain the optimum properties with the proper levels of dimensional change. In some cases, the product is tempered, then cryogenically processed to convert retained austenite to martensite, and then retempered.

Carbonitriding

The gas carbonitriding process is just like carburizing, except a small amount of nitrogen is added at a slightly lower temperature to the atmosphere. As a

result, the case depth and, therefore, the capability of load carrying is not as high as with the carburizing process, but the dimensional control and wear resistance are often better. The carbonitriding process can be performed on unalloyed steels; other types of machined parts to make strong and wear-resistant parts can be produced economically.

Nitro Carburizing

The nitrocarburizing process is slightly varied when compared with the other processes. During the nitrogen carburizing diffusion process, nitrogen, carbon, and oxygen atoms diffuse into the steel surface, forming a compound layer and diffusion layer at the surface. The operating temperature for the gas nitriding/nitrocarburising process is 482°–650°C. The aim of the process is to provide anti-wear resistance on the surface layer and to improve the fatigue and corrosion resistance on the material surface. Nitrocarburizing can be applied to the same materials as those surfaces coated by nitriding, as well as unalloyed materials, where good quality wear resistance and improved fatigue resistance can be produced at a low cost.

Conclusion

There are numerous methods available for the surface coating of wind turbine gear. But the selection of the right method for surface treatment processes along with control of process and equipment variables is essential. According to the findings, surface-coated gear offers effective protection against Gray spotting and pitting. The increase in pitting resistance through the surface coating is 27%. Generally, the life of an uncoated gear is 1.35X106, but after the surface coating, the expected life of the gears is 5.4X107 cycles.

Disclaimer

None.

References

Baldwin, M. P. F. M. J, Haydon, S. C, Kumar, S, Collins, G. A, Short, K. T, and Tendys, J, "*Surface Coating Technology*," pp:1187-1191, 1998.

Davis, J. R, "Surface Hardening of Steels-Understanding the Basics," *Davis & Associates*, 2002.

Gebeshuber, Andreas and Ralph Trigueros, "*Plasma Nitriding - Especially in the Gear Industry*," Rübig GmbH & Co KG, Austria.

Lei, M. K, Zhang, Z. L, "Vacuum, Surfaces, and Films," *Journal of Vacuum Science & Technology*, Vol. 15 pp: 421, 1997.

Long, H, Al-Tubi, I. S, Martinze, M. T. M, "Analytical and Experimental Study of Gear Surface Micropitting due to Variable Loading," *Applied Mechanics and Materials* Vol. 750, pp: 96-103, 2015.

Menthe, E, Rie, K. T, Schultze, J. W and Simson, S, "*Surface and Coatings Technology*," Vol. 74-75, pp: 412-416, 1995.

Pye, D, "Practical Nitriding and Ferritic Nitrocarburising," *Materials Park*, ASM International, 2003.

Ragheb, Adam M. and Magdi Ragheb, "*Wind Turbine Gearbox Technologies, Fundamental and Advanced Topics in Wind Power*," www.intechopen.com, pp:189-206.

Renevier, N, Collignon, P, Michel, H, and Czerwiec, T, "*Surface and Coatings Technology*," Vol. 111, pp: 128-133, 1999.

Sheng, Shuangwen (Shawn), "Wind Turbine Gearbox Failure Modes – A Brief," *National Renewable Energy Laboratory, ASME/STLE 2011 International Joint Tribology Conference*, October 24-26, 2011.

Sheng, Shuangwen, "Wind Turbine Micropitting - Technical Report," *National Renewable Energy Laboratory* (NREL/TP-500-46572), February 2010.

Somers, Marcel, A. J, "Thermodynamics, Kinetics and Micro Structural Evolution of the Compound Layer; A Comparison of the states of Knowledge of Nitriding and Nitrocarburizing," *Heat Treatment of Metals*, Vol. 2000. 4, pp:92-102, 2000.

Sule Yildiz Sirin, Kahraman Sirin, Erdinc Kaluc, "*Effect of the Ion Nitriding Surface Hardening Process on Fatigue Behavior of AISI 4340 Steel*," Elsevier, Materials Characterization, Vol. 59, pp: 351 – 358, 2008.

Sun, Y and Bell, T, "*Materials Science and Engineering*," Vol. 140, pp: 419-434, 1991.

Wallace (Jack) Titus, AFC-Holcroft, "Improving Heat Treating Flexibility for Wind Turbine Gear Systems through Carburizing, Quenching and Material Handling Alternatives," *American Gear Manufacturers Association (AGMA) Technical Paper*, ISBN: 978-1-55589-9776, October 2010.

Yang, Mei, "*Nitriding - Fundamentals, Modeling and Process Optimization*," Thesis, April 2012.

Zagonela, L. F, Bettini. J, Basso, R. L. O, Paredez. P, Pinto. H, Lepienski, C. M, Alvarez, F, "Nanosized Precipitates in H13 Tool Steel Low Temperature Plasma Nitriding," *Surface and Coatings Technology*, 2012.

Chapter 4

Comparison of Artificial Neural Network Techniques in Prediction of Wind Speed Using Combinations of Metrological Variables

S. Sivakumar[1], W. Rajan Babu[2], A. Ravikumar[3], S. Sam Karthik[4], L. Krishna Kumar[5] and R. Senthilkumar[1,6,*]

[1]Department of Computer Science and Engineering, Nehru Institute of Engineering and Technology, Coimbatore, Tamilnadu, India
[2]Department of Electrical and Electroincs Engineering Sri Eshwar College of Engineering, Coimbatore, Tamilnadu, India
[3]Department of Computer Science and Engineering, Sridevi Women's Engineering College, Hyderabad, India
[4]Department of Electrical and Electroincs Engineering, Dhanalakshmi Srinivasan College of Engineering, Coimbatore, Tamilnadu, India
[5]Anna University, Chennai, Tamilnadu, India
[6]Department of Computer Science and Engineering, Nehru Institute of Engineering and Technology, Coimbatore, Tamilnadu, India

Abstract

In this study, wind speed is predicted using Feed Forward Neural Networks with a Backpropagation Algorithm (FFNNBA) and Generalized Regression Neural Network (GRNN) in 60 cities in India. The input variables used in this analysis are longitude, latitude, air temperature, elevation, relative humidity, cooling degree-days, heating degree-days, daily solar radiation-horizontal, earth temperature, and

* Corresponding Author's Email: sentinfophd@gmail.com

In: The Future of Wind Energy
Editors: M. Dhurgadevi, P. Sakthivel and K. Gunasekaran
ISBN: 979-8-88697-232-0

atmospheric pressure. The Mean Square Error (MSE) of the two models is compared, and GRNN gives better results than FFNNBA. The accuracy of FFNNBA and GRNN is 98.07% and 96.05% for the training phase and 98.97% and 96.54% for the testing phase, respectively.

Keywords: feed forward neural networks with back propagation algorithm, generalized regression neural network, artificial neural network, mean square error, and wind speed prediction

Introduction

Wind energy is one of the most abundant and easily available sources of energy. Adoring this fact, responsibility should be raised to obtain maximum usage. India is in the second position in terms of population. (A. K. Yadav, Hasmat Malik, and S. S. Chaudhry, 2015). The population explosion panics with the demand for energy utilization. Most of the sources for meeting this demand are non-renewable and are on the verge of extinction. There are many renewable sources that can be utilized for generating energy. Among the available resources, wind energy is surplus and can be used very efficiently. The most common method used for electricity generation from wind is by using wind turbines. To install the wind farm in any particular area, the wind speed prediction in that area must be accurate. The wind is uncontrollable and has properties of randomness. Due to this, it is difficult to predict the wind speed correctly (A. K. Yadav, Hasmat Malik, and S. S. Chandel, 2014). Many models have been developed for the prediction of wind speed. The most commonly used model is the Artificial Neural Network (ANN). For various subjects like wind energy assessments, including pattern recognition, approximation, and time-series prediction, raised to obtain maximum usage. India is in the second position in terms of population. (A. K. Yadav, Hasmat Malik, and S. S. Chaudhry, 2015). The population explosion panics with the demand for energy utilization. In this study, we have developed two models using FFNNBA and GRNN. Then these two models are compared to find out which one gives a better result. There are several models developed for the prediction of wind speed. The most commonly used model is the Artificial Neutral Network (ANN). In this paper we have developed two models using FFNNBA and GRNN. Then these two models are compared to find out which one gives a better result.

Methodology

In this section, the dataset used for this study is described along with a brief introduction of FFNNBA, GRNN, and the implementation of the GRNN for predicting the long-term wind speed.

Database Collection

The selected 24 cities of India are used for training the GRNN model; 15 cities of Tamilnadu are used for testing; and 15 cities of Tamilnadu are used for prediction (Chow S. K. H., Lee E. W. M., Li D. H. W.). The training, testing, and predicted values of selected cities are shown in Table 1. Monthly data samples of these locations are collected from a publicly available online dataset from NASA (D. F. Specht). Using this data for long-term wind speed prediction is done. The variables which are used as input are longitude, latitude, air temperature, elevation, relative humidity, cooling degree–days, heating degree–days, daily solar radiation–horizontal, earth temperature, and atmospheric pressure. The average monthly values for a year using these variables are recorded.

Table 1. Datasets

Data sets of 25 Locations of India are used for training											
S.No	City	Lat (Deg)	Long (Deg)	S.No	City	Lat (Deg)	Long (Deg)	S.No	City	Lat (Deg)	Long (Deg)
1	Patna	25.61	85.13	9	Panjim	15.49	73.81	17	Chennai	13.08	80.27
2	Kolkata	22.39	88.27	10	New Delhi	28.35	77.12	18	Vishakhapatnam	17.43	83.14
3	Bangalore	12.57	77.38	11	Jaipur	26.92	75.82	19	Hyderabad	17.36	78.48
4	Ahmedabad	23.04	72.38	12	Srinagar	34.08	74.79	20	Mumbai	19.07	72.51
5	Dehradun	30.16	78.02	13	Jodhpur	26.18	73.01	21	Nagpur	21.09	79.07
6	Thiruvanthapuram	08.05	76.90	14	Varanasi	25.45	82.85	22	Pune	18.52	73.84
7.	Hamirpur	31.68	76.52	15	Bhopal	23.25	77.42	23	Bhavnagar	21.77	72.15
8.	Minicoy	8.28	73.03	16	Shilong	25.34	91.53	24	Port Blair	11.61	92.72
Data sets of 15 cities are used for Testing Purpose											
1	Kanchipuram	12.87	79.87	6	Dharmapuri	12.09	78.20	11	Nagapattinam	10.76	79.84
2	Cuddalore	11.74	79.77	7	Erode	11.34	77.71	12	Tiruvarur	10.77	79.63
3	Villupuram	11.95	79.29	8	Coimbatore	11.01	76.95	13	Tiruchirappalli	10.79	78.70
4	Vellore	12.91	79.13	9	The Nilgiris	11.49	76.73	14	Karur	10.88	78.15
5	Tiruvannamalai	12.22	79.07	10	Madurai	9.95	78.11	15	Pudukkottai	10.37	78.82
Data sets of 15 cities are used for Prediction Purpose											
1	Thanjavur	10.78	79.13	6	Tirunelveli	8.71	77.75	11	Perubalur	11.24	78.86
2	Ramnad	9.37	78.83	7	Thoothukkudi	8.76	78.13	12	Salem	11.66	78.14
3	Theni	10.01	77.47	8	Kanniyakumari	8.08	77.53	13	Sivagangai	9.97	78.56
4	Namakkal	11.21	78.16	9	Krishnagiri	12.51	78.21	14	Tirunelveli	8.71	77.75
5	Virudhu nagar	9.56	77.96	10	Ariyalur	11.23	79.29	15	Thoothukkudi	8.76	78.13

Artificial Neural Network (ANN) Models

An artificial neural network (ANN) is primarily designed to model the internal operational features of the human brain and nervous system. ANN models can be used for various applications, including pattern recognition, pattern classification, nonlinear mapping, and general computer simulation. There are different types of ANN models for a problem depending on various parameters such as the complexity of the function, the architecture, the training algorithm, and the number of training cases (A. K. Yadav, Hasmat Malik, and S. S. Chandel, 1991). Among the various types of ANNs, we chose the FFNNBA and GRNN models.

Generalized Regression Neural Network (GRNN) Models

GRNN is normally used for function approximation. It is a learning algorithm with an extremely parallel structure. The main purpose of this algorithm is to acquire the perfect mapping between the input vector and the target vector with minimum error (Dowell J., Weiss S., Hill D., Infield D., 2014). The general regression neural network (GRNN) was suggested by Donald F. Specht, with the theoretical basis of nonlinear regression analysis as shown in Figure 1. The GRNN consists of four components:

The input layer: the original variables enter the network, which resembles the neurons one by one, and are submitted to the next layer.

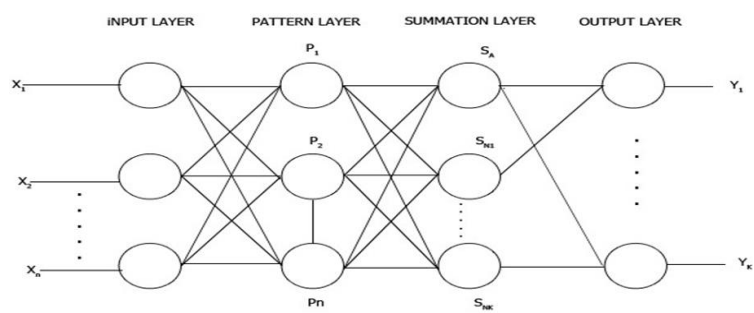

Figure 1. The Structure of the Generalized Regression Neural Network (GRNN).

The pattern layer consists of two things: A nonlinear transformation is applied to the values obtained from the input layer. The transfer function of the ith neuron in the pattern layer is:

$$P_i = \exp[-(X - X_i)^T (X - X_i)/2\sigma^2]\ i = 1,2,..n \quad (1)$$

where X represents the input variable, Xi is the learning sample corresponding to the ith neuron, and σ is the smoothing parameter.

The summation layer calculates the sum and weighted sum of the pattern outputs. The summation layer has two types of neurons, in which one neuron SA makes an arithmetic summation of the output of all pattern layer neurons, and the weight of each neuron in the pattern layer to this neuron is 1. Its transfer function is:

$$\mathrm{S_A} = \sum_{\mathrm{i=1}}^{\mathrm{n}} \mathrm{P_i} \quad (2)$$

The outputs of all neurons in the pattern layer were weighted and summed to gain the other neurons' SNj in the summation layer. The transfer function of the other neurons in the summation layer is:

$$S_{Nj} = \sum_{i=1}^{n} y_{ij} P_i\ j = 1,2,3 \ldots., k, \quad (3)$$

where y_ij is the connection weight between the i^{th} neuron in the pattern layer and the j^{th} neuron in the summation layer. y_ij is the jth element in the ith output sample y_i. The output layer is where the forecasting results can be derived. The output of each neuron is:

$$y_j = \frac{S_{Nj}}{S_A}\ j = 1,2, ...,\mathrm{k} \quad (4)$$

where y_i is the output of the jth neuron.

Feed Forward Neural Networks with Backpropagation Algorithm (FFNNBA)

The input vector of independent variables pi is related to the target ti (wind prediction) using the architecture depicted in Figure 2. This figure shows one of the frequently used networks, namely, the layered feed-forward neural network with one hidden layer. In this place, every single neuron is connected to those of the previous layer through adaptable synaptic weights. Knowledge is generally stored as a set of connection weights. Training is the process of making changes to the network using a learning mode in which an input is

supplied to the network along with the desired output, and then the weights are adjusted so that the network attempts to produce the desired output. The weights after training contain significant information, whereas before training they are random and have no meaning.

The architecture of the network examined in the study was such that $p_i' = (p_{i1,}p_{i2,\ldots,}p_{10})$ p_10) contained values for 10 input independent variables from distinct i.

The input variables are associated with each of the N neurons in a hidden layer by using the specifications specified for each independent variable (j) to neuron (k) connection. The mapping has two forms for the relationship between output t and independent variables:

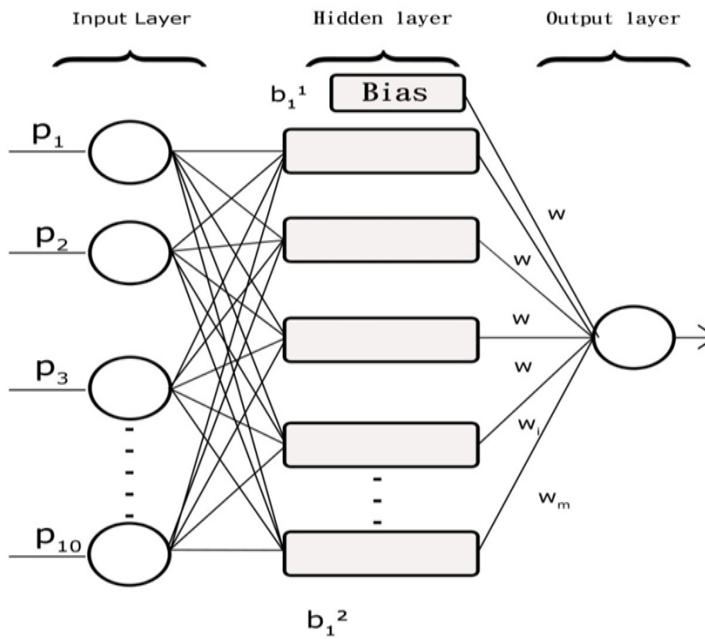

Figure 2. The architecture of an artificial neural network.

$$Hidden\ layer\ n_k^{(1)} = \sum_{j=1}^{R} w_{kj}^{(1)} p_j + b_k^{(1)}; a_k^1 = f_{level-one}\left(n_k^{(1)}\right) \quad (5)$$

$$output\ layer\ n_k^{(2)} = \sum_{j-1} w_k^{(2,1)} a_k^1 + b_1^{(2)}; \widehat{t_\iota} = a_k^{(2)} = f_{level-two}\left(n_k^{(2)}\right) \quad (6)$$

In the case of N neurons in the neural network, the biases are $b_1^{(1)}, b_2^{(1)} \ldots\ldots b_N^{(1)}$. Prior to activation, the input value for neuron k is $b_k^{(1)} + \sum_{j=1}^{10} w_{kj} p_j$. An activation function f(.) (linear or nonlinear) is then applied to the input in each neuron and gathered as $\sum_{ki=1}^{N} w_k' f_k\left(b_k^{(1)} + \sum_{j=1}^{10} w_{kj} p_j\right) + b^{(2)}$ where $w_k (k = 1,2, \ldots, N)$ are $b_{(1)}$and$b_{(2)}$) bias parameters in the hidden and output layers. At the end of the process, this activated total quantity is carried out again with function g(.) as $g\left[\sum_{K=1}^{N} w_k' f_k(.) + b^{(2)}\right] = f_k\left(n_k^{(2)}\right)$, which then becomes the estimated target variable (Wind prediction) value of ti in the training data set, or

$$\hat{t}_i = g\left\{\sum_{k=1}^{N} w_k' f\left(\sum_{j=1}^{R} w_{kj} p_j + b_k^{(1)}\right) + b^{(2)}\right\}; j = 1,2, \ldots..R \; k = 1,2, \ldots., N \quad (7)$$

In this study, 70% of the organized data set was used for the training set, and the rest (30%) of the data set was used for the test set.

1 fhidden layer (.) = linear (.) and foutput layer (.) = linear (.)

2 fhidden layer = Tangent sigmoid (.) and foutput layer = linear (.)

In this study, 70% of the organized data set was used for the training set and the rest (30%) of the data set was used for the test set.

Implementation of GRNN and FFNN

First, data from 60 Indian cities, monthly data samples of these cities are collected from a publically available online dataset from NASA. Then this data is divided into training, testing, and prediction. The selected 24 cities are used for training the GRNN model; 15 cities are used for testing the model, and the remaining 15 cities are used for prediction. The input variables used in this analysis are longitude and latitude, air temperature, elevation, relative humidity, cooling degree-days, heating degree-days, daily solar radiation-horizontal, earth temperature, and atmospheric pressure. The training data contains 250 samples of 10 variables, the testing data contains 210 samples of 10 variables, and 200 samples of 10 variables are used for prediction.

Wind speed is used as the target. After preparing the data, the code for GRNN After preparing the data, the code for GRNN is implanted, and then the code is processed. The proposed algorithm for this model is shown in Figure 3.

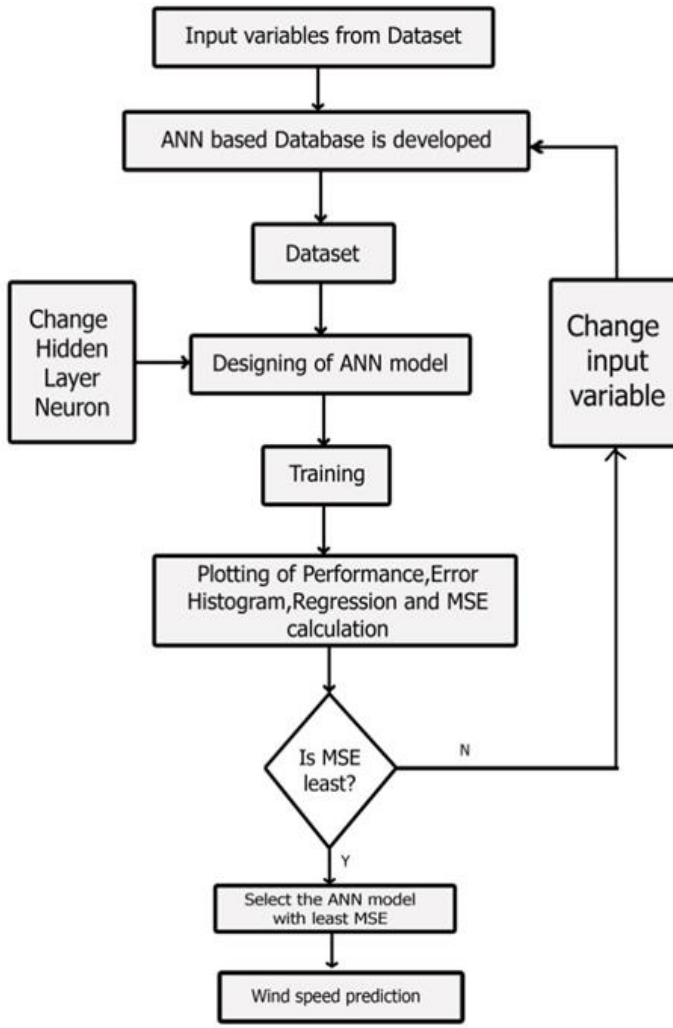

Figure 3. Proposed feed forward neural networks with back propagation algorithm.

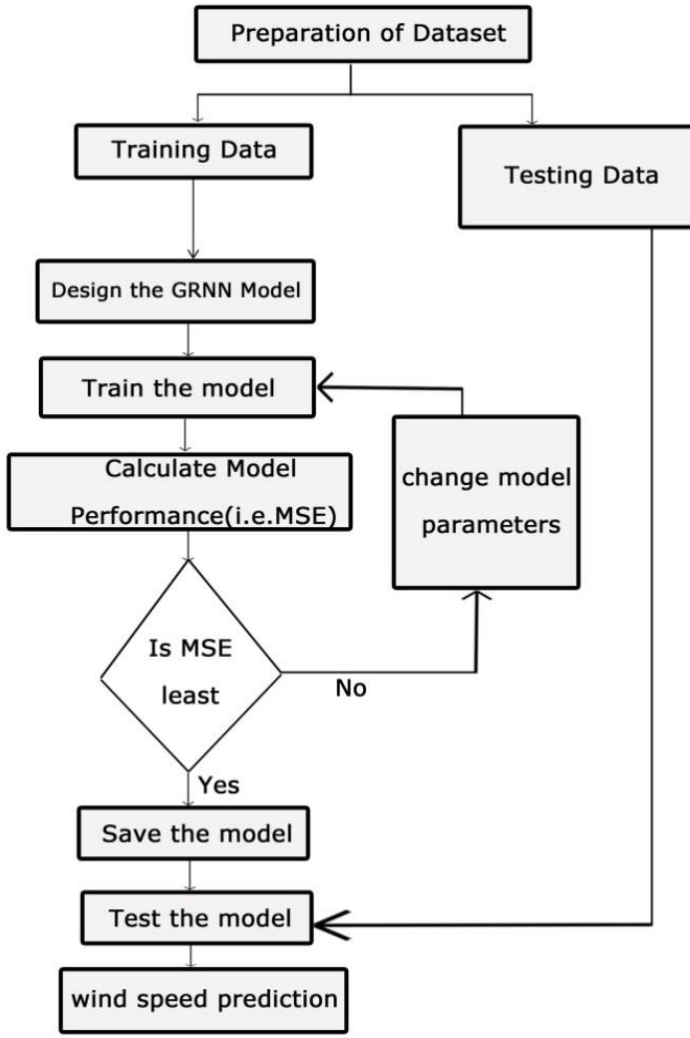

Figure 4. Proposed generalized regression neural network algorithm.

The FFNN with the backpropagation model was developed using the ANN fitting tool (D. F. Specht, 2001). The variables used are the same as in GRNN. The input and target data are entered and randomly divided into 70%, 15%, and 15%, which are used in training, testing, and validation respectively, resulting in an ANN-based model. After that, the network is trained by changing the hidden layer of neurons. The number of neurons in the hidden

layer is calculated by Eq. (Murat Kayri, 2015). The algorithm which is derived is shown in Figure 3.

$$h = \frac{i+o}{2} + \sqrt{s} \tag{8}$$

where s and h are the total number of data samples and the number of neurons in the hidden layer, o and I represent the output and input variables, respectively.

GRNN is used due to some drawbacks of the FFNN model. Some of the drawbacks are that the model has to be run again and again for the different numbers of neurons and has low prediction accuracy. The GRNN model does not have these drawbacks, which is why it is used to develop the model.

Results and Discussion

Wind Speed Prediction Using FFNNBPA

The results of the FFNNBPA-based model are shown in Figure 5. The regression plots for training, testing, validation, and overall are shown in Figure 5(a) to Figure 5(d). The performance plot of the FFNNBPA model is shown in Figure 5(e). This is a plot of the Mean Square Error and the number of epochs. From this plot, it is found that with the increase in epochs, the MSE is decreasing. The validation set error and test set error to have comparable characteristics at epoch 19. The error histogram is shown in Figure 7.

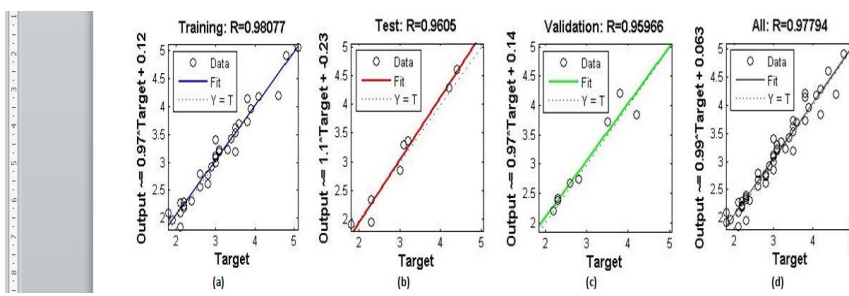

Figure 5. Graphical Results of FFNNBA (a) Regression plot for training, (b) Regression plot for testing, (c) Regression for validation (d) over all Regression plot for ANN model.

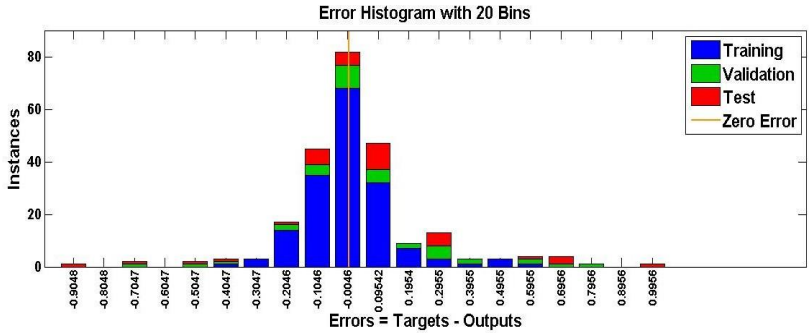

Figure 6. Error histogram plot for FFNNBA.

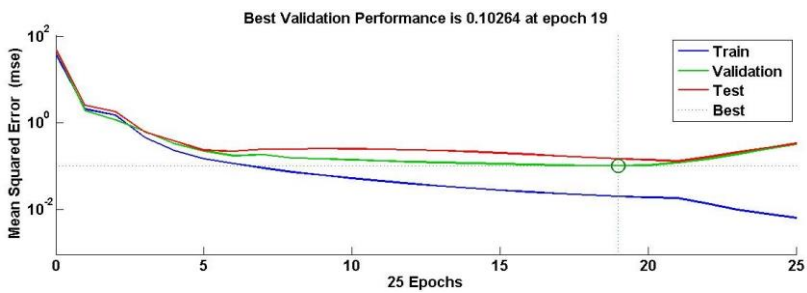

Figure 7. Performance plot for FFNNBA.

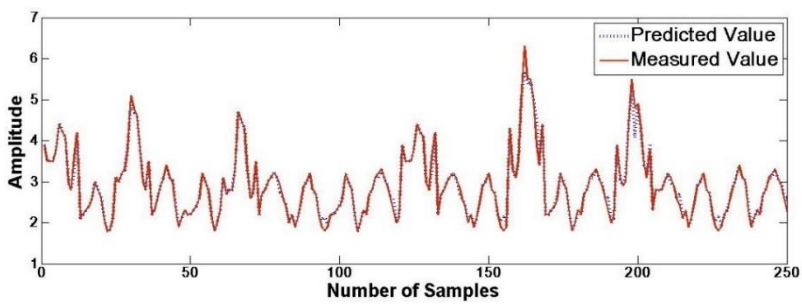

Figure 8. Comparison between the measured and predicted values of predicted cities.

It provides authentication for the model. It is a plot of instance versus error values. Table 2 shows the performance of the FFNNBPA model for the training and testing phases. The measured and predicted values of the wind speed for some cities in Tamilnadu are shown in the table. Figure 8 shows the comparison between the measured and predicted values of the predicted cities.

Wind Speed Prediction Using GRNN

Figure 9(a) shows the graphical results for the GRNN model during the training phase, and Figure 9(b) shows the results during the testing phase. The regression plot for training and testing is shown. The accuracy for the training is 98.97% and the testing is 96.54%. The model output and the target plot are shown in Figure 9(d). Figure 9(d) shows the comparison between the measured and predicted values of the predicted cities.

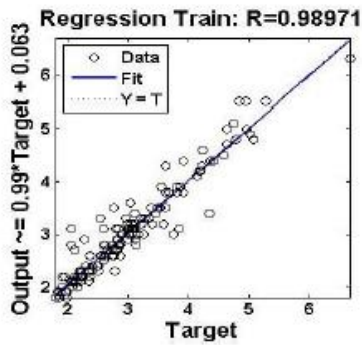

(a) Regression plot of training phase

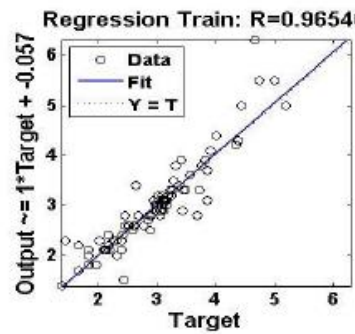

b) Regression plot of testing phase

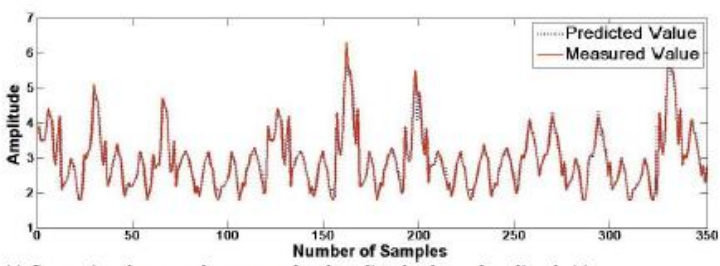

(c) Comparison between the measured and predicted values of predicted cities.

Figure 9. Training and testing phase results of GRNN.

Result Comparison of FFNNBA and GRNN Model

In this paper, two models are developed using the FFNNBA and GRNN techniques. On comparing these two models, it is found that GRNN gives better results than FFNNBA, as shown in Table 2. By analyzing Table 2 and Figure 5 to Figure 10, we conclude that GRNN gives comparable results to

FFNNBA. Therefore, GRNN can be used to predict the wind speed at a new location. The comparison of the measured and predicted values of wind speed for both models is shown in Figure 10. The wind speed of some cities in Tamilnadu, India has been predicted by using both models and compared with the measured values obtained from NASA and is shown in Table 3.

Table 2. Result comparison

Model	Training Phase Results			Testing Phase Results		
	MSE	RMSE	Accuracy (%)	MSE	RMSE	Accuracy (%)
GRNN	0.0117	0.1073	98.971	0.0394	0.1874	96.05
FFNNBA	0.0391	0.1987	98.07	0.0392	0.1894	95.4

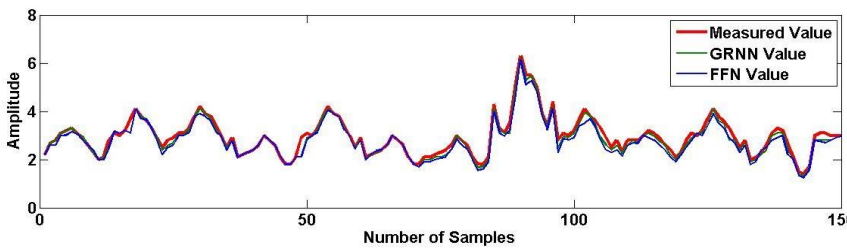

Figure 10. GRNN and FFNBA model result comparison with measured value.

Table 3. Predicted values of wind speed using GRNN and FFN models

Cities	Model	Jan	Feb	Mar	Apr	May	Jun	July	Aug	Sep	Oct	Nov	Dec
Thanjavur	Measu	2.2	2.7	2.8	3.1	3.2	3.3	3.1	2.9	2.6	2.3	2.1	2.1
	GRNN	2.1747	2.6689	2.6664	3.0643	3.0473	3.2620	3.0643	2.8666	2.4756	2.2735	2.0758	2.0758
	FFNN	2.0950	2.5712	2.6664	2.9521	3.0473	3.1425	2.9521	2.7616	2.4756	2.1902	1.9998	1.9998
Ramnad	Measu	2.8	3.1	3	3.2	3.7	4.1	3.8	3.6	3.3	2.9	2.5	2.8
	GRNN	2.6664	3.0643	2.9655	3.0473	3.6574	3.904	3.7574	3.558	3.2620	2.8666	2.4712	2.6664
	FFNN	2.6664	2.9521	2.8569	3.0473	3.5235	3.904	3.6235	3.4282	3.1425	2.7616	2.3807	2.6664
Theni	Measu	2.9	3.1	3.1	3.3	3.8	4.2	3.9	3.8	3.4	3	2.5	2.9
	GRNN	2.8666	3.0643	3.0643	3.2620	3.7574	4.1517	3.71	3.7574	3.3609	2.9655	2.4712	2.8666
	FFNN	2.7616	2.9521	2.9521	3.1425	3.6235	3.999	3.71	3.6235	3.2378	2.8569	2.3807	2.7616
Namakkal	Measu	2.1	2.2	2.3	2.4	2.6	3	2.8	2.6	2.1	1.8	1.8	2.1
	GRNN	2.0758	2.1747	2.2735	2.3724	2.4756	2.9655	2.6664	2.4756	2.0758	1.7804	1.7804	2.0758
	FFNN	1.9998	2.0950	2.1902	2.2855	2.4756	2.8569	2.6664	2.4756	1.9998	1.7189	1.7189	1.9998
Viru.nagar	Measu	2.9	3.1	3.1	3.3	3.8	4.2	3.9	3.8	3.4	3	2.5	2.9
	GRNN	2.866	3.0643	3.0643	3.2620	3.7574	4.1517	3.8551	3.7574	3.3609	2.9655	2.4712	2.8666
	FFNN	2.7616	2.9521	2.9521	3.1425	3.6235	3.999	3.7139	3.6235	3.2378	2.8569	2.3807	2.7616
Perubalur	Measu	2.5	2.9	2.1	2.2	2.3	2.4	2.6	3	2.8	2.6	2.1	1.8
	GRNN	2.4712	2.8666	2.0758	2.1747	2.2735	2.3724	2.4756	2.9655	2.6664	2.4756	2.0758	1.7804
	FFNN	2.3807	2.7616	1.9998	2.0950	2.1902	2.2855	2.4756	2.8569	2.6664	2.4756	1.9998	1.7189
Salem	Measu	2.1	2.2	2.3	2.4	2.6	3	2.8	2.6	2.1	1.8	1.8	2.1
	GRNN	2.0758	2.1747	2.2735	2.3724	2.4756	2.9655	2.6664	2.4756	2.0758	1.7804	1.7804	2.0758
	FFNN	1.9998	2.0950	2.1902	2.2855	2.4756	2.8569	2.6664	2.4756	1.9998	1.7189	1.7189	1.9998

Measu = Measured.

Conclusion

In this paper, GRNN and FFNNBA-based neural network models are developed to predict long-term wind speed. The data sets for the training, testing and prediction phases of these two models are collected by NASA. The variables which are used as input variables for these models are longitude, latitude, air temperature, elevation, relative humidity, cooling degree–days, heating degree–days, daily solar radiation–horizontal, earth temperature, and atmospheric pressure. The wind speed prediction accuracy for FFNNBA is found to be 98.07% for training and 96.05% for testing, while GRNN is 98.97% for training and 96.54% for the testing phase of the model. In the comparison of these models, it is found that GRNN gives better results than FFNNBA. Therefore, GRNN can be used for the effective prediction of long-term wind speed.

Disclaimer

None.

References

Ayodele T. R. and Ogunjuyigbe A. S. O., "Prediction of wind speed for the estimation of wind turbine power output from site climatological data using artificial neural network," in *International Journal of Ambient Energy*, 2015.

Bilgili M., Besir Sahin and Abdulkadir Yasar, "Application of artificial neural networks for the wind speed prediction of target station using reference stations data" in *Renewable Energy* 2007, vol. 32, pp. 2350-2360.

Chow S. K. H., Lee E. W. M., Li D. H. W. Short-term, prediction of photovoltaic energy generation by intelligent approach. *Energy based* 55 :660-7.

Dowell J., Weiss S., Hill D., Infield D., "Short-term spatio-temporal prediction of wind speed and direction" *Wind Energy.* 2014;17(12) :1945-1955.

Kayri M. "Predictive Abilities of Bayesian Regularization and Levenberg-Marquardt Algorithms in Artificial Neural Networks : A Comparative Empirical Study on Social Data," *Mathematical and Computational Applications*. 2016.21.20; doi: https://doi.org/10.3390/mca 21020020.

Monfared M., Rastegar H., Kojabadi H. M., "A new strategy for wind speed forecasting using artificial intelligent methods," *Renewable Energy* 2009;34(3) :845-8.

Ramasamy P., Chandel S. S. and Amit Kumar Yadav, "Wind speed prediction in the mountainous region of India using an artificial neural network model," in *Renewable Energy* 2015, vol. 80, pp. 338-347. https://eosweb.larc.nasa.gov/sse/RETscreen/.

Sheela K. G., Deepa S., "Neural network-based hybrid computing model for wind speed prediction," *Neurocomputing*, 2013; 122 :425-9.

Specht D. F. "A general regression neural network," IEEE transactions on neural networks 1991; 2 :568-576. *MATLAB user's Guide.* The Mathworks, INC., NATICK, MA 01760, 1994-2001.

Varshney K., Poddar K., Prediction of wind properties in urban environments using artificial neural network. *Theoretical and Applied Climatology* 2012; 104 :322-9.

Yadav A. K., Hasmat Malik and Chandel S. S., "Application of rapid miner in ANN based prediction of solar radiation for assessment of solar energy resource potential of 76 sites in North western India," in *Renewable and Sustainable Energy Reviews* 2015, vol. 52, pp. 1093-1106.

Yadav A. K., Hasmat malik, Chandel S. S, Selection of most relevant input parameters using WEKA for artificial neural networks solar radiation, prediction models. *Renewable and sustainable energy reviews*, 2014, 31 :509-519.

Yadav A. K., Hasmat malik, Hhandel S. S., "Application of rapid miner in ANN based prediction of solar radiation for assessment of solar energy resource potential of 76 sites in northwestern india," *Renewable and sustainable energy reviews*, 2015, 52 :1093-1106.

Chapter 5

A Machine Learning Approach for Thermodynamic Analysis in Wind Turbine with Optimization

K. Gunasekaran[1, *], PhD, M. Dhurgadevi[3], PhD and Vimal Kumar[2]

[1]Department of Computer Science and Engineering, Sri Indhu College of Engineering and Technology, Telungana, India
[2]Department of Computer Science and Engineering, Mahendra Engineering College, Namakkal, Tamilnadu, India
[3]Department of Information Technology, Hindustan Institute of Technology, Coimbatore, India

Abstract

A wind turbine is a machine that converts the energy of the wind into other more useful forms, like mechanical energy. Water pumping wind turbines are generally referred to as wind turbines. Shrouded wind turbines are characterized by a higher mass flow rate of air passing through the turbine blades as compared to bare wind turbines. Thermoeconomic analysis of shrouded wind turbines considers different shroud area ratios and the speed range of the wind turbine. The significant intension of this work is to frame an Artificial Neural Network (ANN) with the assistance of optimization techniques. The ANN is utilized to predict the various thermoeconomic parameters of wind power generation based on wind speed and turbine surrounding area. Different optimization techniques such as Particle Swarm Optimization (PSO), Ant Colony Optimization (ACO), and Harmony Search (HS) algorithms are

* Corresponding Author's Email: drgunak@yahoo.com.

In: The Future of Wind Energy
Editors: M. Dhurgadevi, P. Sakthivel and K. Gunasekaran
ISBN: 979-8-88697-232-0

utilized to arrive at the optimal weight of the ANN process. All the optimum results demonstrate that the error values attained between the output of the experimental values and the predicted values are close to zero in the designed network. From the results, the minimum error of 85.72% is determined by ANN to attain the harmony search (HS) algorithm.

Keywords: wind turbine, speed, thermoeconomic parameters, area ratio, artificial neural network (ANN), harmony search (HS)

Introduction

At present, the wind turbines offer a huge radar signature on account of the turbine tower and also the rotating blades, which stimulate a Doppler spread which is dependent on the blade tip momentum, frequency, and aspect angle. (Alessio Balleri et al., 2013) In fact, the wind turbine has emerged as one of the best methods to extract power from the wind. Further, it is common knowledge that the power extracted from wind by a wind turbine is in direct proportion to the cube of velocity, with the effect that a trivial acceleration of the wind tends to pave the way for a huge enhancement in power extraction (Wen-Xue Wang et al., 2015).

In this regard, the innovative brands of wind turbines point to an inclination towards elevated power levels. Moreover, the added energy harvest capacity in view of the higher tower height and the larger blade diameter resulted in an incredible preliminary installation cost as well as the preservation expenses per unit (Venkata Yaramasu et al., 2014). Thus, it is evident that the actuator disk continues to be in its hey-days as it has been afforded a red-carpet welcome as a highly thriving and extensively employed brand for replicating the open and ducted wind turbine wakes.

Furthermore, there is a lot of excitement surrounding the comparison of open and ducted wind turbines in terms of realising an incredible increase in the power extracted by the rotor (Bontempo and Manna, 2014). Incidentally, the flow fields of a small wind turbine with a flanged diffuser illustrate the fact that the power coefficient of the shrouded wind turbine is approximately four times that of the bare wind turbine (Chen, Liao, and Cheng, 2012). Further, increasing attention has been evinced by many investigators throughout the cosmos to diffuser technology exploration, enthused by the significant improvement in the efficiency which the diffuser is competent to generate in

wind turbines, especially for minute systems (Deborah Aline et al., 2014). On account of the inconsistent wind flow in the urban area, certain wind turbines deploy stator vanes to further propel the efficiency to superior levels. The Sistan wind mill system, triggered by the drag force with added wing wall, top and bottom disk, significantly ushers in supreme overall efficiency of the turbine (Wong et al., 2014), which is likely to depend on certain contributing features like the generator efficiency, the ratio of the gear box system, and the height of the hub from the ground (Seyed Mehdi Mortazavi et al., 2015). In the case of a shrouded turbine, the turbine is enclosed in a shroud which goes on to step up the incoming wind, incredibly scaling up the mass and power available to the turbine (Aniket Aranake et al., 2015). The add-on of a diffuser shroud endowed with a brim has shown its mettle in enhancing the efficiency of a wind turbine by stepping up its output power.

Though there are three-phase generators (Huihui Sun and Yusaku Kyozuka, 2011) which are offered in the market for employment in wind turbines, the higher phase number generator seems to have an edge over them as a zooming technology as it glistens with glittering advantages which are not within the reach of the three-phase systems (Janarthanan et al., 2014). With the ever-zooming requirement for energy, the setting up of wind turbines has inched towards the deeper waters. Whereas the floating platforms acting as strong pillars for the wind turbines emerge as a preferred choice in deep waters (greater than 90 m), fixed platforms are capable of delivering the goods in the case of transition waters (30–90 m) (Abhinav and Nilanjan Saha, 2015). Several renovations to the deflecting plate concept have been initiated on the Savonius wind turbines, which have computationally standardised the geometry and position of a flat deflector for both the two-blade and three-blade Savonius turbines (Daegyoum Kim and Morteza Gharib, 2013). One of the major mechanisms for this is a blend of enhanced mass flow rate and decreased wake rotation downstream of the turbine.

With a diffuser-shrouded turbine, the mass flow rate of air through a turbine is enhanced because of the sub-atmospheric pressure at the diffuser exit plane (Buyung Kosasih and Andrea Tondelli, 2012). Thermo-economics, in essence, integrates the theories of thermodynamics and economics with an eye on furnishing functional data on cost-conscious energy renovation mechanisms that cannot be generally accomplished by means of traditional energy and economic modelling (Iman Janghorban Esfahani and Changkyoo Yoo, 2014). The thermo-economic technique is employed to allocate the cost of the entire procedure onto the internal streams by way of energy and non-energy. The stream-cost equations are organised in a matrix form and resolved

to evaluate the financial outlay of the process streams (Seyed Reza et al., 2011). In fact, the thermo-economic assessment is highly significant in studying the nature of the cycles thermodynamically and financially. The energy elimination and cost flow in the segments of the cycles can be tracked and comprehended by means of thermo-economic techniques (Rabi Karaali and Ilhan Tekin Oztürk, 2015). The comprehensive formulations for the energy, exergy, and exergy-economic evaluation for the plant segments and the whole tri-generation systems have been effectively developed.

The thermodynamic and exego-economic systems embrace the efficiency and performance parameter definitions and the cost assessment formulation according to the Specific Energy Cost (SPECO) technique (Ozgur Balli et al., 2010). The blend of thermodynamic performance and economic factors is shortlisted as the objective function. The thermo-economic optimization of the biomass-based integrated energy system employs the total cost rate of the system and the energy efficiency as objective functions (Yongqiang Feng et al., 2015).

Literature Review

In 2015, Goldstein (Leo Goldstein, 2015) made a name for himself by bringing to light an innovative wind turbine with a downwind rotor that was tilted upward. An external cable appended to the centre of force of the blades acts as a support for each rotor blade, and the tower is supported by guy wires at the top. The innovative wind turbine does not employ either a gearbox or a direct drive generator. The novel mechanism is structurally assessed and contrasted vis-a-vis a traditional wind turbine. The assessment reveals the fact that developing the novel technique may entail an outlay of around 2.5 times less than that required for a traditional wind turbine of the same power on land. The cost benefits tend to perk up in offshore scenarios as well.

In 2015, Fahad Al-Sulaiman et al. (Fahad Al-Sulaiman and Bekir Yilbas, 2015) fantastically proposed the thermo-economic evaluation of the shrouded wind turbines after integrating various area ratios of the shroud. It was established that the wind turbine efficiency scaled up depending on the enhancement in the shroud area ratio. Further, it was proved that the expenses were incredibly elevated by the low wind speed. In addition, the outcomes revealed that the energetic improvement potential escalated as the wind speed was stepped up, and it went up further at high shroud area ratio. The expenditure was minimum for an area ratio of 1.5 and maximum for 1.1 The

overheads of the energy lost were also evaluated, and it was found that the area ratio of 1.5 was the minimum energy cost, while that of 1.1 entailed the maximum energy cost, which was in harmony with the cost of the power generated.

In 2014, Jafari et al. were afforded a bouquet of applause for their novel proposal by which the Computational Fluid Dynamic (CFD) simulations of a miniature commercial wind turbine were performed with a simple frustum diffuser shrouding. The diffuser was modelled with various shapes with the intention of comprehending the impact of length and area ratio on the power expansion. This factor was greatly influenced by the diffuser area ratio. The outcomes of their investigation offered a technique to evaluate the effective frustum diffuser geometries for a miniature wind turbine. The results can be extended to any kind of wind turbine intended for the nominal wind speed.

In 2014, Canan Cimsit et al. had the conviction and courage to advocate the performance of comprehensive energy-based thermo-economic evaluations, thermo-economic assessment with exergo-economic variables, and thermo-economic optimization by employing the non-linear simplex direct search technique for the cascade refrigeration cycle. The exergetic effectiveness and the least cost of the objective function are decided as 7.30% and 4.05 ($/h) respectively for the optimum case of sample application. In comparison to the base case, the least cost of objective function is reduced by approximately 3.3%, whereas the coefficient of performance (COPcyclegen) and energetic efficiency of the cascade cycle have increased by approximately 7% and 3.1%, respectively.

In 2013, Chonga et al. were instrumental in launching a novel shrouded wind turbine mechanism studded with a multitude of prospective advantages over the traditional wind turbine. The incorporation of the PAGV into the 3-in-1 wind, solar, and rain water harvester on high-rise buildings is demonstrated. From the wind tunnel testing measurements where the wind turbine is in a free-running state, only the rotor inertia and bearing friction were initiated, and the wind rotor rotational speed (with the PAGV) was enhanced by 75.16%. By means of a semi-empirical technique, the power output increment of the rotor with the PAGV went up by 5.8 times at a wind speed of 3 m/s.

In 2013, Gandiglio et al. came up with a grandiose proposal, shelling out the thermodynamic and financial performance of the two plant configurations.

The exergy assessment has illustrated an augmented exergetic accomplishment for the pressurised cycle, which envisages components with superior efficiency and a resultant reduced rate of exergy damage (20% less than the atmospheric plant). The cheering outcomes have clearly proved that the pressurised plant has incredibly overwhelmed the atmospheric one, with an outlay (based on the exergo-economic base) of electricity of 47.7 $/MWh in place of 64.2 $/MWh. Taking into account the exergy and financial outcomes integrated in a meticulous thermo-economic analysis, the thermo-economic outlay of electricity was brought in and deployed to underscore the sterling overall performance of the pressurised plant, with a TCOE in the PSOFC plant 25% lower than in the atmospheric one.

Proposed Methodology

An artificial neural network structure is utilised to predict the thermoeconomic parameters with the various wind speeds and wind turbine surround area ratios. Thermoeconomic parameters, which are air mass flow rate, power of the wind, energy efficiency, energy loss, improvement potential, cost of power produced, and cost rate of energy loss of the wind power generation. From the above mentioned parameters, the ANN structure is generated with the input layer, hidden layer, and output layer of the structure. This is utilised to train and test the process. For the training process, 80% of the data is used in preliminary stage prediction with known input data values and during the testing process. The 20% of data used in validation for the ANN structure is based on the input constraints that predict the thermoeconomic parameters. In the input and hidden layer processes, the weights α and β are used in the ANN structure. For the better value produced in the ANN structure, optimise the weight of the structure. To optimise the weight of α and β various optimization techniques are utilised to arrive at the optimal weight of the structure. If the achieved results are not up to the level expected, then the training process is repeated again to adapt the structure to the appropriate level necessary to predict the output. Once the attained error values between the output of the experimental values and the predicted values are close to zero, the designed model is utilised for predicting the unknown values in the input and minimising the time interval of the process. The ANN structure with the Harmony Search (HS) optimization process is shown below in pseudo code.

Pseudo Code for the Proposed Method

Step 1: Structure initialization
{
Initialize the input ($I_i ; i = 1,2$)
Initialize the input layer weight {
$\alpha_i ; i = 1,.....n \; and \quad -10 \le \alpha \le 10$ }
Initialize the hidden layer weight {
$\beta_{ij} ; j = 1,2..20 \; and \quad -10 \le \beta \le 10$
Number of hidden layer ($H_l = 1$)
Number of output layer ($O_l = 1$)
}
Step 2: Input layer (L_l)
Basic function computation (B_f)
Step 3: Hidden layer H_l
For optimizing weight ($\alpha_i \; and \quad \beta_{ij}$) by using HS algorithm
Step 4: HS algorithm
{
Initialize the weights (α_i , β_{ij})
Fitness computation (F_i) $for(W_i)$
Based on fitness update the New Harmony solution
Initialize the Harmony Memory (HM)
Improvise a New Harmony memory
Find the fitness for the New Harmony solution ($F_{i(new)}$)
}
Step 5: Store the best behavior of the solution so for ined
Stop until optimal solution ($F_{optimal}$) ined
Iteration=Iteration+1
Step 6: Output layer
Obtain the basics function of the output layer (O_i)
Step 7: Find the error value (E_i)

An Artificial Neural Network

The artificial neural system is an adapted computational model that aims to copy the neural structure and workings of the human cerebrum. It contains an interconnected structure of misleadingly delivered neurons where capacity is used as a pathway for information exchange. With every different inner or outer boost, artificial neural systems are adjustable and flexible, learning and conforming. Artificial neural systems are employed as a part of the arrangement, for example, gratitude frameworks, information handling, mechanical technology, and demonstrating. The information sets are classed out by the framework for knowing the base sneak past misusing the weights α and β, which are altered with the end goal of deciding the motions of the input stipulations. Designed for improving weights α and β diverse improvement systems are utilised to optimise the weights of some algorithms, which are Harmony Search (HS), Particle Swarm Optimization (PSO), and Ant Colony Optimization (ACO). These are adequately used to land at the perfect weights

of the target capacity, which is given by the contrast between the test and gauge values.

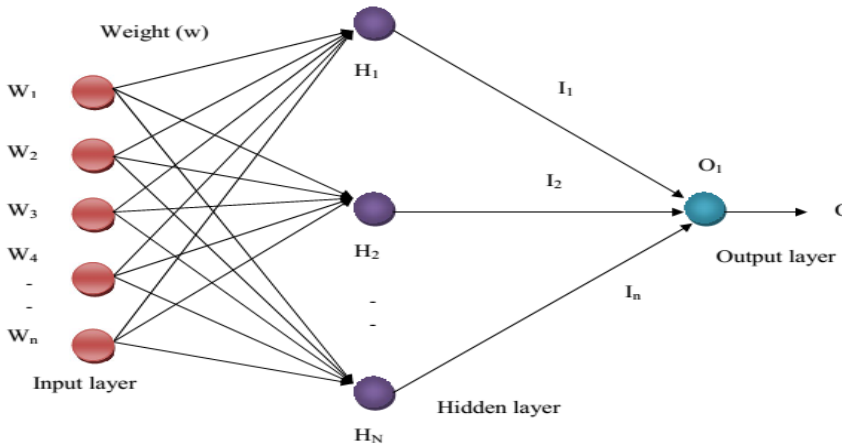

Figure 1. Neural network structure.

In Figure 1, the important structural planning of the artificial neural system is pointed out. It has a multi-layer neural system that consists of three layers, for instance, the input layer, concealed layer, and output layer. Neural networks carry out these functions together and in parallel by the units, rather than there being an obvious delineation of subtasks to which different units are allocated. The term "neural network" frequently refers to models used in statistics, cognitive psychology, and artificial intelligence. Neural network models that follow the central nervous system are part of theoretical neuroscience and computational neuroscience. In this methodology, the necessary ANN structure, the shrouded layer is 1, and the unseen neuron is 1 to 20.

The mathematical result of ANN equation includes F_i that is an input layer parameter; O_i is an output layer parameter.

Structure Initialization

In the initialization process, three inputs, which are based on the input layer weight and the hidden layer weight, are initialized. Input parameters considered are wind speed and different area ratios.

Input Layer

The input layer contains a number of neurons. All input layer neurons are connected to the hidden layer. It has four inputs i_1, i2….i_n and the input neurons possess a weight W_1, W_2….W_n, which is represented as the ith input layer neuron connected with the jth neuron of the hidden layer. Like the input layer basic function equation, which is defined as equation 1 where L is a basic function of hidden neurons, l is the number of hidden units, β is the weight of the input layer neuron, N is the number of data, and W is the input value. In these value-based calculations, the basics function

$$L_f = \sum_{j=1}^{N} W_i \times \beta_{ij} \tag{1}$$

Where Li is a basic function, b_{ij} is an input layer weight, and i is a number of input W_{i1}= wind speed and W_{i2} = Area ratio.

Hidden Layer

The hidden layer contains a number of neurons which are named as $h_1, h_2, ...h_n$, the hidden layers are connected with the output layer by using the neurons. Weight obtaining equation is α_i where L_i is the number of input layers, and the weight α_i and β_{ij} based obtains the activation function. The ANN is usually based on several optimizations of the weights. In this arithmetic demonstration, the harmony search (HS) optimization strategy is observed to achieve the optimal weight.

The Harmony Search (HS) Algorithm

The Harmony Search was inspired by the improvisation of jazz musicians. Specifically, the process by which the musicians (who have never played together before) rapidly refine their individual improvisation through variation, resulting in an aesthetic harmony.

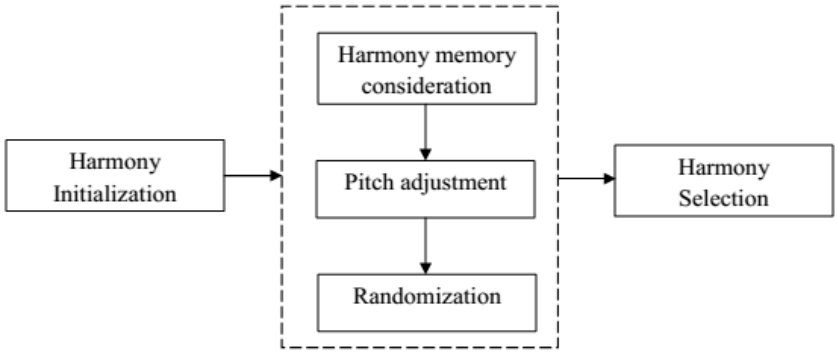

Figure 2. Harmony search process.

Initialization of Solution and Algorithm Parameters

Initialize the input parameters such as weight α and β which is defined as the α_i , β_i , is an initial solution, and i is a number of solutions, and also initialise the parameters such as step. This process is known as the "initialisation process."

$$I_i = (W_{oj}, W_{1j} \ldots W_n)$$

Where, I_i defines an initial solution, i ε [1, 2 … 10] and jε [1, 2 … 140]. Since the ith value represents the number of solutions and the jth value represents the length of the solution.

The HS algorithm parameters are also specified in this step. These parameters are

- Harmony Memory Size (HMS) or the number of solution vectors in the harmony memory;
- Harmony Memory Considering Rate (HMCR), HMCR;
- Pitch Adjusting Rate (PAR);

$$W_i = \left[\begin{array}{l} (No\ \ of\ \ hidden\ \ neuron * No\ \ of\ \ input\ \ data) + \\ \\ No\ \ of\ \ hidden\ \ neuron \end{array} \right] \tag{2}$$

where Total input = 2; Hidden neuron = 20.

Based on equation (2), the attained solution length is 140 and the solution range lies between $-10 \le I_{ij} \le 10$ according to the initial solution-based output as thermoeconomic parameters.

Fitness Function

Evaluate the fitness value of each harmony solution by using this equation (3) and then calculate the best solution values.

$$F_i = \sum_{j=1}^{h} \alpha_j * \left(\frac{1}{1+\exp(-\sum_{i=1}^{N} W_i \beta_{ij})} \right) \tag{3}$$

Where, Fi is a fitness function α and β are weights, is the input parameters, is the number of inputs; j is the number of weights, and h is the number of hidden neurons. This equation is based on the fitness value of the process.

The new solutions for the process of updating the new harmony memory are based on the following process.

Initialize the Harmony Memory (HM)

In this step, the HM matrix is filled with as many randomly generated solution vectors as the HMS.

$$HM = \begin{bmatrix} W_1^1 & W_2^1 & ..... & W_n^1 \\ W_1^2 & W_2^2 & ..... & W_n^2 \\ & & & \\ W_1^{HMS} & W_2^{HMS} & ..... & W_n^{HMS} \end{bmatrix}$$

Improvise a New Harmony

A new harmony vector is generated based on three rules such as memory consideration, pitch adjustment, and random selection. Generating a new harmony is called improvisation. In the memory consideration, the value of the first decision variable for the new vector is chosen from any of the values

in the specified HM $(W_1^1 - W_1^{HMS})$ range. HM is similar to the step where the musician uses memory to generate a tune. The values of the other decision variables are chosen in the same manner. The $HMCR \in [0,1]$ is the rate of choosing one value from the historical values stored in the HM, while $(1 - HMCR)$ is the rate of randomly selecting the value from the possible range of values.

$$W_i^{'} = \begin{cases} W_i^{'} \in \{W_i^1, W_i^2 .... W_i^{HMS} \ with \quad probability \quad HMCR \\ \quad W_i^{'} \in W \quad with \quad probability \quad (1 - HMCR) \end{cases} \tag{4}$$

For example, a HMCR of 0.90 indicates that the HS algorithm will choose the decision variable value from historically stored values in the HM with a 90% probability or from the entire possible range with a (100–90%) probability. Every component obtained by the memory consideration is examined to determine whether it should be pitch-adjusted or not. This operation uses the $PAR \in [0,1]$ parameter, which is the rate of pitch adjustment, as follows:

The value of (1-PAR) sets the rate of doing nothing. If the pitch adjustment decision for is YES, is replaced as follows:

Where, is an arbitrary distance bandwidth, which is a random number between 0 and 1.

Update Harmony Memory

For each new value of harmony, the value of the objective function is calculated. If the new harmony vector is better than the worst harmony in the HM, the new harmony is included in the HM and the existing worst harmony is excluded from the HM.

Optimal Solution

Based on the abovementioned process, the optimal weights and also optimal fitness are attained, which is defined as this optimal fitness based on the output. The optimal values are based on predicting the output, which is air mass flow rate, power of the wind, energy efficiency, energy loss, improvement potential, cost of power produced, and cost rate of energy loss.

Output Layer

The output layer has a number of neurons. The neurons in the hidden layer are connected with the output layer by the neurons. Each connection has a weighted value, such as $\alpha_1, \alpha_2, \ldots\ldots \alpha_n$. The basis function of the output units is expressed by the equation is O_l .

$$O_l = \sum_{i=1}^{n} \alpha_i \, \sigma(F_{i(optimal)}) \tag{5}$$

The calculation of the error value and weights ranges from -50 to 50, I represents the input parameters, i represents the number of inputs, j represents the number of weights, and h represents the number of hidden neurons.

$$E_i = \sqrt{\frac{\sum_{i=1}^{ND} (D_i - P_i)^2}{ND}} \tag{6}$$

Where ND is the number of the data, D is the desired value, and P is the predicted value, i = 1, 2,..., n. By using this formula, the error value is calculated from the difference between the desired value and the predicted value.

Results and Discussion

The results are taken on the working platform of MATLAB 2014 with the system configuration, i5 processors with 4GB RAM using the ANN process. Wind turbine considerable parameters like wind speed and area ratio with the output parameters like air mass flow rate, power of the wind, energy efficiency, energy loss, improvement potential, cost of power produced and cost rate of energy loss are obtained by utilising the artificial neural network (ANN). For developing the optimal artificial intelligence network with the HS algorithm, optimising the fascinating function of finding the optimal solutions of α and β is elegantly performed. Subsequently, the optimal solutions for the weight with input constraints are arrived at with the assistance of the amazing HS process. The major objective of the ANN is to forecast the output like a

real-time experiment to minimise the error. In other words, the differential error between real-time output and the attained output from ANN is found to be near to zero. As a result, the related output is evaluated by utilising the thermoeconomic parameters.

Convergence Graph

The graphs shown below successfully show the wind power generation parameters fitness graphs based on iteration of the HS, PSO, and ACO by altering the weights in the range of -500 to 500, and thus the error values are determined. The error graph is drawn with the iteration symbolised on the X-axis and fitness on the Y-axis.

Figure 3 illustrates the convergence graph for thermoeconomic parameters for wind generation with the fitness values. The graph basically resolves the harmony search (HS) procedure, which presents the minimum fitness in a maximum iteration. From the graph, the minimum wind power generation that is achieved in the HS technique is 0.04 in the 44th iteration. The minimum error of the proposed work compared to other optimizations is 72.3%. The wind power generation parameter, which is based on speed and area ratio, shows that the predicted values are almost equal to the experimental values. The HS process compared to the ACO error difference is 72.3% and the PSO is 70.23%. The harmony search optimization approach obviously specifies the ideal fitness value with competent results.

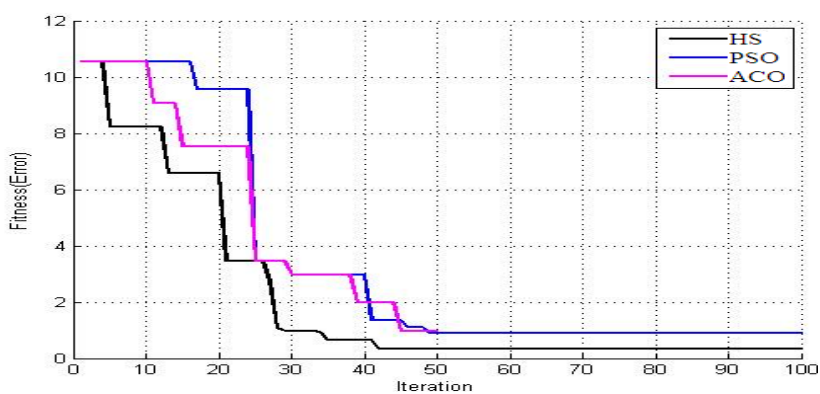

Figure 3. Convergence graph.

The Error Values of Output Parameters in Different Algorithms

In this section, the number of testing data is varied and an error value is calculated for some input data like wind speed and area ratio, based on the predicted wind power generation parameters. The parameters such as air mass flow rate, power of the wind, energy efficiency, energy loss, improvement potential, and cost of power produced and cost rate of energy loss are determined. The predicted results are shown below.

Figure 4 shows the thermodynamic parameters for the different techniques with error values. Figure (4a) shows that the air mass flow rate error values for the different algorithms are similar. The minimum error value for this parameter is 3.51 for HS, and this value compared to the ACO, the error value is 91.70, and the PSO is 201.3. In PSO, the maximum error value of the initial testing data is 210.27 and the HS is 1.13. The behaviour of the air mass flow rate graph is initially minimised and maximised according to the value based on the testing inputs. Figure (4b) shows that the power produced in wind power generation of the proposed technique is compared to the ACO where the error difference is 90.4% and the PSO is 85.5. In the initial testing data, the error value is 176.4, 230.83 in the HS process. This technique contrasts with the other two algorithms by 11.56%, and the Figure (4c) also shows the energy efficiency for the testing data where the error is set at 2.5 for the initial data in all algorithms, and the error will be decreased and then again increased. The energy efficiency error value of all the testing data is 0.017 for HS, 0.27 for ACO, and 1.56 for the PSO process.

Figure (4d) shows that the energy minimum error value is 0.19 for HS, 0.27 for ACO, and 1.56 for PSO. The next figure (4e) shows the potential error value for the optimization technique. The minimum error value is 0.107 in HS. This technique is compared to ACO and the difference is 91.45% and the PSO difference is 91.07%. The predicted value of the wind power produced is shown in Figure (4f). The minimum error value of testing data is 0.6 in ACO and similar values for the other techniques. Then the energy loss values are shown in Figure (4g), where the minimum error value is 0.19 in HS. All the testing data minimum error value is compared to other techniques and the difference is 5.63%. In all the theromodyamic parameters, the minimum error value is attained in HS technology.

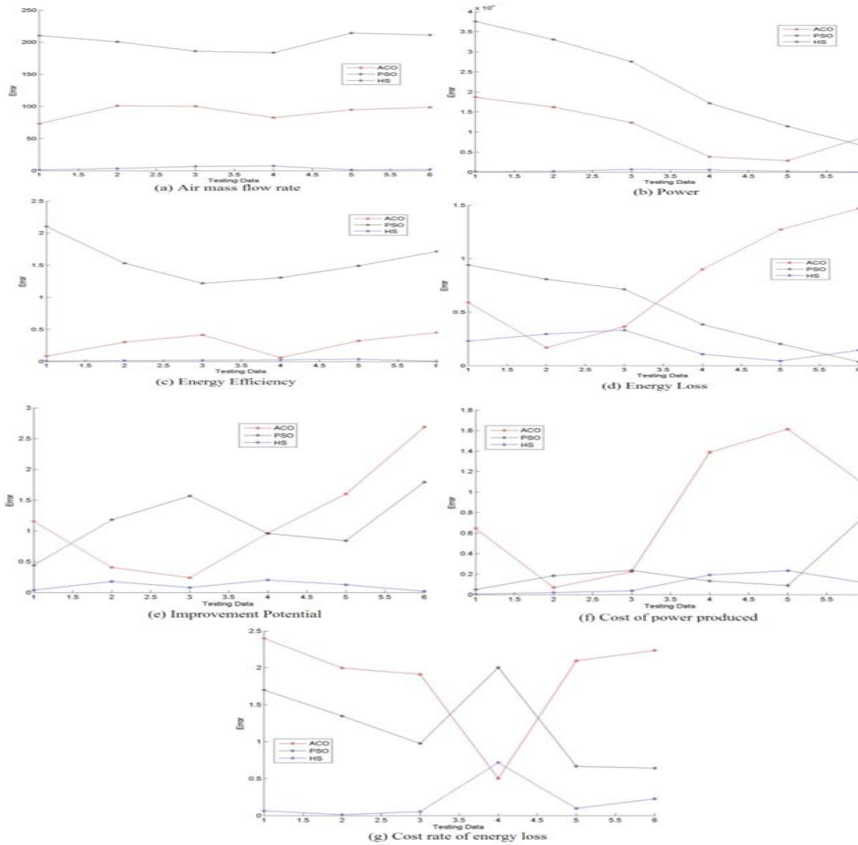

Figure 4. Error graph for testing data.

Experimental Results and Predicted Values for the Proposed Method

Using the neural network process, the testing results and original values for the wind power generation and thermodynamic parameters are shown in the Table 1.

Table 1 displays the actual and predicted values of the proposed method, in which the wind speed and the surrounded area ratio are calculated using the thermodynamic parameter. For the first testing data, the actual value of the air mass flow rate is 130 and the nearby value that occurs in the HS technique is 128.8. The optimum weights with the minimum error value of thermodynamic parameters are attained in the HS approach.

Table 1. Original value and Predicted values for testing data

Input		Output													
Wind Speed	Area Ratio	Air mass flow rate		Power		Energy efficiency		Energy loss ratio		Improvement potential		Cost of power produced		Cost of energy loss	
		Actual value	HS	Actual value	HS	Actual value	HS	Actual value	HS	Actual value	HS	Actual value	HS	Actual value	HS
7	1.3	130	128.86	500	676.44	0.28	0.284	0.68	0.41	0.7	0.75	0.6	0.58	1.9	1.949
8	1.3	140	43.0	2000	2230.9	0.45	0.443	0.59	0.29	1.5	1.39	0.3	0.31	1.8	1.708
9	1.3	170	163	4500	3842.2	0.55	0.543	0.45	0.15	1.65	1.53	0.16	0.16	1.6	1.68
11	1.5	245	237	10000	10578.1	0.69	0.711	0.3	0.16	2.6	2.89	0.11	0.30	2.75	2.033
12	1.3	220	221	13000	12749.4	0.71	0.678	0.23	0.27	2.95	3.06	0.11	0.34	1.3	1.73

Hidden Neuron- Based Thermoeconomic Parameters

All the thermodynamic parameter error values of the artificial neural network process with different optimization algorithms This ANN process considers the one hidden layer and the neurons varying from 10 to 30. In each neuron, the parameters error values vary in the graph shown below.

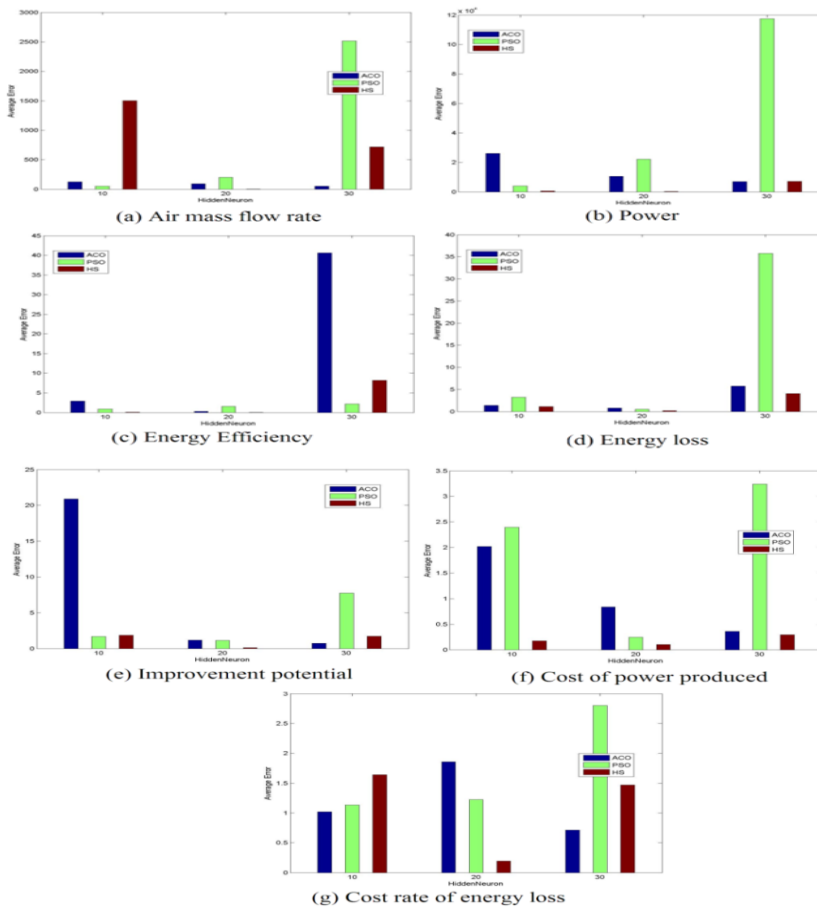

Figure 5. Hidden neuron-based error values.

Figure 5 shows that the neural network structure with neurons varying predicts the error value. Figure (5a) shows the air mass flow rate for the different neurons in 10 neurons. The error value of this parameter is 52.69 for the PSO process. It's compared to the 20 neuron PSO technique, and the

difference is 73.7%, and the 30 neuron PSO technique has a difference of 80.23%. The proposed technique of the 10 neurons is compared to 20 and 30, and the difference is 75.5%. Figure (5b) shows that the power generation for the wind mill is if the neuron varies the performance of the proposed method and the other techniques also vary these thermodynamic parameters. The difference between 10 neurons compared with 20 and 30 neurons will be 98.45% of the proposed technique. The particle swarm optimization process has obtained a maximum error value of 30 neurons in the process. Figure (5c) shows the energy efficiency of the error and in this graph, the minimum error is attained in the HS technique with 10 neurons varying and also the maximum value is arrived at in the ACO process with 30 neurons varying.

Energy loss as a thermodynamic parameter is shown in Figure (5d). In this process, the maximum difference is predicted and experimental values are shown in the ACO technique with 30 neurons. The minimum deviation compared to the HS and PSO processes of 30 neurons is 98.27%. The next Figure (5e) shows that the improvement potential maximum error value of the proposed method is attained in the 10 neuron process, and the next Figure (5f) shows that the cost for power produced in the proposed method of the 20 neuron is compared to the ACO with 20 neurons, where the difference is 74%, similar to the other techniques. The final graph shows the cost rate of energy loss of the 10 neurons where the maximum error value is 1.7 in the HS technique and 20 neurons is 1.89 in the ACO process.

Conclusion

The thermoeconomic parameters of wind turbines are predicted by using the artificial neural network (ANN) with the HS algorithm, which amazingly attains the accurate ideal values of the weights in the model. Multivariable optimization issues are resolved in the universal optimum solution and illustrate the adaptability of choosing the design variables based on the weights. During this process, consider the wind speed and area ratio of the turbine. The convincing output results are observed to be nearly equal to the data set minimum error value achieved in the optimization method. The minimum error of ANN with HS process, the air mass flow rate, power of the wind, energy efficiency, energy loss, improvement potential, cost of power produced, and cost rate of energy loss is 98.14%, 95.58%, 96.9%, 52.85%, 95.42%, 72.4%, and 88.80% of the prediction process. In future, the ANN investigators will look towards further unbelievable improvement

methodologies for the production of diminished errors with their excellent techniques for the thermo-economic parameters of wind power generation.

References

Abhinav and Nilanjan Saha. (2015). "Coupled hydrodynamic and geotechnical analysis of jacket offshore wind turbine", *Journal of Soil Dynamics and Earthquake Engineering*, Vol. 73, pp. 66-79.

Alessio Balleri1, Allann Al-Armaghany, Hugh Griffiths, Kinfai Tong, Takashi Matsuura, Takashi Karasudani and Yuji Ohya. (2013). "Measurements and analysis of the radar signature of a new wind turbine design atX-band", *Journal of of Engineering and Technology*, Vol. 7, No. 2, pp. 170-177.

Aniket Aranake, Vinod Lakshminarayan and Karthik Duraisamy. (2015). "Computational analysis of shrouded wind turbine configurations using a 3-dimensional RANS solver", *Journal of Renewable Energy*, Vol. 75, pp. 818-832.

Bontempo and Manna. (2014). "Performance analysis of open and ducted wind turbines", *Journal of Applied Energy*, Vol. 136, pp. 405-416.

Buyung Kosasih and Andrea Tondelli. (2012). "Experimental study of shrouded micro-wind turbine", *Journal of Procedia Engineering*, Vol. 49, pp. 92-98.

Canan Cimsit, Ilhan Tekin Ozturk and Olcay Kincay. (2014). "Thermo economic optimization of LiBr/H2O-R134a compression absorption cascade refrigeration cycle", *Journal of Applied Thermal Engineering*, pp. 1-11.

Chen, Liao and Cheng. (2012). "Development of small wind turbines for moving vehicles: Effects of flanged diffusers on rotor performance", *Journal of Experimental Thermal and Fluid Science*, Vol. 42, pp. 136-142.

Chonga, Pan, Poh, Fazlizan, Oon, Badarudin and Nik-Ghazali. (2013). "Performance investigation of a power augmented vertical axis wind turbine for urban high-rise application", *Journal of Renewable Energy*, Vol. 51, pp. 388-397.

Daegyoum Kim and Morteza Gharib. (2013). "Efficiency improvement of straight-bladed vertical-axis wind turbines with an upstream deflector", *Journal of Wind Engineering and Industrial Aerodynamics*, Vol. 115, pp. 48-52.

Déborah Aline Tavares Dias do Rio Vaz, André Luiz Amarante Mesquita, Jerson Rogério Pinheiro Vaz, Claudio José Cavalcante Blanco and João Tavares Pinho. (2014). "An extension of the Blade Element Momentum method applied to Diffuser Augmented Wind Turbines", *Journal of Energy Conversion and Management*, pp. 1-8.

Fahad Al-Sulaiman and Bekir Yilbas. (2015). "Thermo economic analysis of shrouded wind turbines", *Journal of Energy Conversion and Management*, Vol. 96, pp. 599-604.

Gandiglio, Lanzini, Leone, Santarelli and Borchiellini. (2013). "Thermo economic analysis of large solid oxide fuel cell plants: Atmospheric vs. pressurized performance", *Journal of Energy*, Vol. 55, pp. 142-155.

Huihui Sun and Yusaku Kyozuka. (2011). "Analysis of Performances of a Shrouded Horizontal Axis Tidal Turbine", *Journal of Earth system science and technology*, pp. 1-7.

Iman Janghorban Esfahani and Changkyoo Yoo. (2014). "A highly efficient combined multi-effect evaporation-absorption heat pump and vapor-compression refrigeration part 2: Thermo economic and flexibility analysis", *Journal of Energy*, pp. 1-11.

Jafari and Kosasih. (2014). "Flow analysis of shrouded small wind turbine with a simple frustum diffuser with computational fluid dynamics simulations", *Journal of Wind Engineering and Industrial Aerodynamics*, Vol. 125, pp. 102-110.

Janarthanan, Selvakumar, Jagadeeshwaran and Vijayshankar. (2014). "Design and Analysis of Multiphase Permanent Magnet BLDC Generator for Domestic Wind Turbine Application", *Conference on Electrical Energy Systems*, pp. 290-293.

Leo Goldstein. (2015). "A proposal and a theoretical analysis of a novel concept of a tilted-axis wind turbine", *Journal of Energy*, Vol. 84, pp. 247-254.

Ozgur Balli, Haydar Aras and Arif Hepbasli. (2010). "Thermodynamic and thermoeconomic analyses of a tri generation (TRIGEN) system with a gas–diesel engine: Part I – Methodology", *Journal of Energy Conversion and Management*, Vol. 51, pp. 2252-2259.

Rabi Karaali and Ilhan Tekin Oztürk. (2015). "Thermo economic optimization of gas turbine cogeneration plants", *Journal of Energy*, Vol. 80, pp. 475-485.

Seyed Mehdi Mortazavi, Mohammad Reza Soltani and Hamid Motieyan. (2015). "A Pareto optimal multi-objective optimization for a horizontal axis wind turbine blade airfoil sections utilizing exergy analysis and neural networks", *Journal of Wind Engineering and Industrial Aerodynamics*, Vol. 136, pp. 62-72.

Seyed Reza Hosseini, Majid Amidpour and Ali Behbahaninia. (2011). "Thermo economic analysis with reliability consideration of a combined power and multi stage flash desalination plant", *Journal of Desalination*, Vol. 278, pp. 424-433.

Venkata Yaramasu, BinWu, Marco Rivera and Jose Rodriguez. (2014). "A New Power Conversion System for Megawatt PMSG Wind Turbines Using Four-Level Converters and a Simple Control Scheme Based on Two-Step Model Predictive Strategy—Part II: Simulation and Experimental Analysis", *Journal of IEEE Emerging and Selected Topics in Power Electronics*, Vol. 2, No. 1, pp. 14-25.

Wen-Xue Wang, Terutake Matsubara, Junfeng Hu, Satoru Odahara, Tomoyuki Nagai, Takashi Karasutani and Yuji Ohya. (2015). "Experimental investigation into the influence of the flanged diffuser on the dynamic behavior of CFRP blade of a shrouded wind turbine", *Journal of Renewable Energy*, Vol. 78, pp. 386-397.

Wong, Chong, Yap, Fazlizan, Omar, Poh and Hsiao. (2014). "The design and flow simulation of a power-augmented shroud for urban wind turbine system" In *proceedings of Applied Energy*, Vol. 61, pp. 1275-1278.

Yongqiang Feng, Yaning Zhang, Bingxi Li, Jinfu Yang and Yang Shi. (2015). "Sensitivity analysis and thermo economic comparison of ORCs (organic Rankine cycles) for low temperature waste heat recovery", *Journal of Energy*, pp. 1-14.

Chapter 6

Design, Modeling and Analysis of Wind Turbine Gear and Modified Wind Turbine Blades

P. Sakthivel*, PhD
Department of Mechanical Engineering, Sri Krishna College of Technology, Coimbatore, India

Abstract

A wind turbine is a device that converts kinetic energy from the wind, also called wind energy, into mechanical energy, a process known as wind power. If the mechanical energy is used to produce electricity, the device may be called a wind turbine or wind power plant. A utility wind turbine's typical design lifetime is 20 years, but the gear boxes that convert the rotor blades' rotational speed of 5 to 22 RPM to the generator's required rotational speed of 1000 to 1600 RPM frequently fail within 5 years of operation and must be replaced. The surface and sub-surface damages lead to fatigue crack initiation followed by crack growth and eventual fracture. This paper presents the design of wind turbine gear using Pro-E and analysis was carried out by ANSYS software. Through analysis, it was identified that chromium-vanadium material is better than EN-36 material for making wind mill gears, thereby providing higher strength and lifetime. Another part is to design a windmill gear using Pro-e Wildfire 2.0 and the stress analysis of the gear is done by using ANSYS Work Bench and the results are calculated. By achieving this concurrent engineering concept, the product development cycle time can be reduced considerably for any kind of model with the required quality. Based on the computation process and

* Corresponding Author's Email: skt4design@gmail.com.

In: The Future of Wind Energy
Editors: M. Dhurgadevi, P. Sakthivel and K. Gunasekaran
ISBN: 979-8-88697-232-0

the detailed analysis, the life of the windmill has increased by up to 10% of the desired life. So it tends to reduce the breakdown of the windmills and also increase the power production range. The next step is to analyze and modify the wind turbine blades. There are two electromagnetic induction generators that are preferred to share the loads through a single shaft over straight-level gears. The poles of these generators will be changed from alternate to parallel. The output electric current is stored by a series of batteries for utilisation through the converter and step-up transformer. The wind energy conversion process is done by the control system to extract extreme energy from the incident wind. The maximum power point tracker (MPPT) control schemes have been reported, which are operated by varying the speed of the generator in order to optimize wind turbine aerodynamic efficiency. However, for the implementation, the measurement of accurate wind speed is required. The optimum value depends upon the accuracy of the loss model parameters.

Keywords: wind turbine, helical gear, pitting, Pro-E & ANSYS, power, MPPT, HAWT, VAWT, MATLAB, pitting, gear, Pro-e, and ansys

Introduction

Helical gears are extensively used in numerous engineering applications, including gearboxes. Failures of gears not only result in replacement costs but also in process downtime. The causes of gear failure are numerous, including faulty designs, improper applications, and manufacturing errors. Design errors include improper gear geometry, improper materials, poor material quality, and an inappropriate lubrication system. Application errors include improper mounting and installation, poor cooling and lubrication, and poor maintenance. Manufacturing errors could be from poor machining and faulty heat treatments. Surface pitting is one of the principal modes of failure of mechanical elements that are subjected to rolling contacts, like gears and bearings, and it governs the service life of the components. The complete contact fatigue process starts with micro-pit formation, followed by crack initiation, crack growth, and the breakaway of the surface material layer. In practice, it is common that contact fatigue damage will first occur in the dedendum of the smaller gear (which is usually the driving gear) of a gear set. Damage due to contact fatigue in gear teeth usually occurs in one of three areas: along the pitch line, in the addendum, or in the dedendum. The pits formed on the surface lead to stress concentrations that serve as initiation sites for the cracks and eventually the failure. The reducer gearbox failed after

approximately 15,000 hours, which was much lower than the expected working life of 30,000–50,000 hours in continuous running conditions.

The wind is a clean source of energy that does not pollute the air, and it is a renewable energy source that is available at no cost. The kinetic energy of the wind can be used to produce electrical energy by wind turbines (Chaware. K.D., Dr. P.V. Washimkar, 2016). A wind turbine is a type of power plant. The different configurations can be used for wind turbines. One of two different modes of operation can be used in the function of the wind turbine, one being MPPT and the other being a Fuzzy logic controller. These types of operations are used for both fixed-speed and variable-speed wind turbines (Ashwin P. Joseph, Suraj P. Chavhan, Pravesh K. Sahare, Abdul Arif, and Tanveer A. Hussain, 2015). In previous years, fixed speed was used to achieve maximum efficiency for a given wind speed. But, power conversion is not an efficient method. To avoid this reason, nowadays, variable speed wind turbines are used. Maximum efficiency over a wide range of wind speeds has been achieved by this design.

Power generation from wind has emerged as one of the most successful renewable energy technologies. Despite the facts of unpredictability and lack of control over wind energy, windmills are preferred as the source of power generation because of growing environmental concerns with respect to the use of other conventional fuels and to preserve the finite resources of fossil fuels. The field reliability study of modern wind turbines shows a reduction in failure rates of the gearbox subsystem in comparison with other subsystems. However, the gearbox has a low availability due to its high downtime per failure, and gearbox failure incurs high repair costs. However, for gear systems used in wind turbine applications, the demand for gearboxes designed with extremely high gear ratios and operating under conditions subject to a broad spectrum of load and speed variations makes reliability prediction and failure prevention difficult. Current research initiatives in this area include the Gear Reliability Collaborative (GRC) of US NREL/DOE, which has committed research efforts to tackle this challenging problem. The failure mode is an important method in reliability analysis appropriate at the design stage. It provides benefits by improving designs by identifying weaknesses in subassemblies and components of a complex system. Identification of weak points in design also prompts further improvement in the configuration design of the system.

The output range of a single windmill is small, and it can’t be used for commercial purposes. Therefore, a large number of windmills are erected over a large area, which is called a wind energy farm (FarhaKhanam, NeeleshSoni,

2016). Wind farms are created with multiple numbers of windmills placed in the same area for the purpose of generating a greater amount of electricity. Due to increasing energy prices and the resultant search for alternatives, nowadays there are thousands of wind farms available in many countries around the world. Each and every windmill is coupled together to get the electricity for commercial applications. For the production of electricity, the rated wind speed should be greater than 15 km/hr. In recent years, demand for increasing numbers of power plants has been renewed, sparking an interest in Vertical Axis Wind Turbines (VAWT) (Pravesh K. Sahare, Tanveer A. Hussain, Sangita N. Kakde, Sujata R. Ingle, and Ambikaprasad O. Chaubey, 2016). The VAWT withstands high wind speeds when compared with the Horizontal-Axis wind turbines (HAWT).

Literature Review

In the wind turbine (Deng, ZheChen, Fujin Deng, 2010), a multiple permanent magnet synchronous generator (MPMSG) system is engaged in the wind turbine. A multilevel converter interface based on MPMSGs is established to combine a desired high ac voltage output that is directly connected to the grids. A phase angle shift strategy is proposed in this paper, which effectively reduces the fluctuation of the electromagnetic torque sum and results in good performance for the MPMSG structure.

The authors (Matthias Kinzel, Quinn Mulligan, and John O. Dabiri, 2012) analyzed the flow field of an array of 18 counter-rotating vertical-axis wind turbines (VAWTs), with an emphasis on the fluxes of turbulence kinetic energy and mean. The turbine wakes up the recovery of the average wind speed between the turbines. The rows are derived from the measurements of the velocity using a meteorological tower. The flow fields in wind farms are highly complex due to the contact between the wind turbines and the atmospheric boundary layer. The average horizontal wind speed during the measurement was 8.05 m/s1 at 10 m, which means above the top of the wind turbine canopy, with a deviation of 2.1 m/s. The turbine is commercially available with a lift-based rotor design consisting of three airfoils, and a 1200-watt generator is connected to the base of the turbine shaft.

By means of placing seven sensors at different positions, we get the average mean horizontal flow velocity at the mid-height of the rotor at each location. This is done to average the velocities. The experimental field study has analyzed the flow field along with the center line of an array of nine pairs

of full-scale counter-rotating VAWTs. The velocity field result shows the blockage effect of the wind turbines and individual turbine pairs within the array.

The authors (B. Bittumon, AmithRaju, Harish Abraham Mammen, AbhyThamby, and Aby K Abraham, 2014) considered high torque, which would be useful in self-starting and rotor having a high tip speed ratio for electrical generation. VAWTs have traditionally been more expensive to operate and maintain than HAWTs. The wind turbine rotors and stator are levitated correctly by using permanent magnets, which allow negligible friction with smooth rotation. At reasonable wind speeds, the power output of the generator satisfies the specifications needed to supply the LED load. Finally, the SEPIC circuit operated effectively and to the specifications that were slated at the beginning of the circuit design.

This paper investigates and models the performance of a VAWT (Vertical Axis Wind Turbine) with PMSG. A careful and wide-ranging investigation is required since different environmental locations call for different wind speeds. For example, Nigeria is a country that has low and unsteady wind speeds. The wind turbine system consists of three main parts; wind speed, turbine, and generator.

A three-phase PMSG was chosen for the experimental work due to its higher efficiency and less maintenance when compared to other generators. It does not require rotor windings, which involves a reduction in weight and cost. These elements, and the entire idea of this work, have been modelled and simulated by using MATLAB and SIMULINK. Results show the good system performance. The wind turbine system is designed to generate a three-phase current with a peak value ranging from 2.27A to 7.35A for a comparatively low wind speed range of 3m/s to 6m/s. From these values, the generated current is sufficient at low and unsteady wind speeds. Voltages from the steady state values generated range from 32.9Vrms/phase to 117.2Vrms/phase for the wind speed range of 3 m/s to 6 m/s. The power generated ranges from 32.08w to 335.6w for a relatively low wind speed range of 3m/s to 6m/s. If the methodology is implemented, the cost of design and cost of maintenance is reduced, making it economical and affordable.

In (Peter J. Schubel and Richard J. Crossley, 2012), the design of a wind turbine blade is presented, which includes the value of maximum theoretical efficiency, propulsion and practical efficiency, HAWT blade design, and the amount of load acting on the blade. A detailed review of design loads for wind turbine blades is offered by relating aerodynamic, centrifugal, gravitational, gyroscopic, and different operational conditions. For efficiency reasons,

control, noise, and aesthetics of the modern wind turbine market are dominated by a horizontally mounted three-blade design. The use of yaw and pitch is to operate under different wind speed conditions. The basic load analysis result shows that the blade can be modelled as a simple beam with inbuilt support at the hub ends. A uniformly distributed load is used to represent aerodynamic lift during the blade operation.

Design and Construction

Wind turbines are designed to exploit the wind energy that exists at a location. Aerodynamic modelling is used to determine the optimum tower height, control systems, number of blades, and blade shape. Wind turbines convert wind energy to electricity for distribution. Conventional horizontal axis turbines can be divided into three components:

1. The rotor component, which is approximately 20% of the wind turbine's cost, includes the blades for converting wind energy to low-speed rotational energy.
2. The generator component, which is approximately 34% of the wind turbine cost, includes the electrical generator, the control electronics, and most likely a gearbox.
3. The structural support component, which is approximately 15% of the wind turbine cost, includes the tower and rotor yaw mechanism.

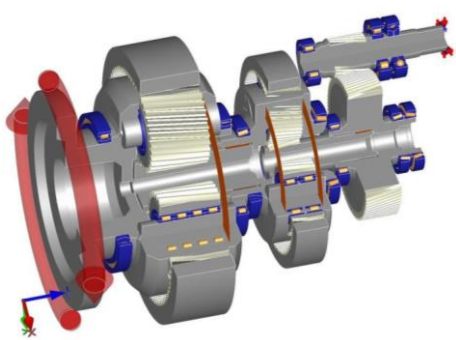

Figure 1. Gear Box Arrangements.

A 1.5 MW wind turbine of a type frequently seen in the United States has a tower 80 meters (260 ft) high. The rotor assembly (blades and hub) weighs 48,000 pounds (22,000 kg). The nacelle, which contains the generator component, weighs 115,000 pounds (52,000 kg). The concrete base for the tower is constructed using 58,000 pounds (26,000 kg) of reinforcing steel and contains 250 cubic yards (190 m3) of concrete. The base is 50 ft (15 m) in diameter and 8 ft (2.4 m) thick near the center.

Power Control

A wind turbine is designed to produce a maximum of power at a wide spectrum of wind speeds. All wind turbines are designed for a maximum wind speed, called the "survival speed," above which they do not survive. The survival speed of commercial wind turbines is in the range of 40 m/s (144 km/h, 89 MPH) to 72 m/s (259 km/h, 161 MPH). The most common survival speed is 60 m/s (216 km/h, or 134 MPH). Wind turbines have three modes of operation. They are below-rated wind speed operations; around-rated wind speed operations; and above-rated wind speed operations.

Gear Box Arrangements

Wind-turbine gearboxes convert low-speed input from the turning blades to high-speed output to the generator, which is shown in Figure 1. The function of the gearbox in a wind turbine is to transmit torque from the rotor to the generator shaft, providing the desired conversion ratio for speed and torque. Gearbox failure is among the failures resulting in the longest average downtime and thus has a strong impact on production availability. It can cause severe secondary damage, e.g., in the main bearing or the rotor shaft. An additional failure cause of general validity for different gearbox components is manufacturing and installation deficiencies, which lead to increased friction or inappropriate high cyclic loading, resulting in damage.

The Design of a Gear Blade

Sixty-five percent of gears fail from pitting fatigue, and the gear fails completely after 60 thousand hours. The new gearbox is designed by replacing

the gear material, and new gear geometry is introduced. Pitting is a form of surface fatigue that may occur soon after an operation begins, and it is due to overloading. Improper lubrication and sudden starting and stopping may lead to micro pitting.

Micro Pitting

More recently, a microscopic pitting phenomenon—generally referred to as micro pitting—has become a very problematic failure mode in certain applications. Typically, high loading is present at lower speeds under low or marginal film thickness conditions, and micropitting becomes a significant risk. It is important to note that although it usually appears in a somewhat different presentation, micro pitting is also a factor in the operation of higher-speed gears as well.

Macropitting

Until fairly recently, the surface durability of gears has been defined by macropitting, in which a crack initiates at a subsurface location where the shear stress exceeds the shear allowable. When such a crack propagates to the tooth surface, a small piece or, more often, several small pieces of material are liberated, leaving an inverted, cove-shaped defect. As this process is repeated, more and more pits appear, and eventually, the tooth surface is heavily damaged.

Figure 2. 3D View of Gear Arrangement.

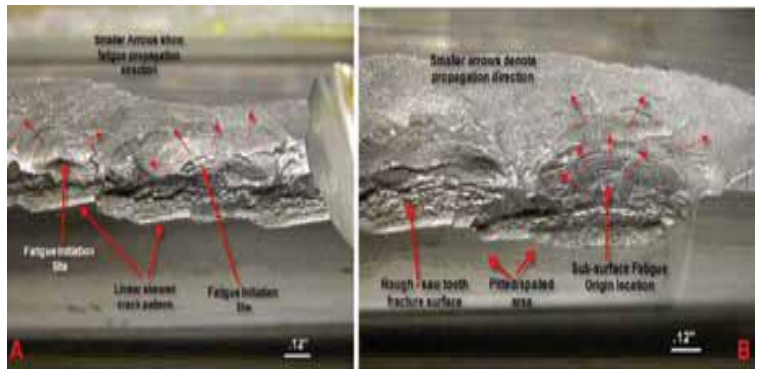

Figure 3. Helical Gear Tooth after Partial Tooth Fractures.

Reason for Pitting

The simple model is based on linear momentum theory. The analysis is assumed by a control volume, which consists of the surface of a stream tube and double cross-sections of the stream tube (Figure 5). The wind turbine model is represented by the actuator disk, which has a uniform discontinuity of pressure in the stream tube of air flowing through it. This analysis is not limited to any particular type of wind turbine.

There are three different reasons for pitting on a gear surface: The surface contact stress of the gear is higher than the permissible surface fatigue stress of the material. When using helical gears, the axial force is produced in the gear shaft. For this reason, the clearance value in the bearing is increased. For this reason, the percentage of tooth contact is reduced from 99% to 90%.

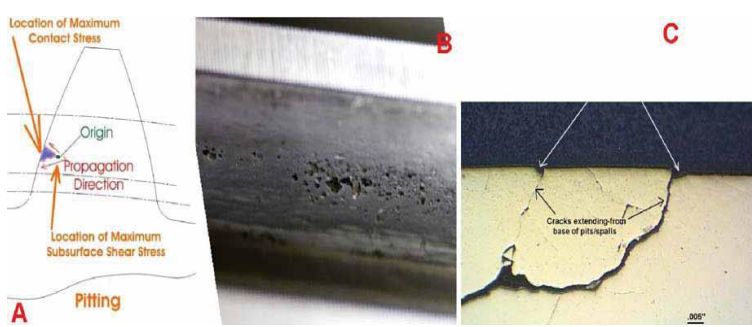

Figure 4. Classic Macropitting Fatigue.

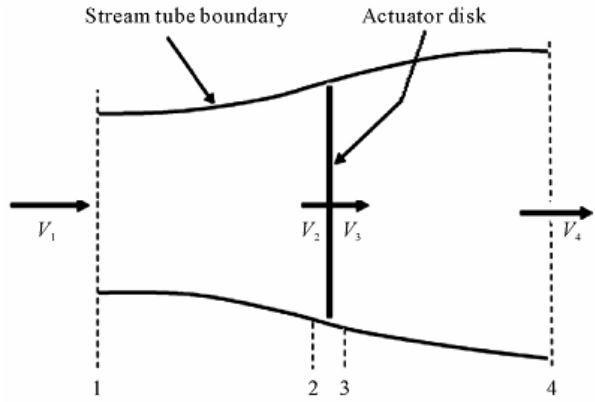

Figure 5. Actuator disk of a wind turbine.

Power Obtained from Wind Turbines

The simple model is based on linear momentum theory. The analysis is assumed by a control volume, which consists of the surface of a stream tube and double cross-sections of the stream tube (Figure 5). The wind turbine model is represented by the actuator disk, which has a uniform discontinuity of pressure in the stream tube of air flowing through it. This analysis is not limited to any particular type of wind turbine.

The total static pressure upstream and downstream of the rotor system is equal to the undisturbed ambient static pressure. By applying the conservation of linear momentum to the control volume enclosing the entire system, it is possible to find the force on the filling of the control volume. The net force is equal and opposite to the thrust, which is the force of the wind on the wind turbine.

The momentum for a 1D incompressible, time-invariant flow is,

$$T=V\_1\ (\rho AV)\_1- V\_4\ (\rho AV)\_4$$

ρ is the density of air, A is the value of the cross-sectional area, V is the velocity of the air, and the subscripts indicate the values at the numbered cross sections in Figure 1. For steady-state flow,

$$(\rho AV)\ 1 = (\rho AV)\ 4 = m,\ T = \dot{m}(V\_1- V\_4\ )$$

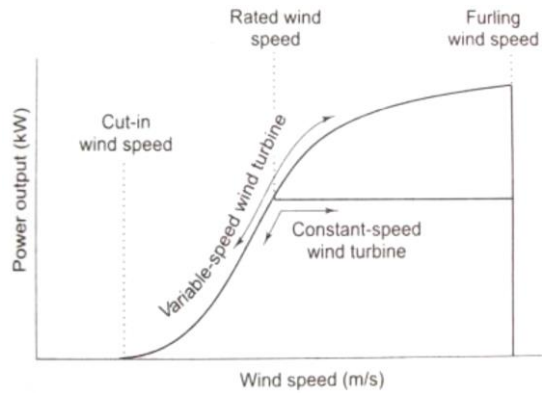

Figure 6. Wind turbine power versus wind speed.

The thrust value is positive, so the velocity behind the rotor V4 is less than the velocity of the free stream V1. The Bernoulli equation is used in the two control volumes on both sides of the actuator disk. The stream tube upstream of the disk

$$p_1 + 1/2 [pv]_1^2 = p_2 + 1/2 [pv]_2^2$$

The stream tube downstream of the disk,

$$p_3 + 1/2 [pv]_3^2 = p_4 + 1/2 [pv]_4^2$$

The upstream and downstream pressures are equal (p1 = p4) and the velocity across the disk remains the same (V2 = V3). The thrust of the actuator disc:

$$T = A_2 (P_2 - P_3)$$

It is possible to obtain by solving the equations:

$$T = 1/2 \rho A_2 (V_1^2 - V_4^2)$$

Equating the thrust values and the mass flow rate is

$$A2V2, V_2 = (V_1 + V_4)/2$$

Wind velocity at the rotor plane is calculated by the average of the upstream and downstream wind speeds. The axial induction factor “a”, then

$$a = (V_1-V_2)/V_1; V_2 = V_1 (1-a); V_4 = V_1 (1-2a)$$

The axial thrust on the disk is:

$$T = 1/2 \rho A V_1^2 [4a (1-a)]$$

The non-dimensional thrust coefficient is as

$$C_T = T/(1/2 \rho A V^2) = (\text{Thrust Force})/(\text{Dynamic Force})$$

Construction of a Wind Mill

The windmill can be divided into two major parts: the mechanical turbine and the electric generator. The following section gives a brief description of the wind energy system, including the main components, design, and operation. Among the above, the nacelle is a casing that houses the key components of a windmill, such as the gear, generator, electronic control unit, yaw controller, brakes, etc. The rotor blades capture the wind’s energy and convert it to rotational energy for the shaft. The hub in turn transfers the energy to the low-speed shaft. Blade designs operate on either the principle of drag or lift. The low-speed shaft of the wind turbine connects the rotor hub to the gearbox.

Gear Box

Most wind turbine installations are equipped with similar gearboxes; a typical example is the three-stage spur wheel gearbox (lower capacity area), the one-stage planetary gearbox with two spur wheel stages (middle capacity area), and the two-stage planetary gearbox with one spur wheel stage (higher capacity area). In addition to that, there are currently some interesting variants. As you can see, the majority of wind turbine installations have one rotor only, which generally is up. Likewise, most installations have one generator only i.e., the gearbox has exactly one input and one output. These are the four combinations conceived and partially implemented. Several generators, or

rotors, are unusual. The author does not know of any installation with several rotors and several generators. The wind turbine gearbox's mission is to transform the low speeds and high torques at the gearbox input into higher speeds and lower torques at the output.

Methodology and Material Selection

Wind Turbine Gear: Design and Analysis

A gear rating is parametric in nature. The approximate tooth size needed to carry a specified load is too small. As the dynamic factor decreases as size decreases, the rating is slightly higher (10%) than the minimum acceptable values.

For this work, two different types of materials were selected for analysis. They are EN-36 alloy steel and Chromium Vanadium alloy steel. The chemical and mechanical properties of the materials are shown in Table 1. The design parameters of both materials are shown in Table 2. As per the design calculation, the required gear sets were designed by Pro-E Wild Fire modelling software, and then the simulation was carried out by ANSYS software.

Table 1. Material properties

Material	**EN-36**	**Chromium Vanadium**
Chemical composition		
Carbon	0.15%	0.55-0.65%
Manganese	0.45%	0.70-0.90%
Silicon	0.20%	0.20-0.35%
Nickel	3.50%	-
Chromium	0.80%	0.80-1.10%
Sulphur	0.025%	0.040%
Phosphorous	0.025%	0.040%
Mechanical properties		
Young's Modulus	200×10^3 N/mm^2	206×10^3 N/mm^2
Density	7.85×10^{-6} Kg/mm^3	6.59×10^{-6} Kg/mm^3
Tensile strength	1180 N/mm^2	1370 N/mm^2
Yield strength	765 N/mm^2	915 N/mm^2
Factor of safety	0.27	0.29

Table 2. Design parameters of existing & new gear materials

EN-36	**Chrome-vanadium**
$\sigma_u = 1180 \times 106$ N/m^2	$\sigma_u = 1370 \times 106$ N/m^2
$\sigma_c = 909.28 \times 106$ N/m^2	$\sigma_c = 622.85 \times 106$ N/m^2
$\sigma_b = 109.17 \times 106$ N/m^2	$\sigma_b = 41.45 \times 106$ N/m^2
Power P = 103.452 Kw	P = 103.452 Kw
Gear ratio1:2	1:2

Corrective Action

Nowadays, so many corrective actions are there to prevent the pitting of gear. They are:

Increasing the hardness of the gear material, improving the surface hardness of the material, redesigning the gear geometry, providing a proper lubrication system, and eliminating the axial force of the rolling element are all options.

Design and Analysis of Wind Turbine Blades

Windmill Using a Multi-Generator

The two electromagnetic induction generators are connected to the end of the shaft by coupling. The wind turbine rotor transmits the power to the two generators through a bevel gear. The output power of a multi-generator wind turbine will be double that of a single-generator wind turbine.

The Methods' Guiding Principle

The wind turbine works by the conversion of wind energy to electrical energy by using the generator. The blades of a wind turbine rotate due to the force of air striking them. Due to the blade rotation, electricity is generated by the shaft.

Construction of the Methods

The main components of the horizontal blade wind turbine are as follows: blades and rotor; electromagnetic induction generator; gear and shaft. The blades are attached to the rotor. The rotor is connected to the gear through a shaft and balanced by bearing mountings. The gearbox consists of the driven gear and driver gear. The driven gear teeth are meshing with the driver gear. The low-speed shaft is connected by a driver gear, and the other side is connected by the turbine rotor of the wind turbine. The high-speed shaft is

connected by the center of the driven gear. Both ends of the shaft are connected to the same or different generators through coupling. For vertical blade wind turbines, the main parts are as follows: blades and rotor; electromagnetic induction generator; gears and shaft. Of these two types of generators, one is rotated in a clockwise direction and the other one is rotated anticlockwise. Due to the anticlockwise rotation of the generator, it does not produce the current.

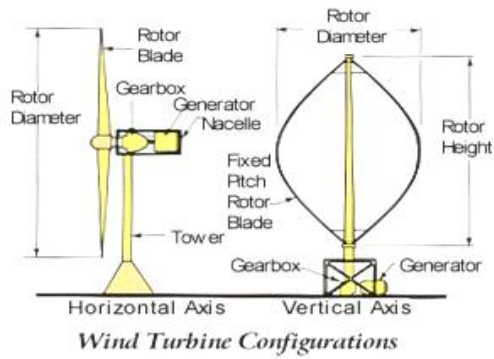

Figure 7. Wind turbine configuration.

Power and Torque Transmission in Bevel and Spur Gears

The power produced from the wind turbine rotor flows through the spur gear and it is divided into two ways: one part goes straight and another side goes to the driven gear, then it is divided into two sides; one is the right side, which is used by the generator, and the other side is the loss of power and torque. So, the windmill carries on with an efficiency of 50%.

In a bevel gear system, the power and torque generated by the wind turbine flow to the driver gear and then to the driven gear. Then it is divided into two sides. One is on the right side by Generator G2 and the opposite side by Generator G1. So, the windmill has increased efficiency when compared with the spur gear arrangement.

Parts of a Windmill

Blades

The blades are basically the wings of the wind turbine. Blades act as barriers to the wind. When the wind forces the blades to rotate, it transfers some

amount of energy to the rotor. Blades are generally available in two types as follows: horizontal and vertical.

Shaft

The wind-turbine shaft is connected to the rotor. And the rotor transfers its mechanical energy to the shaft, which enters into the generator at the other end of the shaft. The shaft is a machine member which has high strength to support the total weight of all three blades.

Gear (Bevel Gear)

Bevel gears are drive systems that convert the direction of a shaft's rotation exactly perpendicular. It is usually fixed on shafts that are 90 degrees, but it can be designed to work at other angles as well.

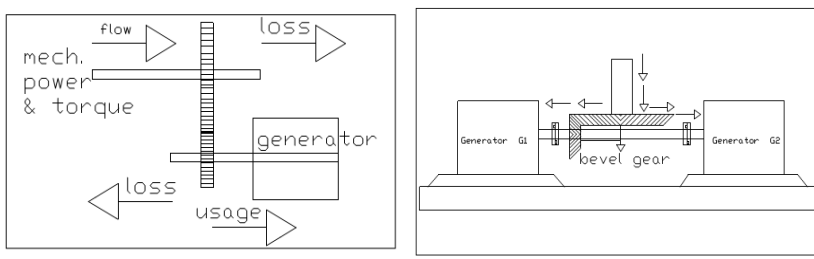

Figure 8. Power and torque flow of the transmission in spur and bevel gears.

Table 3. Chemical composition

Name of Material	**Composition**
Carbon C	0.35 - 0.45%
Chromium Cr	1.0 - 1.40%
Nickel Ni	1.30 – 1.40%
Manganese Mn	0.45 - 0.70%
Molybdenum Mo	0.20 - 0.35%

Table 4. Mechanical properties

Tensile Strength (N/mm^2)	**Yield Strength (N/mm^2)**	**Hardness Value BHN**
800 to 1300	600 to 1200	300 to 400 BHN

Generator

A generator is a device that uses electromagnetic properties to produce electrical energy. A simple generator consists of a conductor and magnets. The conductor is typically a coiled wire. The generator shaft connects to an assembly surrounded by permanent magnets that the coil of wire winds around.

Tower

The turbine is usually positioned upwind of its supporting tower. It supports the rotor, the drive train mechanism, and other types of equipment, including control mechanisms, ground support equipment, and interconnection devices.

Material Specification

The material that is used to make the shaft, gear, bolt, and nut is alloy steel. [Case Hardened] 40 Ni 2 Cr 1 Mo 28.

Schematic of Wind-Hybrid System

Figure 9 shows the schematic layout of a 3-phase, 4-wired autonomous system. The two back-to-back connected with insulated gate bipolar transistor systems (IGBTs), pulse width modulation (PWM), and voltage source converters (VSCs) are connected among the stator windings of SCIG and PMSG to facilitate bidirectional power flow. The tip speed ratio determines the SCIG rotor-speed set point for a given wind speed. The mechanical energy generated at this speed lies at the maximum energy of the turbine. The load-side converter is controlled by the regulation of load-voltage magnitude and frequency. For maintaining the load-frequency constant, it is also essential that excess power in the system be side tracked to the battery source.

The BESS on the DC bus of the PWM converter is to transfer the power from the battery without any converter. The role of the transformer and converter is to recompense the unbalanced condition with the load currents.

The new system consists of three different modes of operation. For the first mode, the necessary power of the load is less than the power produced by the synchronous generator. The excess power generated by the PMSG is transformed into the BESS through the load-side converter. In the second

mode, the power generated by SCIG is supplied through the converter on the load-side, and the remaining power is stored in BESS. In the third mode, the shortage power is supplied by the BESS, the generated power by PMSG, and the shortage by BESS is supplied to the load-side converter.

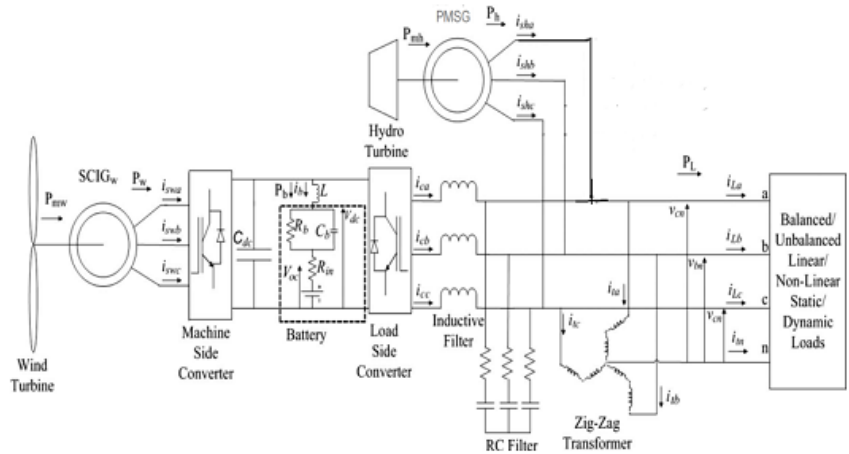

Figure 9. Schematic layout of the hybrid system.

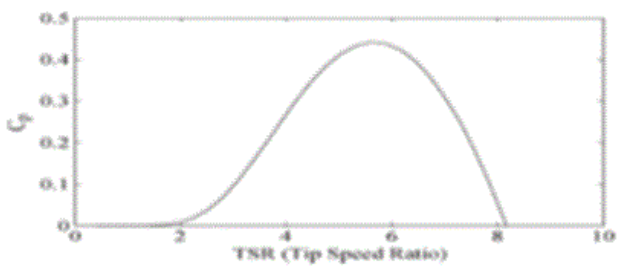

Figure 10. Performance coefficient vs. tip speed ratio.

The Wind Turbine Design

The hybrid system being considered has a wind turbine capacity of 55 kW and a hydro turbine of 60 kW, respectively. The voltage of the battery bank is considered 700V. The maximum value of the RMS line voltage at the load terminals is 415 V. By considering the ability of the new system to provide

electricity at a load rate of 60 kW for 10 hours, the storage capacity of the battery power bank is taken as 600 kWh. The commercially available battery bank contains cells at 12 V. The capacity of each cell is taken as 150 Ah. To achieve a voltage range (700 V) through series linked cells of 12 V, the battery bank has 59 (700/12) cells in series. The storage capacity of this combination is 150 Ah and the total ampere per hour required is (600 kWh/700 V) = 857 Ah, and the number of sets required to be linked in a parallel connection is (857 Ah/150 Ah) = 5.71 = 6. The battery bank contains six parallel-connected sets and 59 series-connected battery cells.

Gear Ratio of Wind Turbine

The wind turbine will produce 55 kW at a rated wind speed of 1.2 m/s. Mechanical power Pm is calculated for wind speeds less than the rated wind speed by multiplying wind speed Vw, turbine radius rw, the density of air, and coefficient of performance (Cpis). The maximum coefficient of performance is achieved at the optimal tip ratio (λ∗w). The values of Cpmax and tip ratio are 0.4411 and 5.66. Consider the values of wind speed Vw = 11.2 m/s, Pm = 55 kW, Cp = 0.4411, and density of air ρ = 1.1544 kg/m3 for 4.1. The wind turbine's radius, rw, is discovered to be 7.5m. The gear ratio is thus 12 [(100*705)/5.66*11.2].

Pitting Analysis of Wind Turbine Blades

The first step in this exercise was to design the anticipated gear sets. As gear ratings are parametric in nature, the approximate tooth size needed to carry a specific load has to be selected. The rating is slightly higher (10%) than the minimum acceptable values as the dynamic factor decreases with size. The required gear sets were designed by Pro-E wildfire and then the simulation was carried out by ANSYS WORKBENCH.

Eliminating Methods

(i) Replacing the gear material to have higher hardness.
(ii) Reworking the gear geometry
(iii) Removing axial force.

Specification of the Present Double Stage Gear

1. Power of the gearbox (P) = 500KW
2. Type of gear: Helical gear.
3. The gearbox material is Chromium-Vanadium.
4. Rockwell hardness of the Material (HRC) = 41
5. The ultimate tensile strength of the material is13700kgf/cm^2
6. Lubrication- Flash type.
7. Type of bearing: Roller bearing.

Design Calculation for New Gear (Herringbone Gear)

Two-stage Herring bone gear calculation:

First Stage Gear

Alloy steel (40 Ni 2 Cr 1 Mo 28) is used.
N1 pinion, N2 main wheel.
N2 = 15 rpm, P = 500 kw
HRC = 57 i = 10.
Design surface contact stress: $[\sigma_c] = 933.66 * 10^6$ N/m^2
Design bending stress: $[\sigma_b] = 309.16 * 10^6$ N/m^2
Calculation of initial design torque (M_t):
$[M_t] = 21107.58$ N-m
Calculation of centre distance:a = 1.04211 m
Calculation of normal module (M_n): $M_n = 7.98 * 10^{-3}$ m
Calculation of the number of pinion and gear teeth (Z_1 and Z_2):
Assume Z1 is equal to 20 [Z1 is equal to 20]. & Z2 = 200
Calculation of pitch circle diameter of pinion and gear:
$d_1 = 0.208865$ m & $d_2 = 2.08865$ m

Revised Calculation

Calculation of normal module (M_n): $M_n = 7.25 * 10^{-3}$ m
Calculation of centre distance (a):a = 1.14875 m
Calculation of design torque $[M_t]$: $[M_t] = 22211.66$ N-m
Checking design calculation: $\sigma_c = 827.56 * 10^6$ N/m^2
$[\sigma_c] > \sigma_c$, Design is Safe.
$\sigma_b = 122.61 * 10^6$ N/m^2
$[\sigma_b] > \sigma b$, Design is Safe.

Surface fatigue stress is permissible.
$(\sigma_{cp}) = 1425 * 10^6$ N/m^2 : $(\sigma_{cp}) > \sigma_{c.,}$ Design is Safe.
Surface wear strength condition is satisfied.

Second Stage Gear

While N2 = 150 rpm, N1 = 1500 rpm.
$[M_t] = 2110.7666$ N-m
Where,
$[\sigma_c] = 933.66 * 10^6$ N/m^2
$[\sigma_b] = 309.16 * 10^6$ N/m^2
Calculation of centre distance (a): a = 0.483709 m
Normal module calculation: Mn = 3.67 4*10-3 m
Revised Calculation:
Normal module calculation: Mn = 3.86 4*10-3 m
The center distance is calculated as a = 0.574375 m.
Design torque is calculated as [Mt] = 22221.1 N-m.
Calculation of design torque: $[M_t] = 22221.1$ N-m
Check calculation: $\sigma_c = 740.16 * 10^6$ N/m^2
$[\sigma_c] > \sigma_c$, Design is Safe.
$\sigma_b = 91.72 * 10^6$ N/m^2 $[\sigma_b] > \sigma_b$, Design is Safe.
Surface fatigue stress permissible
$(\sigma_{cp}) = 1425 * 10^6$ N/m^2
$[\sigma_c] = 933.66 * 10^6$ N/m^2: $(\sigma_{cp}) > \sigma_{c.}$
The condition is satisfied.

Comparison Table for Present and New Gear

Table 5. Present and new gear

Title	**Present Gear (Helical)**	**New Gear (Herring bone)**
Material	Chrome-vanadium	Nickel-chromium
HRC	41	57
Ultimate tensile strength	$\sigma_u = 1370 * 10^6$ N/m^2	$\sigma_u = 1550 * 10^6$ N/m^2
Surface contact stress	$\sigma_c = 635.60 * 10^6$ N/m^2	$\sigma_c = 933.66 * 10^6$ N/m^2
Bending stress	$\sigma_b = 279.7 * 10^6$ N/m^2	$\sigma_b = 309.66 * 10^6$ N/m^2
Module	First Stage gear Mn = $13 * 10^{-3}$m Second Stage gear Mn = $6 * 10^{-3}$m	First Stage gear Mn = $8 * 10^{-3}$m Second Stage gear Mn = $4 * 10^{-3}$m
Power	P = 500KW	P = 500KW
Gear ratio	1:10	1:10
Gear type	Helical gears	Herring bone gears

Results and Discussion

The helical gear is modelled using Pro-E software. Then the different types of analysis like stress deformation, displacement vector, and strain deformation are carried out by using ANSYS software. Table 6 summarises the analysis values for both materials.

Table 6. Analysis values

Particulars	**EN-36**	**Chrome-Vanadium**
Displacement vector	0.20284×10^{-3} m	0.20924×10^{-3} m
Stress Deformation	3321×10^{-6} N/m^2	3340×10^{-6} N/m^2
Strain Deformation	0.016493	0.017636

The analysis result shows that Chrome-Vanadium material has high values of stress, displacement, and strain compared with EN-36 material. By changing the material to Chrome-Vanadium instead of EN-36, pitting failure is minimized to the desired level. The chromium vanadium material is better than EN-36 material for making wind turbine gears, thereby providing higher strength and longer life.

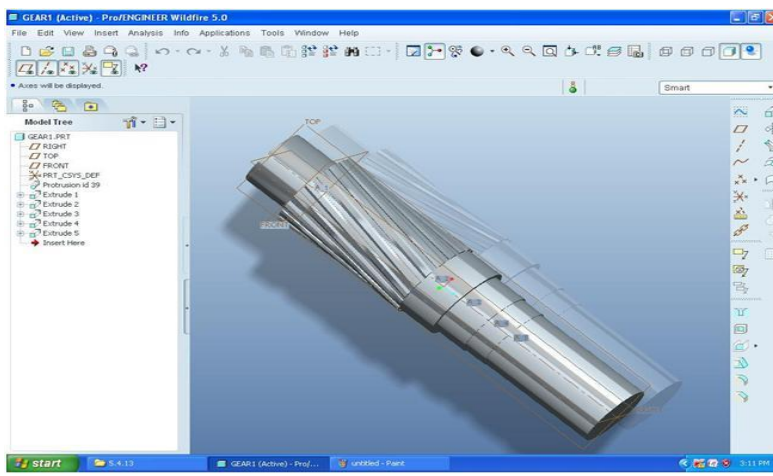

Figure 11. Helical gear.

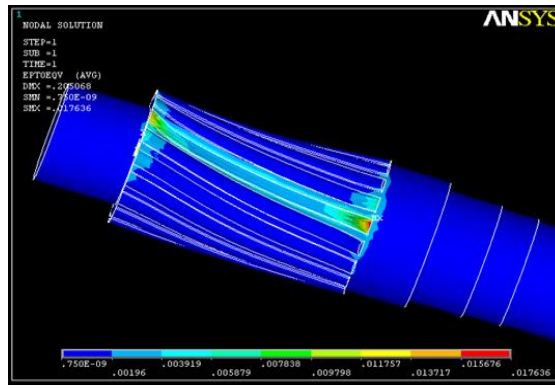

Figure 12. Stress deformation (EN-36).

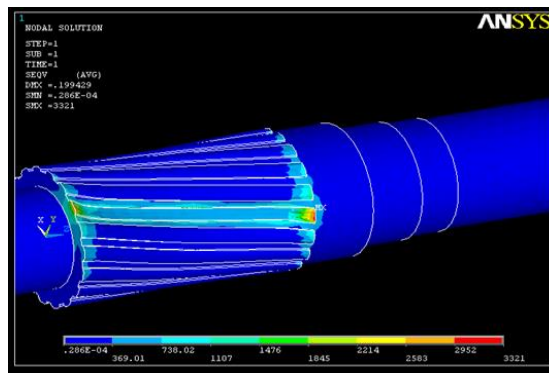

Figure 13. Stress deformation (chromium vanadium).

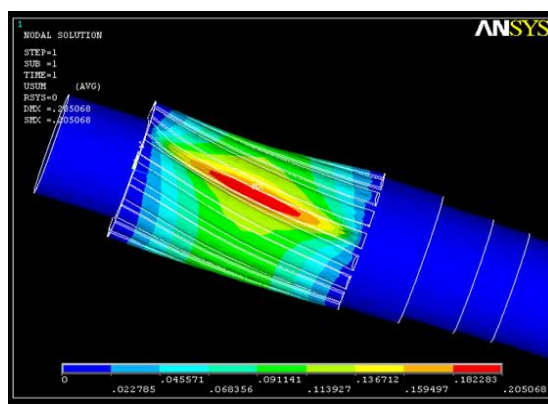

Figure 14. Displacement vector (chrome-vanadium).

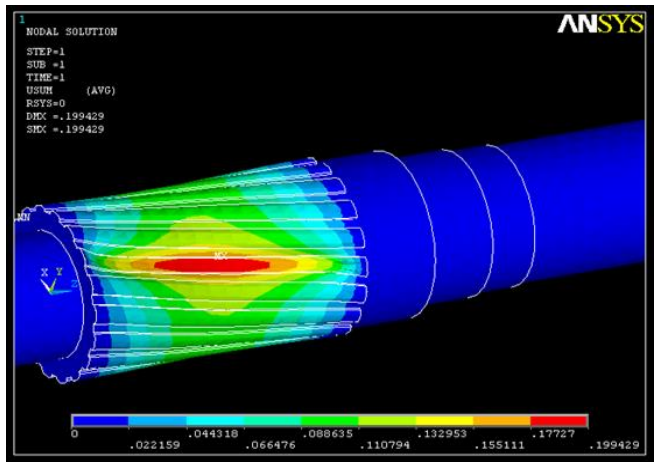

Figure 15. Displacement vector (EN-36).

Analysis of Modified Wind Turbine Blades

A balanced load and a secondary dynamic load at a wind speed of 11 m/s are connected to the network. At this wind speed, the wind turbine produces 55 kW and the hydro turbine produces 60 kW. So the total power generation is 115 kW. The model is tested with a half load of 57.5 kW, a full load of 115 kW, and a 10% overload. The waveforms are purely sinusoidal, as expected for the above conditions. The magnitude and frequency of the load voltage are also maintained at constant levels.

Double Multiple Stream Tube Model

The Double Multiple Stream Tube (DMST) models are used for the difference between the upwind and downwind passes through each blade. This is done by dividing the stream tube into an upwind and downwind half. The turbines interact with the wind upwind and downwind, which separately bypass through the blades. The upstream wind-induced velocity (V∞) is the average of the far upstream (V) and downstream equilibrium (Ve) air velocity. $V_{au} = \frac{1}{2}(V_\alpha + V_e)(or)V_e = 2V_{au} - V_\alpha$.

The conventional airfoils used for the Darrieus VAWTs were NACA0012, NACA0015, and NACA0018. These blades are of symmetrical geometry with minimum or negative torque generations at lower TSRs. Among these blade profiles, NACA0018 was selected for the analysis. The airfoil selected is to vary the trailing edge, which is from the original dimensions. For this analysis, the conventional NACA0018 symmetrical airfoil was used for the analysis of the double multiple stream tube (DMST) model. The trailing edge axis inclination of the blade is set to 15.

Figure 16. NACA0018 modified airfoil.

Table 7. Flow conditions

TSR (λ)	**0.25**	**0.5**	**0.75**	**1**	**1.5**	**2**	**3**	**3.5**	**4**	**5**
Velocity m/s	4	4	4	4	4	4	4	4	4	4
Turbine angle Velocity (rad/s)	0.5	1	1.5	2	3	4	6	7	8	10

CFD Analysis

In the VAWT analysis, the modified airfoil limit is set to 0.2 m in chord length with a radius of 2 m. The 2D model of the turbine is created by Gambit software, the mesh of the model is generated, and the commercial CFD fluid is used for numerical solution. The RNG k-epsilon model was adapted for the turbulence closure.

DMST Analysis

In the VAWT analysis by using DMST, the normal NACA0018 airfoil is set to 0.2m chord length and the radius of the turbine radius is 2m. The wind

velocity used for this analysis is 4 (m/s) and the tip speed ratios (λ) are 0.5, 1, 1.5, 2, 3, 4, 5, and 6. The number of stream tubes used for the analysis is 12, with an angle of $\Delta\theta = 15°$.

The coefficient of power for the modified airfoils is calculated by combining the performance of the turbine trailing edge angle of 15 for TSR limit is 0.1 to 1 and without inclination of the trailing edge for TSR value is greater than 1. The Cp was found from the ratio between the modelled turbine power and the available wind power in the air. In DMST, the Cp value is less than about 2.6. The CFD analysis for the modified airfoil system indicates that positive torque occurs at low tip speed ratios.

The Cm values are obtained from the average moment of three airfoils, which is modelled and analyzed through computational analysis. The modified airfoil tip speed ratio has values of 0.1, 0.25, 0.75, and 1. As can be seen, the value of Cm is higher and seems to reduce up to TSR = 0.5 and then starts to rise. The torque values were calculated from the coefficient moment (Cm) by using the value of the modelled airfoil, turbine area, air density, free stream velocity, and the radius of the turbine. As the graph shows, the average torque values at each of the TSR simulated values are positive.

The analysis result shows that the minimum stress value is 7.63607X10-7 N/mm2 (MPa) at node 16099 and the maximum stress value is 0.304129 N/mm2 (MPa) at node 11002. The maximum displacement value is 0.101712 mm at node 8538.

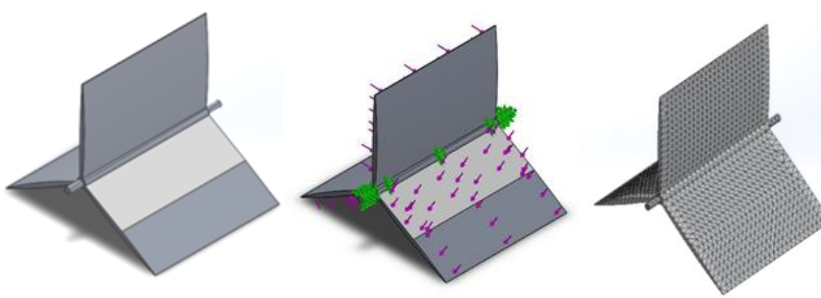

Figure 17. Simulation of a blade.

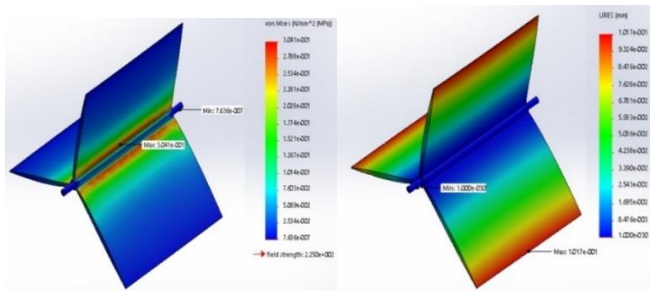

Figure 18. Stress and displacement analysis of the blade.

Table 8. Results of the analysis

Particulars	Helical gear	Herringbone gear
Stress deformation	$453.24*10^{-6}$ N/m^2	$554.97*10^{-6}$ N/m^2
Strain deformation	$0.0028328*10^{-3}$ m	$0.0022652*10^{-3}$ m
Total deformation	$0.0001382*10^{-3}$m	$0.0008076*10^{-3}$ m

Pitting Analysis

The maximum amount of pitting is eliminated by the use of material and gear changes. The best-suited gear to be used in a windmill is herringbone gear.

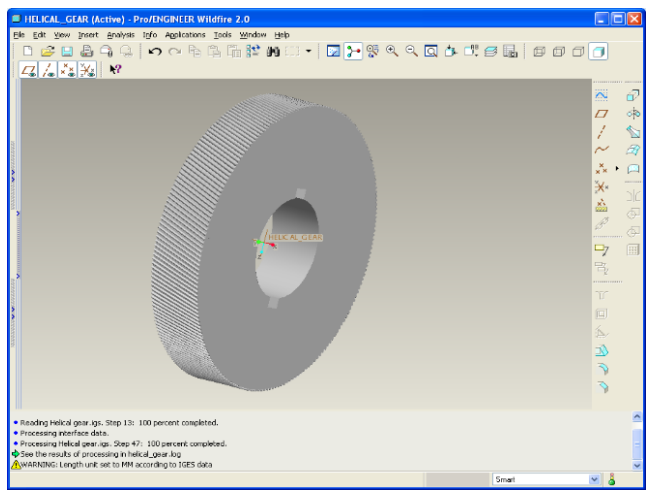

Figure 19. Helical gear design.

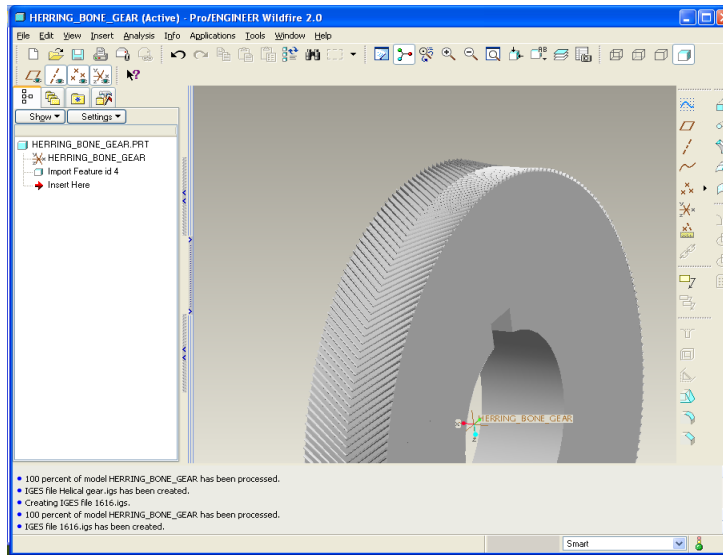

Figure 20. Herringbone gear design.

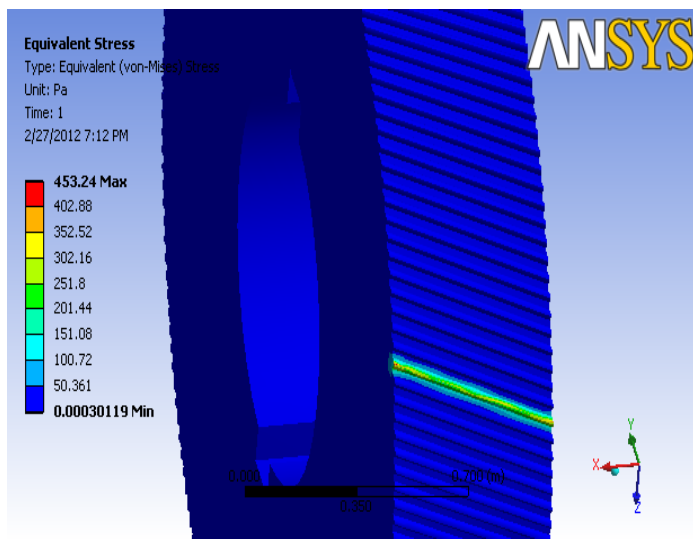

Figure 21. Helical gear stress distribution.

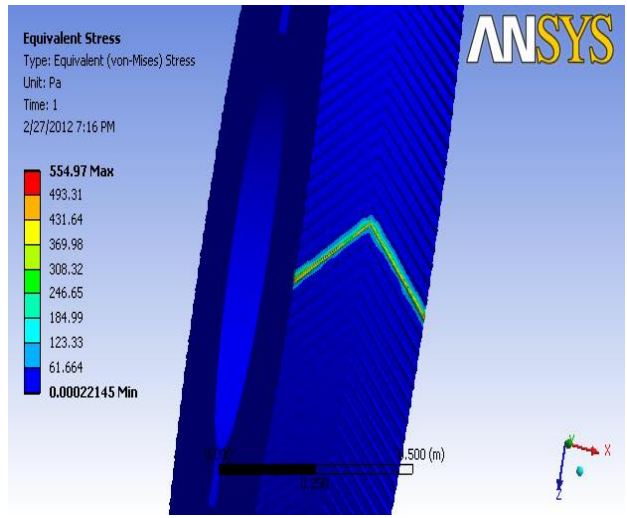

Figure 22. Herringbone gear stress distribution.

Conclusion

Windmills have been around for thousands of years. They almost resulted in failure due to gear. In this work, it was finally found that herringbone gear is the most suitable gear to be used in the windmill. Furthermore, the gear's lifetime at full load increased to nearly 85,000 hours. The present scenario is all about wind energy, so this project would hold up well regarding the construction of windmills. Through this design, it is concluded that herringbone would be the better choice to be used in windmills. By achieving this concurrent engineering concept, the product development cycle time can be reduced considerably for any kind of model with the required needs. Theoretical and experimental work is carried out to confirm the validity of the analytical work. The control system of the induction generator, in combination with the MPPT of the wind turbine, has developed with minimum resistive power loss. The simulation was carried out using MATLAB and the results have been tabulated. From the simulated result, the total ohmic loss has been reduced to 5.79% in the grid side inverter, the power output has increased to 100w, and the efficiency has increased to 11.5%, so it can be one of the efficient wind energy conversion systems. Among the renewable energy sources, small hydro systems and wind systems have the ability to match each other. Further, there are many isolated locations that cannot be linked to the

grid where wind potential and hydro potential exist simultaneously. For such locations, a type of three-phase four-wire autonomous wind-hydro hybrid system is used, with one cage generator driven by a wind turbine and another synchronous generator driven by a hydro turbine, which includes the BESS. The system has been modelled and simulated in MATLAB and Sim Power System. The performance of the hybrid system has been demonstrated by consumer load variation and mechanically by wind speed variation. The performance of the system is within the load range while maintaining constant voltage and frequency ranges.

References

Abhay, K. J., and Diwakar, V. (2002). "Metallurgical Analysis of Failed Gear", *for Engineering Failure Analysis*, vol. 9(3), June 2002, pp. 359-365.

Adam Ragheb., and Magdi Ragheb. (2010). "Wind Turbine Gearbox Technologies". AGMA6006-A03, (2003), "*Standard for Design and Specification of Gearboxes for Wind Turbines*".

Ashwin P. Joseph, Suraj P. Chavhan, Pravesh K. Sahare, Abdul Arif, and Tanveer A. Hussain. (2016). "Review Paper on Wind Turbine using Magnetic Levitation", *International Journal of Research in Mechanical Engineering & Technology*, Vol. 6, Issue 1, Nov 2015-Apri l 2016, pp.87-90.

Bittumon, B., Amith Raju, Harish Abraham Mammen, Abhy Thamby, and Aby K., Abraham. (2014). "Design and Analysis of Maglev Vertical Axis Wind Turbine", *International Journal of Emerging Technology and Advanced Engineering*, Volume 4, Issue 4, April 2014, pp. 374-379.

Chaware. K. D., and Dr. Washimkar, P. V. (2016). "A Review on Experimental Investigation of Windmill to Generate Electric Power using Magnetic Levitation", *International Advanced Research Journal in Science, Engineering and Technolog*, Vol. 3, Issue 4, April 2016.

Crabheer, C. J., Fen, Y. and Taurar, P. J. (2010), "*Detecting Incipient Wind Turbine Gearbox*".

Farha Khanam, and Neelesh Soni. (2016). "Performance Improvement of Horizontal Axis Wind Turbine by Using Modified Blade of NACA 5510", *International Journal of Advanced Research in Science, Engineering and Technology*, Vol. 3, Issue 2, February 2016, pp. 1575-1580.

Fernandes, P. J. L. (1996). "Tooth Bending Fatigue Failure in Gears", *Engineering Failure Analysis*, vol. 3(3), September 1996, pp. 219-225.

Fujin Deng. (2010). "Variable Speed Wind Turbine Based on Multiple Generators Drive-train Configuration", *2010 IEEE PES Innovative Smart Grid Technologies Conference Europe (ISGT Europe)*, pp. 1-8.

Gelman, L., and LaPayne, G. (2012). "Novel Detection of Local Tooth Damage in Gears by the Wavelet Bicoherence", *Mechanical Systems and Signal Processing*, vol. 26, November, pp. 218-228.

Lei, Y., and Zuo, M. (2009). "Gear Crack Level Identification Based on Weighted K Nearest Neighbor Classification Algorithm," *Mechanical Systems and Signal Processing*, Vol. 23, No. 6, pp. 1535– 1547.

Matthias Kinzel, Quinn Mulligan. and John O. Dabiri. (2012). "Energy exchange in an array of vertical-axis wind turbines", *Journal of Turbulence*, Volume 13, September 2012.

Musial, W., and Butter, S. (2007). "Improving Wind Turbine Gearbox Reliability". National Renewable Energy Laboratory.

Omijeh, C. S., and Nmom, E. Nlewem. (2013). "Modeling of a Vertical Axis Wind Turbine with Permanent Magnet Synchronous Generator for Nigeria", *International Journal of Engineering and Technology*, Volume 3 No. 2, February, 2013, pp. 212-220.

Peter J. Schubel, and Richard J. Crossley. (2012). "Wind Turbine Blade Design", www.mdpi.com/*journal/Energies*, 5, 3425-3449.

Pimsarn, M., and Kazerounian, K. (2002). "Efficient evaluation of spur gear tooth mesh load usin pseudo-interference stiffness estimation method," *Mechanism and Machine Theory*, pp. 769–786.

Pravesh K. Sahare, Tanveer A. Hussain, Sangita N. Kakde, Sujata R. Ingle, and Ambika prasad O. Chaubey. (2016)."Review Paper on Vertical Axis Maglev Wind Turbine", *International Journal of Research in Mechanical Engineering & Technology*, Vol. 6, Issue 1, Nov 2015-Apri l 2016, pp. 76-79.

Ragheb, M. (2010). "*Wind Power Systems*, Harvesting the Wind".

Sandia. (2009). – Wind Plant Taxonomy v1.1. "US Wind Turbine Reliability Workshop".

Schultz, C. D. Beyta Gear Service, "The Effect of Gear box Architecture on Wind Turbine Enclosure Size".

Spinato, F., Tavner, P. J., van Bussel, G. J. W., and Koutoulakos E. (2009). "Reliability turbine subassemblies", *IET Renewable Power Generation*, Vol. 3, Iss. 4, pp. 1–15.

Standard for Design and Specification of Gearboxes, International Organization for, Wind Turbines – Part 4, ISO/IEC 81400-4.

Tavrer Xiong, P. J., and Spinato, J. P. (2006). "Reliability Analysis for Wind Turbines", *Wind Energy*, 10(1).

Thomas, A. C., and Kerman, E. (2005). "*Wind Power in Power Systems*", Wiley and Sons Ltd.

Winder and Wolfe. (1967). "Analysis of Tapered Roller Bearing Damage", American Society for Metals, Report C-7-11.1.

White, D. L., and Musial, W. D. (2004). "The effect of load phase angle on wind turbine blade fatigue damage". *J Solar Energy Eng*.

About the Editors

Dr. M. Dhurgadevi, Associate Professor, Computer Science and Engineering in Mahendra Engineering College, Namakkal, Tamilnadu. She earned her PhD from Anna University, Chennai in the area of Wireless Sensor Networks. She did her post-graduate work (ME) in Computer Science and Engineering with first class and distinction, and did her B-Tech in Information Technology with first class. She has more than 15 years of experience in teaching graduate and postgraduate students. Areas of interests are Wireless Sensor Networks, Distributed Systems, Cyber Security, Cloud Computing and Data Science. She also has three patents published to his credit. She added her credits by NPTEL certification in Introduction to modern application development (Elite) and Wireless adhoc and sensor networks (Elite). She is life member of ISTE. She also certified SAP-ABAP and VM ware Data center Virtualized Trainer. She has published 10 book chapters with Anuradha, Magnus, A.R Publications, Lambert publications and has more than 10 publications to his credit in reputed International Journals and 10 papers in International/National conferences.
Email: dhurgasakthi3@gmail.com

Dr. P. Sakthivel earned his Bachelor's degree in Mechanical Engineering from Government College of Engineering, Salem and Master degree (ME) in Engineering Design from Kongu Engineering College, Perundurai. Then he obtained PhD degree from Anna University Chennai. At present, he is working as an Associate Professor in the Department of Mechanical Engineering at Sri Krishna College of Technology, Coimbatore. He is having 15 years of experience in teaching. His research interest includes Machine Design, Finite Element Analysis, Kinematics, Computer Integrated Manufacturing, Composite Materials, Artificial Neural Networks and Concept

of Engineering Design. He also has three patents published to his credit. He has published 5 papers in national conferences, 7 papers in international conferences and 18 papers in international journals. Dr. P. Sakthivel is a Life member of Indian Society for Technical Education.
Email: skt4design@gmail.com

Dr. K. Gunasekaran received his doctoral degree in the faculty of Information and Communication Engineering from Anna University, Chennai in 2019. Currently he is serving as Associate Professor, Department of Computer Science and Engineering, Sri Indu College of Engineering and Technology, Telangana, India. Earlier he completed under graduate and post graduate degrees in Anna University, Chennai and Bharathidasan University, Trichy respectively. He contributed some of works to few Science Citation Indexed journals and Scopus Indexed journals. His research interests include soft computing, Computational intelligence and Machine learning techniques.
Email: drgunak@yahoo.com

Index

H

I

J

K

L

M

N

O

P

R

S

T

V

W

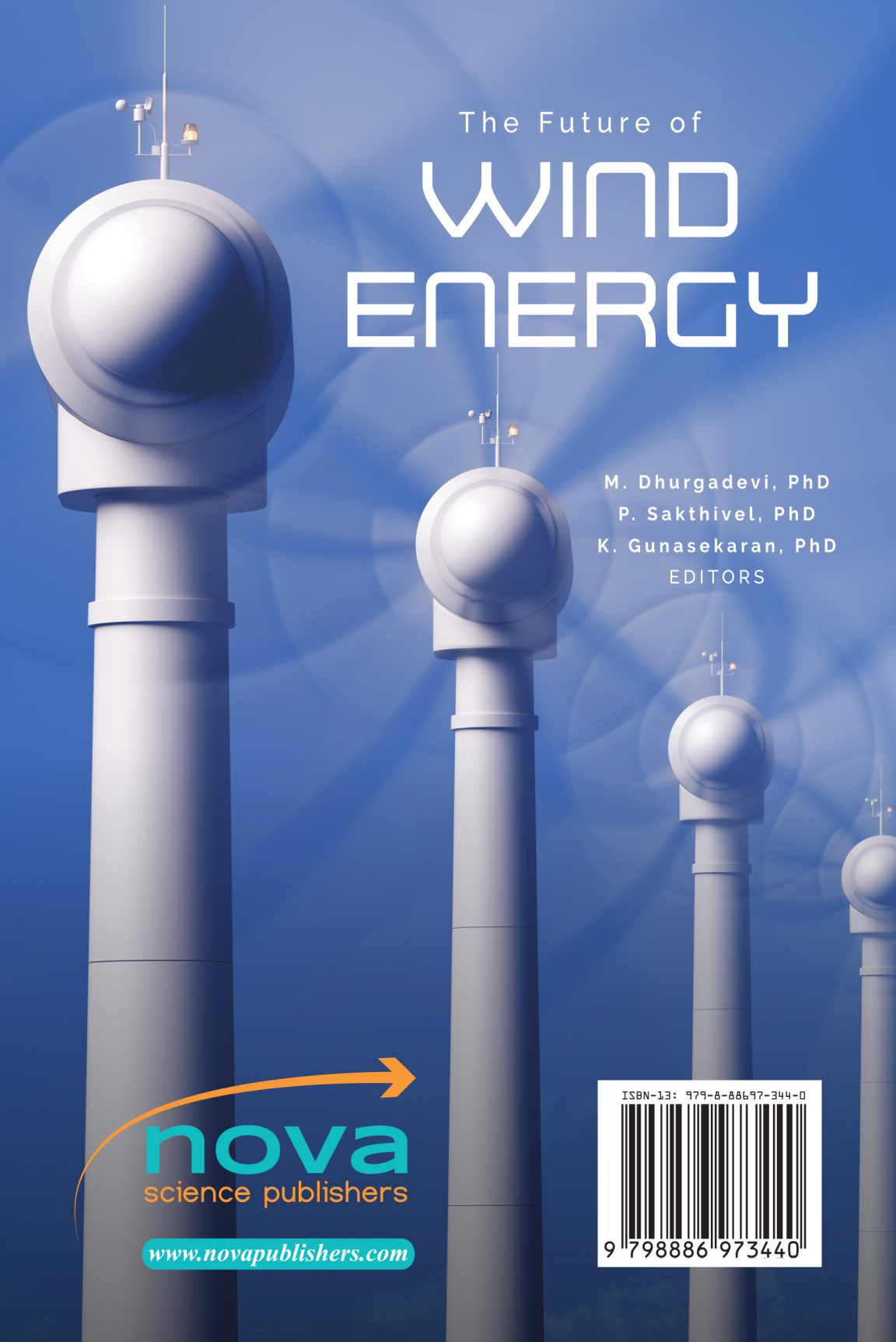
The Future of
WIND ENERGY
M. Dhurgadevi, PhD
P. Sakthivel, PhD
K. Gunasekaran, PhD
EDITORS
nova
science publishers
www.novapublishers.com
ISBN-13: 979-8-88697-344-0
9 798886 973440